Modelling of cumulative groundwater and subsidence impacts in the Surat CMA for UWIR 2025: approach and methods

A technical note

Version 1.0

October2025

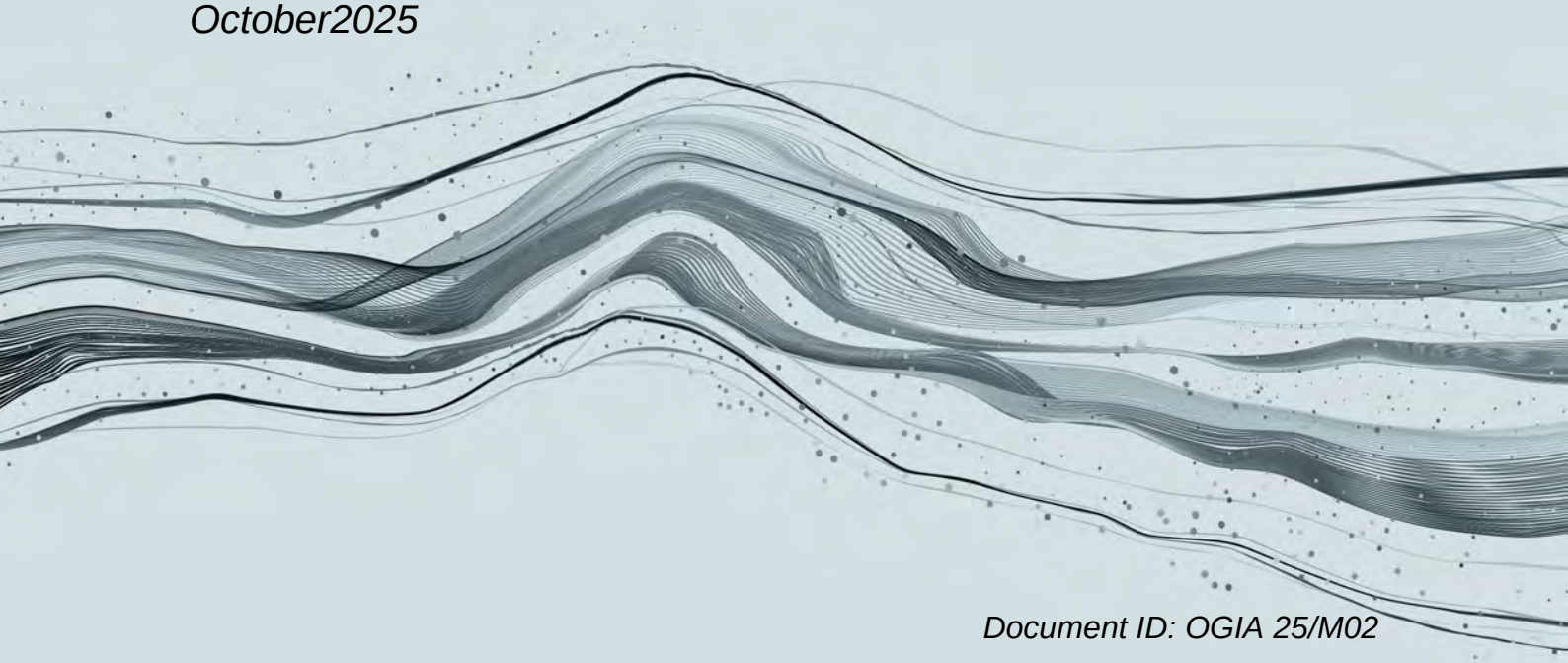

Document ID: OGIA 25/M02

Version	Release date	Authorised by
1.0	October 2025	Sanjeev Pandey

Overall guidance and direction: Tao Cui, Gerhard Schöning, Sanjeev Pandey

Contributors: Tao Cui, Mark Gallagher, Hamid Aghighi, Gengshuo Zhang, Marti Burcet, Yue (Wendy) Zhang, Gerhard Schöning, Sanjeev Pandey, John Doherty, Koray Kalmaz

External review: Noel Merrick

Acknowledgement: Jeremy Wolff and Ryan Davidson (mapping); Hugh Marshall (editorial)

This report should be referenced as:

Cui, T, Gallagher, M, Aghighi, MA, Zhang, G, Burcet, M, Zhang, Y (Wendy), Schöning, G, Pandey, S & Doherty, J (2025). *Modelling of cumulative groundwater and subsidence impacts in the Surat CMA for UWIR 2025: approach and methods* by the Office of Groundwater Impact Assessment, Department of Local Government, Water and Volunteers, Queensland Government, Australia.

This publication has been compiled by the Office of Groundwater Impact Assessment, Department of Local Government, Water and Volunteers.

Table of contents

Appendices

Table of figures

Table of tables

1 Primary target audience

This document is intended for readers seeking to understand the data sources and analytical techniques that underpin OGIA's regional groundwater model developed to support the UWIR 2025. It assumes a basic familiarity with groundwater modelling concepts. A fundamental understanding of geomechanical principles is also expected for readers engaging with sections related to subsidence modelling.

2 Preamble

Each Underground Water Impact Report (UWIR) prepared by the Office of Groundwater Impact Assessment (OGIA 2016a, 2019a, 2021a, 2025; Queensland Water Commission 2012) has been accompanied by a standalone report containing a detailed description of the groundwater modelling method and results (GHD 2012a; OGIA 2016b, 2019b) that underpinned the assessment. While the UWIR is prepared for a broad audience, with a focus on summaries of results and findings, the modelling report provides detailed information about supporting data, modelling methodology, and predictions.

The current UWIR 2025 modelling strategy is built on the significant advances in research and model development in previous UWIRs. For methods and knowledge that have been discussed in previous modelling reports, this report provides only a brief overview. In contrast, more detailed discussions are provided for significant new developments during this UWIR period, such as the coupling of subsidence modelling with the groundwater model and the new workflow to derive transient recharge.

It is noted that most maps and graphs are presented in the appendices to maintain a relatively concise report.

3 Modelling objectives and purpose

The primary purpose of modelling undertaken by OGIA is to predict spatiotemporal change in regional groundwater pressures and subsidence within the Surat Cumulative Management Area (CMA) due to resource development, in both the short and long terms. More specifically, the modelling of cumulative impacts is required to:

- define the immediately affected area (IAA) for each aquifer present within the model domain – the area where water pressures are predicted to decline by more than two metres (unconsolidated aquifers) or five metres (consolidated aquifers) within the next three years
- define the long-term affected area (LAA) for each aquifer present within the model domain – the area where water pressures are predicted to decline by more than the same thresholds at any time in the future
- provide data to identify IAA bores and LAA bores, which are water bores that are predicted to be impacted based on the specified impact triggers during the IAA and LAA assessment periods
- support the identification of potentially affected springs – springs where the groundwater pressures in aquifers underlying the sites of these springs are predicted to decline by more than 0.2 m at any time in the future

- predict impacts to the rate and volume of groundwater movement between coal formations and key aquifers in the CMA
- estimate the quantity of groundwater that is expected to be extracted by coal seam gas (CSG) and coal mining tenure holders in the CMA
- estimate the CSG-induced subsidence magnitude and slope change within the CMA.

4 Unique modelling challenges and previous models

As outlined in the geological model report by Bui Xuan Hy et al. (2025), the geology of the Surat CMA is highly complex. It comprises more than 20 geological formations, with erosional contacts and structural offsets contributing to substantial lateral and vertical heterogeneity. Individual aquifers within this multi-layered system may be exposed at the surface in some locations, while in others they can extend to depths of more than a few kilometres. CSG is produced from coal formations embedded within this system, which contains a large number of coal seams targeted for development. In this context, the key modelling challenges include:

- **a large model domain:** an area of approximately 650×460 km (nearly 300,000 km²) encompassing dozens of geological formations
- **extended timeframes:** CSG and mining development is expected to span more than 75 years, while model predictions must consider long-term impacts extending thousands of years into the future
- **vertical hydraulic connectivity:** vertical connections both within and between aquifers are often more challenging to assess than horizontal connections due to limited data and the slow response of intervening aquitards
- **coal measures upscaling:** coal measures comprising numerous thin coal seams and interburden units, limited seam-specific data and the computational burden of simulating individual seams make it impossible to represent individual seams as separate layers in groundwater models
- **integration of mining and CSG impacts:** coal mines are generally localised in outcrop areas and interact predominantly with shallow hydrogeological processes, whereas CSG development targets the same formations but at greater depth
- **dual-phase flow effects:** depressurisation near CSG wells induces gas–water interactions that must be accounted for within a regional-scale groundwater flow model
- **fault representation:** geological faults extending into both the Surat and Bowen basins that need to be incorporated into the modelling framework
- **parameter upscaling:** defining parameters that are consistent with the regional assessment scale while still honouring borehole measurements
- **big data:** calibrating the model against extensive and diverse monitoring datasets, including water levels, production data and ground motion

- **CSG-induced subsidence:** driven by interacting processes such as poromechanical compaction of coal and interburden, and coal shrinkage – effects not handled by conventional subsidence modelling packages.

In order to address these challenges, OGIA's approach to the assessment of cumulative impacts from resource development has evolved considerably since the UWIR 2012 (Queensland Water Commission 2012) when the first regional groundwater model was developed. This progression reflects expanding data acquisition efforts and enhanced data interrogation that have improved the understanding of key hydrogeological processes operating within the Surat CMA.

The first model iteration in the UWIR 2012 was largely based on information from previous studies. Relatively little primary data interpretation was undertaken and the model was developed by GHD (2012b) using a standard version of MODFLOW 2005 (Harbaugh 2005a).

An entirely new regional groundwater model (OGIA 2016b) was constructed as part of the UWIR 2016 (OGIA 2016a), using several innovative modelling techniques developed by OGIA and a revised conceptualisation of the groundwater flow system, based largely on primary data interpretation. A customised version of the MODFLOW-USG code built by Panday et al. (2021) was used as the modelling platform for the UWIR 2016, to which OGIA made numerous revisions addressing the following challenges unique to the assessment of CSG impact in the Surat CMA:

- simulation of water desaturation due to gas production in coal seams around CSG wells
- dual-porosity formulation for differing hydraulic responses in coal seams and interburden material
- improved representation of CSG wells using a descending MODFLOW drain methodology, including cell-to-well conductance calculations for associated water production, utilising an increased permeability in areas where CSG wells screen multiple coal seams that would otherwise be separated by low-permeability interburden
- upscaling of hydraulic properties from available lithological logging and permeability measurement data for both the CSG target coal reservoir and potentially impacted aquifers using so-called 'numerical permeameters'; this information is subsequently used for initial parameterisation of the regional groundwater model
- explicit representation of major faults via (i) layer juxtaposition incurred through stratigraphic displacement and (ii) incorporation of the hydraulic effects associated with inter-formational flow along the fault planes and enhancement of vertical permeabilities within the damage zones adjacent to the faults
- simulation of CSG water byproduct reinjected into the Precipice Sandstone.

Some of the innovations in UWIR 2016 model were undertaken by OGIA in collaboration with one of the primary developers of the MODFLOW-USG code. One example is the method developed to simulate water desaturation and the approximation of dual-phase flow in and around CSG wells, as described in Herckenrath et al. (2015).

The third iteration of the regional groundwater flow model in 2019 by OGIA (OGIA 2019b) represented a revision of the UWIR 2016 model and included further refinements to the modelling approach, including modifications to the underlying geological model, revision of the pre-calibration model parameterisation using an updated numerical permeameter workflow, incorporation of additional major faults and simulation of CSG wells partially completed into the Springbok Sandstone.

Further refinement and improvements were implemented in the fourth iteration of the UWIR regional groundwater model in 2021 (OGIA 2021b). For the first time, coal mines in the Surat CMA were integrated into the regional groundwater model to enable a cumulative impact assessment from both CSG depressurisation and coal mining. Based on groundwater level drawdown of the regional groundwater model, an analytical model was developed to estimate CSG-induced subsidence.

5 Approach for the UWIR 2025 assessment

In the current UWIR cycle, OGIA has implemented multiple further improvements to the OGIA regional groundwater model in terms of calibration data updates and process representation. Major updates and added values of the current modelling include the following:

- **Integrated groundwater flow and geomechanical model (Cui et al. 2025):** development and implementation of a coupled hydro-mechanical model that is simultaneously calibrated to groundwater and ground motion data. This enables concurrent prediction of groundwater impacts and subsidence, while maximising the value of available calibration datasets.
- **New recharge estimation workflow:** establishment of a new approach that generates a unique transient recharge model for each outcrop zone, based on daily rainfall and evaporation data specific to the zone.
- **Representation of CSG wells:** refinement of the numerical groundwater model to better capture the behaviour of deviated wells and pressure change during well shutdowns, improving the assessment of impacts and water production.
- **Calibration update:** inclusion of additional monitoring data (such as InSAR) and up-to-date monitoring data to extend the calibration period to December 2022, along with improved calibration of water production, resulting in enhanced model performance.
- **Condamine Alluvium sub-regional model:** development of a new high-resolution sub-regional geological model for the Condamine Alluvium footprint. This integrates recent airborne electromagnetic data with comprehensive reinterpretation of seismic, petroleum well, coal hole and water bore datasets. This lays a foundation for a future sub-regional groundwater model.

In addition to the OGIA regional groundwater and subsidence models, two other models are also used in the UWIR 2025 impact assessment. The Condamine model was originally developed by Klohn Crippen Berger (KCB) for the then Department of Natural Resources, Mines and Energy (DNRME) for water allocation purposes and has since been updated by OGIA in collaboration with KCB. The Acland model was developed by New Hope Group for the prediction of impacts from existing and proposed development at the New Acland coal mine. OGIA reviewed the Acland model and determined that it was fit for the purpose of integrating groundwater impacts from that coal mine into the OGIA regional model. Figure 5-1 shows the spatial domain for the above models and Table 5-1 summarises some of the key design features. Further detail on construction and calibration of these models can be found in Chapters 6 and 7, respectively.

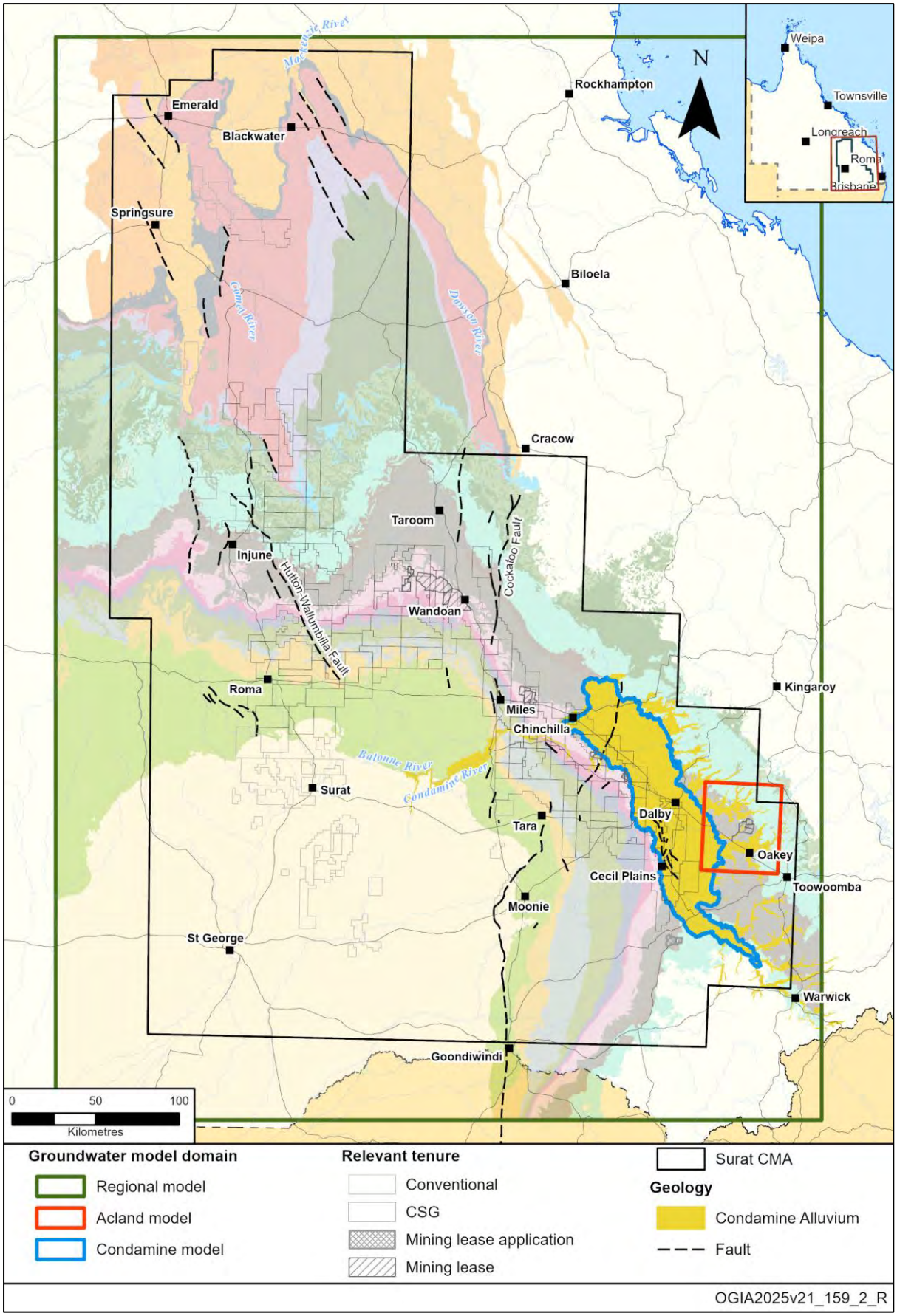

Figure 5-1: Model domains of the suite of models used for UWIR 2025

Table 5-1: Key features of groundwater models used for UWIR 2025

Element	Model		
	Condamine model	**Regional model 2025**	**Acland model**
Purpose	Assist with water management in the Condamine Alluvium	Predict regional cumulative impacts from resource development in the Surat CMA	Predict mining-only impacts from the New Acland coal mine
Layering	2 layers Condamine Alluvium	35 layers Cenozoic – Basement	16 layers Alluvium – Hutton Sandstone
Grid	500×500 m	1,500×1,500 m	25–800 m
Faults	None	35 regional faults	6 fault systems
Domain	~201×55 km	460×650 km	~45×52 km
Modelling code	MODHMS	MODFLOW-USG	MODFLOW-USG

6 Regional model

6.1 Overview

The geological framework and other flow process representation for the 2025 groundwater flow model remained relatively unchanged since the UWIR 2021, except for the coupled hydro-mechanical component and the new recharge estimation workflow. Data, conceptual understanding and modelling methods that have been discussed in the previous reports will be only briefly discussed in this chapter. Further information can be found in OGIA (2016b, 2019b, 2021b).

Key features of the regional model 2025 include the following:

- The geological topology is underpinned by a geological model for the Surat and southern Bowen basins, using 21 layers at 250-m grid resolution, derived from lithostratigraphic interpretation of wireline log data from approximately 8,000 wells, surface geological mapping, stratigraphic interpretation of lithological data from nearly 24,500 water bores and seismic survey data (OGIA 2019c). The regional hydrostratigraphy has been represented numerically, using 35 model layers (Figure 6-2).
- Geological faults are represented through the inclusion of ‘non-neighbour connections’ to simulate flow from one stratigraphic unit to another across fault planes. The widths of the fault cores and damage zones were used, along with detailed lithology information (from geophysical logs where available), to calculate the likely effective horizontal and vertical resistance or conductance created by each fault.
- Because it is always challenging to assimilate hydraulic properties at different scales with a regional groundwater model, local-scale block models of the subsurface (‘numerical permeameters’) were developed specifically to derive effective formation-scale hydraulic properties to integrate data at different scales. Thousands of numerical permeameters were

developed to derive the initial and prior hydraulic conductivity of the regional groundwater model.

- Simulation of CSG extraction wells is achieved using the MODFLOW-USG ‘drain’ boundary condition (descending drains). As each well develops, the drain bottom-hole pressure progressively descends over time until its final bottom-hole pressure is reached.
- The increase in formation-scale horizontal permeability of the Walloon Coal Measures, caused by CSG wells connecting otherwise discontinuous seams, is accounted for by modifying the MODFLOW-USG code and providing a supplementary enhanced permeability field for cell-to-well conductance calculation, to ensure more accurate associated water production simulation.
- Explicit representation of coal mines is simulated through use of a one-way MODFLOW ‘river’ boundary condition, whereby the river stage and river bottom elevations are matched to ensure that water can only be exported from the model. The elevations ascribed to each river cell over time represent the progressive excavation from the pre-mined surface down to the base elevation of the open pit for a given development scenario, as provided by industry.
- MODFLOW-USG functionality was introduced as an approximation of dual-phase (water and gas) flow, to simulate water desaturation in response to a reduction in pressure surrounding CSG wells.
- The hydrogeology of the coal formations is complex in that they comprise highly varied sequences of high- and low-permeability material. It is not practical to represent the individual coal seams within these coal formations as separate layers in the regional groundwater flow model. To address this challenge, a dual-domain setup has been adopted to represent coal (mobile domain) and interburden (immobile domain), to maintain difference head responses in coal seams and interburden.
- Partial completion of CSG wells into the lower parts of the Springbok Sandstone, simulated using MODFLOW-USG drains.
- The thickness and permeability of the non-productive zone (NPZ) of the Walloon Coal Measures is represented, which is a key control on the transmission of CSG impacts into the overlying Springbok Sandstone.
- The groundwater flow model is calibrated in three stages: ‘pre-development’ (1947), to replicate conditions that existed prior to the commencement of any groundwater extraction; pre-CSG extraction conditions, commensurate with 1995; and a transient simulation, to replicate the period from January 1995 to December 2022.

6.2 Key datasets

From developing model architecture to model parameterisation and calibration, significant volumes of data have been collected, integrated and assimilated. While not an exhaustive list of data used for UWIR groundwater modelling, Table 6-1 provides a high-level summary of the datasets and their application in the modelling process.

Table 6-1: A list of the key datasets processed to support the UWIR groundwater modelling

Dataset category	Volume/Note	Use in UWIR modelling
Geology	Seismic data from more than 300 2D surveys and 12 3D surveys; more than 20,000 water bore drill logs; about 7,700 CSG well logs; 18,000 coal holes; and surface and solid geology from GSQ and Cranfield (2017)	Model architecture
Hydrodynamics	Annual estimates of groundwater use from about 30,000 bores; monitoring bore data; monthly volumes for more than 10,000 wells; and about 40,000 records from more than 600 monitoring bores	Processes (non-CSG and CSG extraction); calibration targets
Development plans	CSG development plans and mine development plans	Processes (river package)
Recharge	Precipitation and evapotranspiration data between 1995 and 2023 from 24 stations; long-term recharge based on more than 12,000 chloride samples; and reinjection volumes	Processes (recharge)
Hydraulic properties	Drill stem tests, pumping tests and core tests from about 12,000 measurements; and methane adsorption tests	Parameterisation
Ground motion	InSAR measurements from about 400 million records at around 1 million sites	Calibration target

6.3 Model setup

6.3.1 Model architecture

The Regional Model 2025 retained the hydrogeological model structure of the Regional Model 2021. The numerical groundwater model comprises 35 numerical layers (Figure 6-1 and Figure 6-2). Thickness and depth maps for each of the 35 model layers are provided in Appendix A. For more detailed discussion about the model structure, such as subdivision of the coal formations and non-neighbour connections, please refer to OGIA (2016c, 2019c, 2021c).

Model layer	Formation	Basin
1	All Alluvium and Basalt (including Main Range Volcanics)	Cenozoic
2	Upper Cretaceous (Griman Creek Formation & Surat Siltstone) and the Condamine-Walloon transition zone	Surat & Clarence-Moreton basins
3	Wallumbilla Formation	
4	Bungil Formation	
5	Mooga Sandstone	
6	Orallo Formation	
7	Gubberamunda Sandstone	
8	Westbourne Formation	
9	Upper Springbok Sandstone	
10	Lower Springbok Sandstone	
11	Walloon Coal Measures non-productive zone	
12	Upper Juandah Coal Measures - Layer 1	
13	Upper Juandah Coal Measures - Layer 2	
14	Lower Juandah Coal Measures - Layer 1	
15	Lower Juandah Coal Measures - Layer 2	
16	Lower Juandah Coal Measures - Layer 3	
17	Taroom Coal Measures	
18	Durabilla Formation	
19	Upper Hutton Sandstone	
20	Lower Hutton Sandstone	
21	Upper Evergreen Formation	
22	Boxvale Sandstone	
23	Lower Evergreen Formation	
24	Precipice Sandstone	
25	Moolayember Formation	Bowen Basin
26	Clematis Group	
27	Rewan Group	
28	Bandanna Formation non-productive zone	
29	Upper Bandanna Formation	
30	Lower Bandanna Formation	
31	Lower Bowen 1	
32	Cattle Creek Formation non-productive zone	
33	Upper Cattle Creek Formation	
34	Lower Cattle Creek Formation	
35	Lower Bowen 2	

Regional aquifer | Partial aquifer | Tight aquifer | Interbedded aquitard | Tight aquitard

OGIA_017

Figure 6-1: Model layers and formations represented in the regional groundwater flow model

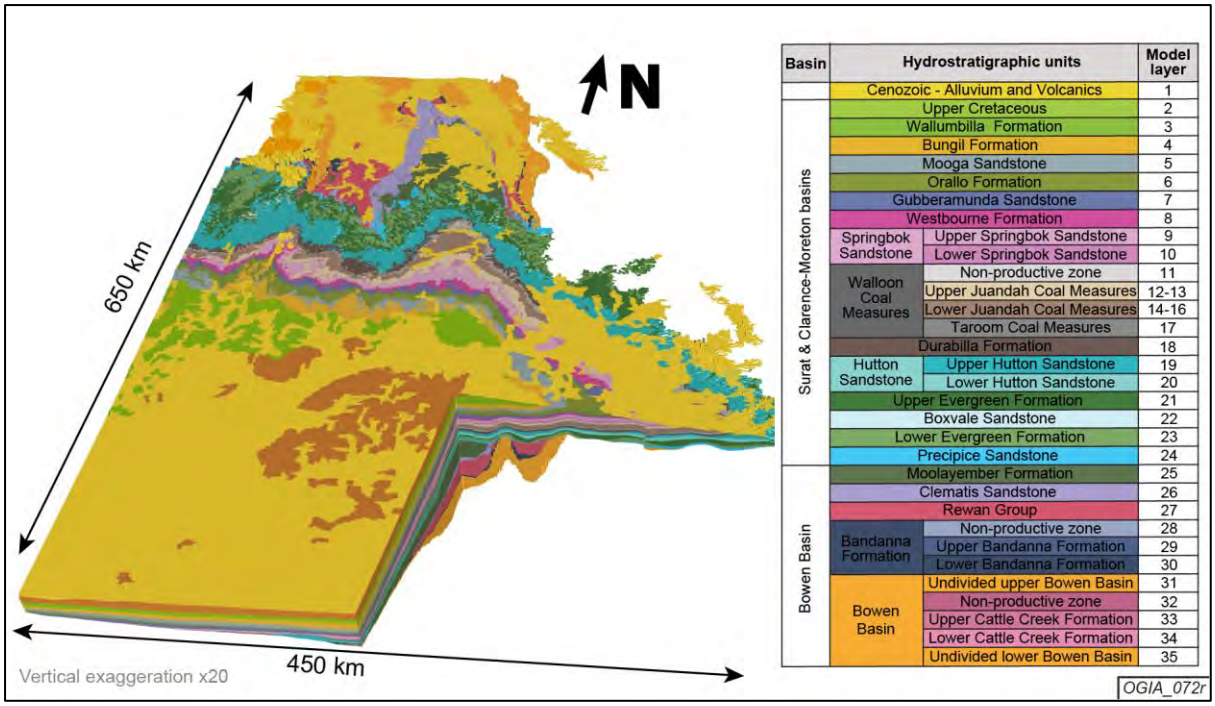

Basin	Hydrostratigraphic units		Model layer
	Cenozoic - Alluvium and Volcanics		1
Surat & Clarence-Moreton basins	Upper Cretaceous		2
	Wallumbilla Formation		3
	Bungil Formation		4
	Mooga Sandstone		5
	Orallo Formation		6
	Gubberamunda Sandstone		7
	Westbourne Formation		8
	Springbok Sandstone	Upper Springbok Sandstone	9
		Lower Springbok Sandstone	10
	Walloon Coal Measures	Non-productive zone	11
		Upper Juandah Coal Measures	12-13
		Lower Juandah Coal Measures	14-16
		Taroom Coal Measures	17
	Durabilla Formation		18
	Hutton Sandstone	Upper Hutton Sandstone	19
		Lower Hutton Sandstone	20
	Upper Evergreen Formation		21
	Boxvale Sandstone		22
	Lower Evergreen Formation		23
	Precipice Sandstone		24
Bowen Basin	Moolayember Formation		25
	Clematis Sandstone		26
	Rewan Group		27
	Bandanna Formation	Non-productive zone	28
		Upper Bandanna Formation	29
		Lower Bandanna Formation	30
	Bowen Basin	Undivided upper Bowen Basin	31
		Non-productive zone	32
		Upper Cattle Creek Formation	33
		Lower Cattle Creek Formation	34
		Undivided lower Bowen Basin	35

Figure 6-2: 3D representation of the regional groundwater model

6.3.2 Process representation

6.3.2.1 Representation of recharge

The approach for estimating recharge within the Condamine Alluvium footprint remains unchanged from previous UWIR models and continues to adopt the outputs of a groundwater model developed by Klohn Crippen Berger (KCB 2011), referred to as the 'KCB Condamine model'. In the Regional Model 2025 model, a revised method was developed to estimate the pre-calibration recharge rates across the model domain, apart from the Condamine Alluvium. Under this approach, each outcrop area is assigned a unique transient recharge model, which is calibrated prior to being applied to the regional model surface cells. Further details of this revised recharge estimation approach are provided in the following subsections.

6.3.2.1.1 Steady-state recharge

In the UWIR 2025, the steady-state recharge adopts the research outputs of Crosbie et al. (2022), which estimated the long-term averaged recharge rate through chloride mass balance for the GAB on a 2,500×2,500-m grid. In Crosbie et al. (2022), comprehensive data sources for chloride concentrations were included to compute point recharges, which were then upscaled using regression kriging to the grid. Additionally, the uncertainty associated with upscaling process was quantified. For the Regional Model 2025, the pre-calibration steady-state recharge rate on each model surface cell was obtained by sampling the long-term averaged recharge rate from the 50th percentile (P50) raster reported in Crosbie et al. (2022). In the Condamine Alluvium area, the steady-state recharge rate was derived from the KCB Condamine model. The distribution of the pre-calibration steady-state recharge rate for the Regional Model 2025 model grid is shown in Figure 6-3. The area and mean long-term recharge rates associated with each outcrop area are provided in Table 6-2.

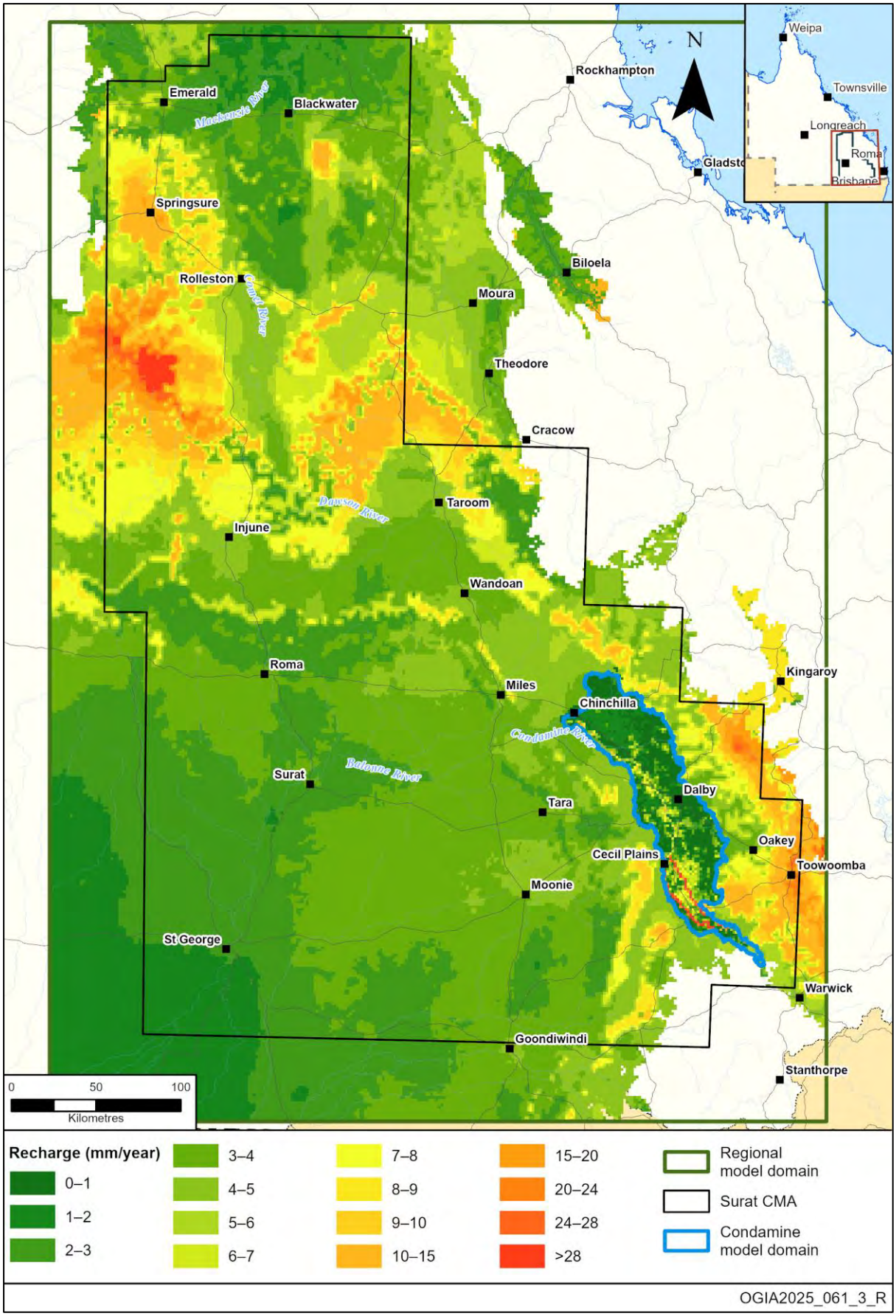

Figure 6-3: Pre-calibration steady-state (long-term average) recharge rate

Table 6-2: Outcrop area and pre-calibration recharge estimates for each outcrop formation

Outcrop dominant formation	Model layers	Outcrop area (km^2)	Mean long-term recharge (m/day)
Condamine Alluvium	1	5,587	9.50E-06 (KCB Condamine model)
Non-Condamine alluvium	1	32,290	7.97E-06
Main Range Volcanics	1	6,217	2.22E-05
Other basalt	1	8,334	2.88E-05
Cenozoic sediments	1	65,817	8.51E-06
Weathered Surat/Bowen	1	1,235	1.22E-05
Upper Cretaceous	2	11,471	8.93E-06
Wallumbilla Formation	3	7,562	9.08E-06
Bungil Formation	4	3,636	7.81E-06
Mooga Sandstone	5	3,274	1.08E-05
Orallo Formation	6	4,561	8.77E-06
Gubberamunda Sandstone	7	2,120	1.73E-05
Westbourne Formation	8	2,268	1.35E-05
Springbok Sandstone	9,10	4,370	1.08E-05
Walloon Coal Measures	11, 12, 13, 14, 15, 16	8,026	1.17E-05
Durabilla Formation	17	2,210	1.30E-05
Hutton Sandstone	18, 19	12,170	2.15E-05
Evergreen Formation/Boxvale Sandstone	20, 21, 22	12,746	2.24E-05
Precipice Sandstone	23	1,231	3.12E-05
Moolayember Formation	24	4,385	2.16E-05
Clematis Group	25	3,782	1.83E-05
Rewan Group	26	4,030	1.60E-05
Bandanna Formation	27, 28, 29	704	1.59E-05
Undifferentiated Bowen Basin strata	30, 34	10,251	1.19E-05

6.3.2.1.2 Transient recharge

For the transient calibration period (1995 to December 2022), time-varying recharge estimates were required. In the Regional Model 2025, a unique LUMPREM transient recharge model built by Doherty (2021) was developed for each of the 24 outcrop zones. These LUMPREM models generate

groundwater recharge time series using daily rainfall and potential evaporation as inputs. Monthly rainfall and evaporation data for each recharge model were obtained from the 'Scientific Information for Land Owners' (SILO) station located nearest to the centroid of the respective outcrop zone. The corresponding SILO stations for each outcrop zone are listed in Table 6-3.

Table 6-3: SILO stations and recharge-to-rainfall ratios in each outcrop formation

Outcrop dominant formation	SILO station	Ratio of long-term averaged recharge to averaged rainfall	
		Minimum (%)	Maximum (%)
Condamine Alluvium	WESTFIELDS	0.58	1.58
Non-Condamine alluvium	BOOMI (BARWON ST)	0.27	2.10
Main Range Volcanics	AUGHAMORE	0.55	3.74
Other basalt	WYNTOON	0.37	5.13
Cenozoic sediments	MARMADUA FORESTRY	0.27	3.84
Weathered Surat/Bowen	BOOMI (BARWON ST)	0.35	3.14
Upper Cretaceous	PECHEY FORESTRY	0.33	0.75
Wallumbilla Formation	GLENMORGAN POST OFFICE	0.36	1.33
Bungil Formation	DULACCA TRUCK STOP	0.36	1.41
Mooga Sandstone	WALLUMBILLA POST OFFICE	0.37	1.47
Orallo Formation	KINDON	0.39	1.59
Gubberamunda Sandstone	POSSUM PARK	0.40	1.75
Westbourne Formation	DUNMORE STATE FOREST	0.41	1.81
Springbok Sandstone	LANCEWOOD	0.43	1.49
Wallon Coal Measures	SOMERSET	0.45	2.38
Durabilla Formation	BROADMERE	0.57	1.96
Hutton Sandstone	LYNWAY	0.43	3.85
Evergreen Formation/ Boxvale Sandstone	WOODSPRING	0.39	3.89
Precipice Sandstone	WOMBALANO	0.41	4.36
Moolayember Formation	REEDY CREEK STATION	0.49	4.27
Clematis Group	BRIGALOW RESEARCH STN	0.45	2.98
Rewan Group	MOUNT NICHOLSON	0.39	3.18
Bandanna Formation	BLUFF POST OFFICE	0.33	2.92

Outcrop dominant formation	SILO station	Ratio of long-term averaged recharge to averaged rainfall	
		Minimum (%)	Maximum (%)
Undifferentiated Bowen Basin strata	CONSUELO	0.33	2.07

Calibration was undertaken prior to applying the LUMPREM-generated recharge series to model cells. Two calibration targets were considered for each transient recharge model:

- mean long-term average recharge rate (Table 6-2)
- annual recharge-to-rainfall ratios within an acceptable range (Table 6-3).

The second calibration target was derived by extracting rainfall data for the transient period across the model domain from SILO and spatially interpolating averaged rainfall onto the UWIR model grid. For each model cell, the ratio of long-term averaged recharge to averaged rainfall was then calculated. A summary of the minimum and maximum ratios for each outcrop zone, excluding non-recharge cells, is presented in Table 6-3. This calibration target plays an important role in constraining the model, as it prevents unrealistic recharge estimates during the transient period, even when the long-term averaged recharge is matched. Figure 6-4 illustrates the calibrated transient recharge series and annual recharge-to-rainfall ratios in transient period for the Main Range Volcanics.

After the calibrated transient recharge time series for each outcrop zone was obtained, these values were translated to the model grid by scaling with a multiplier. The multiplier for each model cell was computed as the ratio of its long-term averaged recharge rate (steady-state recharge rate) to the mean long-term average recharge of its respective outcrop zone. For example, one model cell in the Main Range Volcanics (MRV) has a long-term average recharge rate of 1.11×10^{-5} m/day, whereas the mean long-term average recharge rate for the entire MRV is 2.22×10^{-5} m/day (Table 6-2). This results in a scaling multiplier of 0.5. Consequently, the transient recharge for this cell was obtained by multiplying the calibrated transient recharge of MRV by 0.5.

In summary, by assigning individual recharge models to each outcrop zone, the updated recharge estimation method allows the unique hydrogeological characteristics and recharge response of each outcrop zone to be represented in the model. In addition, the method accounts for the influence of long-term averaged recharge and produces reasonable recharge-to-rainfall ratios that enhance the physical plausibility of the model results. It has been noted in previous UWIR models, however, that errors in recharge are unlikely to promulgate large errors in predictions of CSG impacts, given that a high proportion of recharge is rejected within shallow groundwater systems. Nonetheless, the adoption of an enhanced recharge approach may provide strategic advantages, especially for areas near outcrops. Its capacity to include long-term historical rainfall records and stochastic rainfall or evaporation replicates for future climate-change scenarios across the Surat Basin and paves the way for other hypothesis-testing related to climate variations.

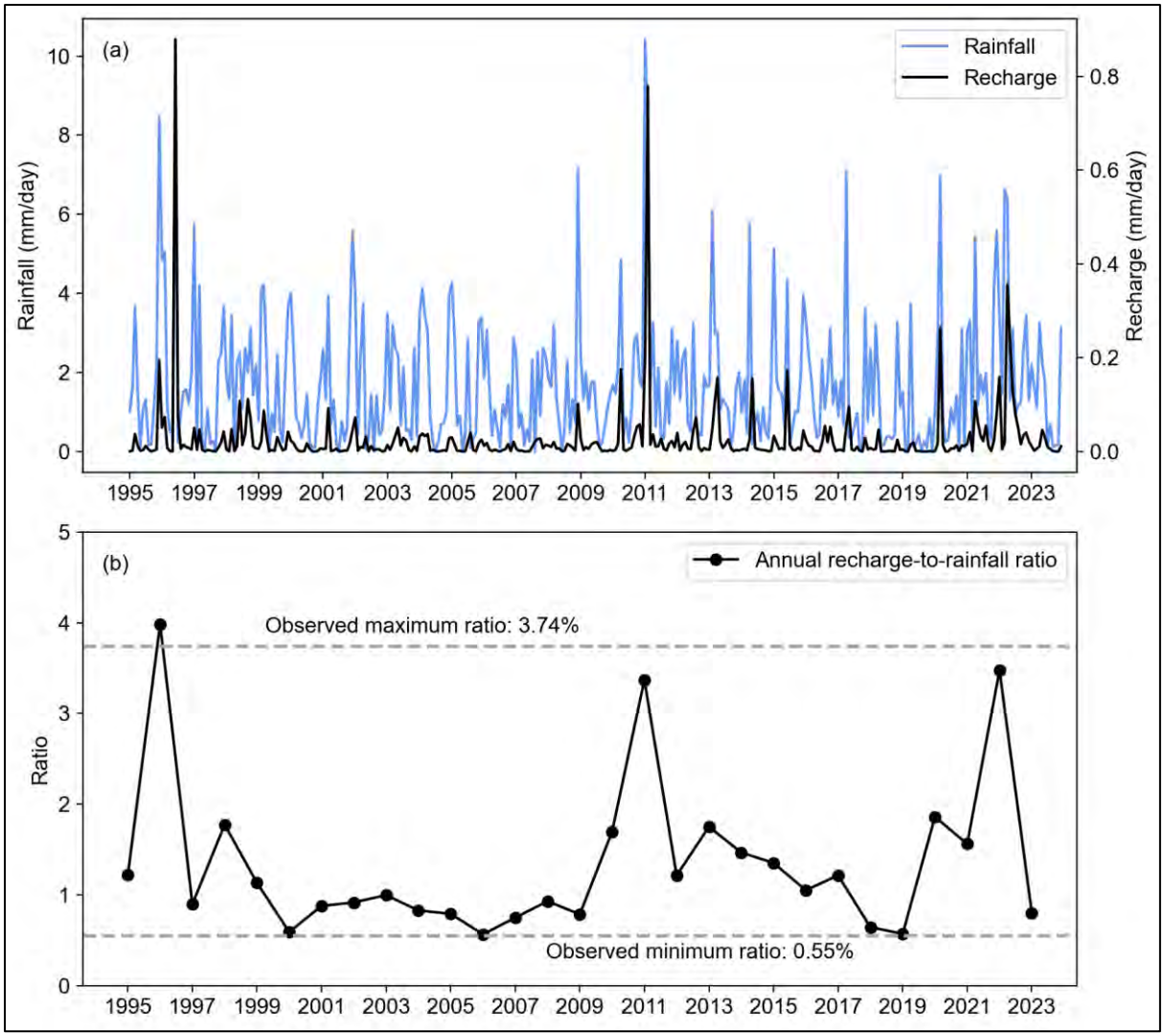

Figure 6-4: (a) Calibrated transient recharge series in Main Range Volcanics and (b) annual recharge-to-rainfall ratio in Main Range Volcanics

6.3.2.2 Representation of non-CSG water extraction

6.3.2.2.1 Assimilation of extractive datasets

Non-CSG extraction includes bores in the Surat and Bowen basins from which water is pumped for irrigation, industrial and mining purposes and for stock and domestic (S&D) supply. It also includes conventional P&G wells that have not yet been decommissioned or converted to water bores. The last of these conventional P&G wells target the Evergreen Formation and Precipice Sandstone in the Surat Basin, including several active fields located to the south and east of Roma. In the Bowen Basin, the primary formations for conventional P&G activities from which water is also extracted are the Showgrounds Sandstone (Clematis Group equivalent) and the Moolayember Formation.

Since the initial UWIR in 2012, the approach for identifying water supply bores and estimating groundwater use has significantly evolved. For the current UWIR, approximately 30,000 water supply bores have been identified in the Surat CMA. The identified water bores need to be assigned to hydrogeological formations ('aquifer attribution') based on their screen information. The process involves the compilation and verification of bore location and construction details – to determine the portion of the bore, in terms of depth, that is 'screened' or open (intake depth) – and the intersection of this with the depths of the geological formations at the same location, taken from the geological

model. There are significant challenges in implementing this fundamental process due to a lack of information and the variable quality of existing data. Since the initial UWIR in 2012, OGIA has continued to evolve the methodology of aquifer attribution in the Surat CMA. The current methodology integrates bore construction information and hydrogeological information in a hierarchical workflow across the regional and sub-regional model domains. Additional details of the methodology are available in an additional technical note (Erasmus et al. 2024).

Another challenge is to quantify the transient groundwater usage of the identified water bores. For the initial UWIR in 2012, a nominal use value was assigned for S&D bores, while for non-S&D bores, 100% of the entitlement volume was applied. The S&D component evolved for the UWIR 2016, with the development of a demand-based approach that utilised property grazing potential to estimate stock demand. In parallel, the University of Queensland (UQ) commenced a metering project in 2016 at 34 properties to provide additional data and information on groundwater use for S&D purposes. Since the UWIR 2021, OGIA has evolved the workflow further, integrating new datasets, information and analysis. As described in Smallacombe et al. (2024), this includes revisions to stock rates, reductions in the daily consumption for stock, and incorporation of spatiotemporal climatic variability into the annual estimates of groundwater demand for S&D purposes. Estimated rates of non-P&G related extraction for major water sources, from 1900 to the end of 2022, are shown in Figure 6-5.

These non-CSG extractions were compiled into MODFLOW-USG well package input files for use in the groundwater model. Non-CSG extractions associated with bores with drill dates prior to 1995 were included in the 1995 steady-state well package input file. For the historical transient simulation, wells were gradually introduced according to the date each bore was drilled and assumed to remain active thereafter unless they have been marked as ‘abandoned and destroyed’ in the same database. The spatial distribution of known non-P&G water bores (those other than conventional P&G and CSG wells) is provided in Figure 6-6.

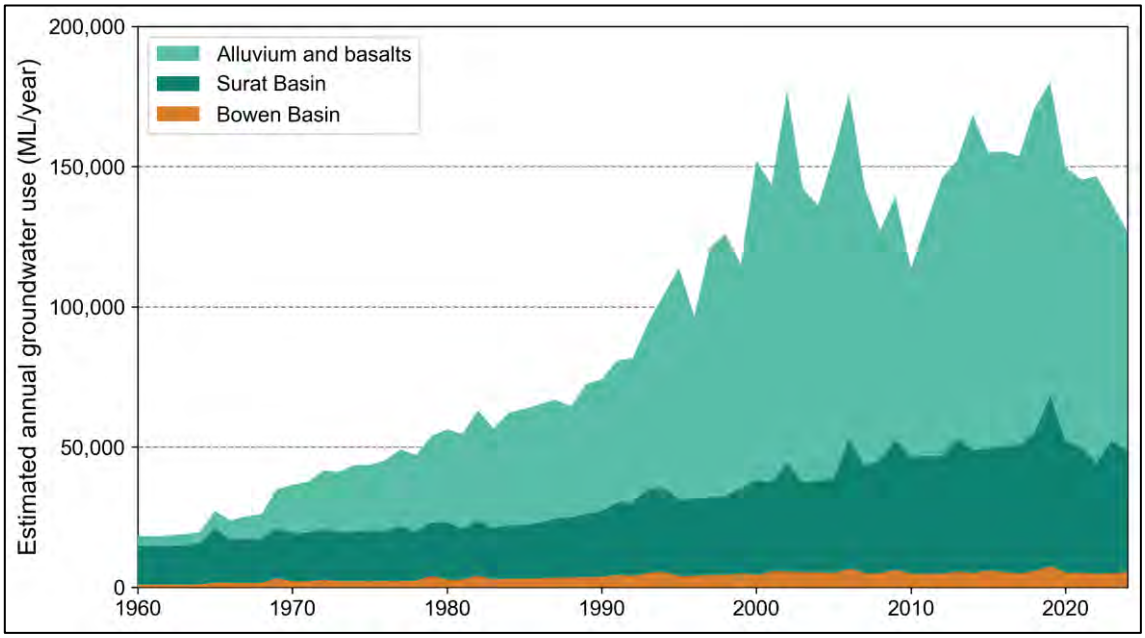

Figure 6-5: Groundwater systems’ estimated rates of non-P&G water supply extraction

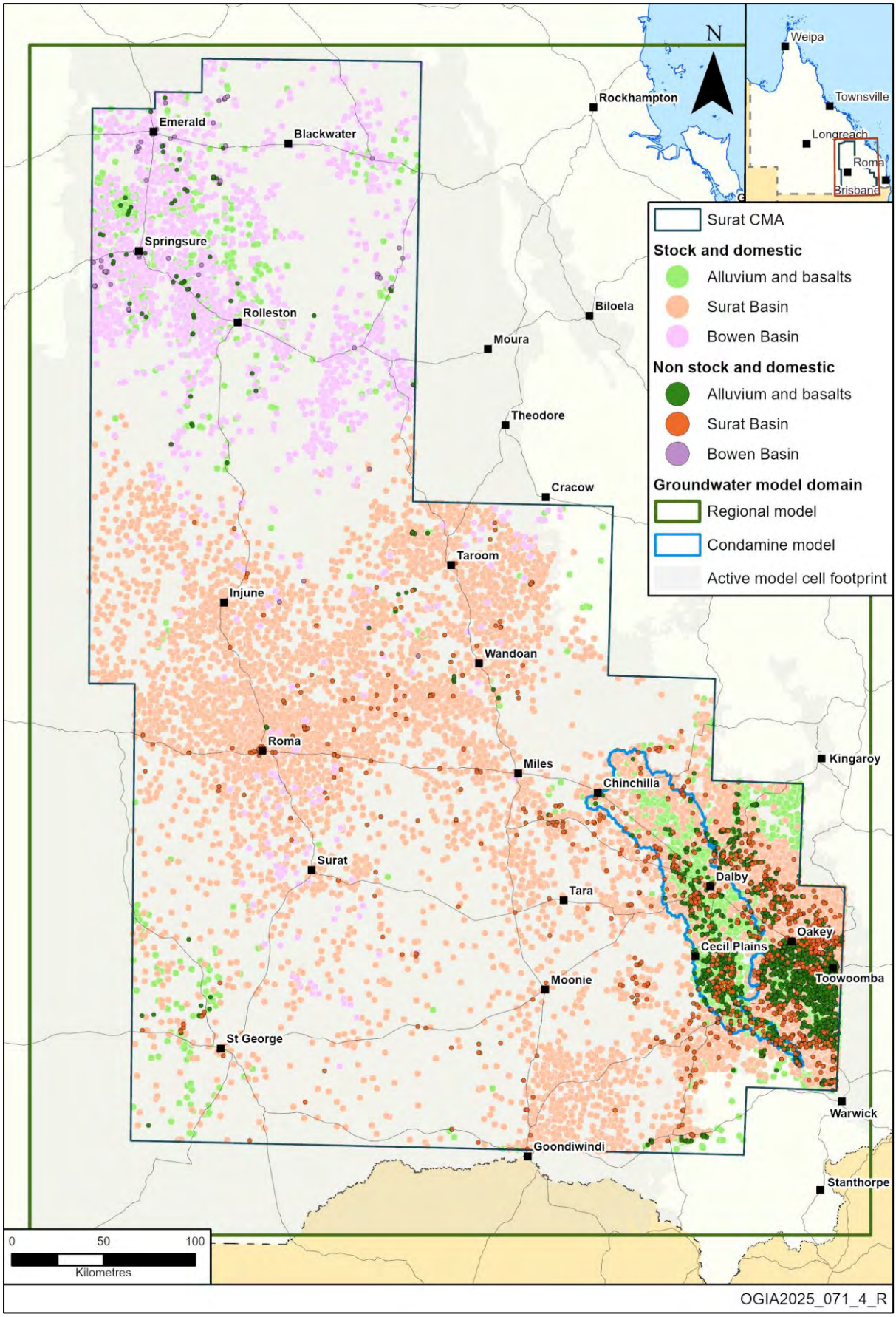

Figure 6-6: Spatial distribution of non-P&G water supply bores within the Surat CMA

Additionally, the following aspects of the extractive input datasets used by the model are of note:

- Extractions from the Condamine Alluvium and Main Range Volcanics are not represented explicitly in MODFLOW-USG well package input file for the Regional Model 2025. Instead, they are presented implicitly as drainage surfaces, which are provided through MODFLOW-USG river input files.
- Also, a small amount of extraction – totalling around 6,500 ML/year from aquitard units in the Regional Model 2025 (namely the Westbourne Formation, Durabilla Formation, upper and lower Evergreen Formation, Moolayember Formation, Rewan Group and undifferentiated Bowen Basin strata) – is not represented in MODFLOW-USG well files. Its exclusion follows experience gained during development of previous model iterations, wherein such extraction precipitated poor model numerical behaviour by generating large drawdowns, on account of the generally low permeability of these units.

6.3.2.2.2 Multiple screened extractions

Simulation of extraction requires that wells spanning multiple model layers be considered. These fall into two categories, the first comprising wells attributed to formations represented by multiple layers in the Regional Model 2025. Stratigraphic units to which this category applies are the Springbok Sandstone, Walloon Coal Measures, Hutton Sandstone, Bandanna Formation and Cattle Creek Formation. The second category comprises wells with screens that tap multiple stratigraphic units. A database maintained by OGIA that contains well screen information and attributes each well to one or more model layers (Erasmus et al. 2024) was utilised for this process.

All multi-layer extractions were subject to transmissivity-weighted flow apportionment considering partial penetration of wells, as far as possible, based on the data available. Flow apportionment is calculated by a model pre-processor that reads MODFLOW-USG input files; hence it is adjusted as model hydraulic properties are adjusted through the calibration process.

For a bore screened across *N* layers, the adjusted extraction rate in each layer *i* is computed using the following formula:

$$Q_i = Q_w \frac{T_i}{\sum_i^N T_i} \quad \textbf{(6.1)}$$

where:

Q_i is the pumping rate attributed to an individual cell,

T_i is the transmissivity of an individual cell,

Q_w is the total well extraction rate.

The individual transmissivity values T_i featured in Equation (6.1) are computed as the product of the horizontal hydraulic conductivity of the respective model cell and the minimum of (i) cell thickness, (ii) screen length and (iii) simulated saturated thickness.

6.3.2.2.3 Well derating

As for the previous UWIR model, the Regional Model 2025 continues to support derating of all non-CSG extraction. This additional functionality enables reductions in extraction rates necessary to ensure that groundwater heads within an extraction well remain above the level of the well screen.

Application of the well derating functionality requires specification of several auxiliary variables for each well. These variables define the well heads at which (i) pump derating is initiated (WELREDELEV) and (ii) pumping ceases (WELOFFELEV). These extra variables are added to standard MODFLOW-USG input files that are written by model pre-processors developed by OGIA. This enables derating variables to be adjusted as model hydraulic properties are adjusted through the calibration process.

In any cell in which extraction takes place, the difference (S_w) between the head calculated for the cell and that pertaining to the extraction well can be calculated using the Peaceman equation (Peaceman 1978). Thus, for any non-CSG extraction well, WELREDELEV = WELOFFELEV + S_w, where S_w is calculated using the Peaceman equation:

$$S_w = \frac{Q}{2\pi T}\ln\left(\frac{0.208a}{r_w}\right) \quad \textbf{(6.2)}$$

where:

- s_w is the cell-to-well correction term,
- Q is the pumping rate,
- a is the length of a square cell (or the square root of the product of lengths of a rectangular cell), equating to 1,500 m,
- r_w is the radius of the well, assumed to be 0.1 m,
- T is the transmissivity of the pumping cell.

WELOFFELEV is set as the top of well screen, if this is known, or the top of the uppermost cell from which extraction takes place, if no screen information in available. If the uppermost cell from which extraction takes place is the highest cell (for example, the outcrop cell) in a model grid column, WELOFFELEV is set to the base elevation of cell + 25% of the cell thickness. However, if WELREDELEV > top elevation of cell, then WELREDELEV = top elevation of cell. For an artesian well, the preservation of “flowing” conditions (head exceeding topography) was considered sacrosanct; WELOFFELEV was set as the top of the uppermost cell in that vertical column.

6.3.2.3 Representation of coal mine stresses

The Regional Model 2025 includes stresses from seven open-cut coal mines in the Surat CMA that target coal seams within the Walloon Coal Measures (Table 6-4). Four of these mines (New Acland, Cameby Downs, Kogan Creek and Commodore) are currently operational, while Wilkie Creek is in ‘care and maintenance’ mode. For two proposed mines, the Wandoan Coal Project and Elimatta, approvals are in place or under consideration. The Range coal mine, which was included in the UWIR 2021, has been excluded from the UWIR 2025 modelling as its application has since been withdrawn. Among the operational coal mines, impact predictions at the New Acland mine are produced separately via the Acland Model (Section 7).

The exploitation depths of coal mines and their proximity to CSG developments are key factors influencing their cumulative impact. Coal mines in the Surat CMA generally have shallow pits and their distances from CSG fields vary. For instance, the Commodore and New Acland mines are located more than 50 km from the nearest CSG developments, while mines in the central area and

the Northern Coal Area (NCA) are situated closer to CSG operations, potentially resulting in cumulative impacts on nearby water levels (Figure 6-7).

Drainage to each mine pit is simulated over time through the addition of MODFLOW-USG RIV cells in each relevant UWIR model 2025 cell, from the pre-mined surface elevation, down to the minimum elevation of the surveyed pit shell. Figure 6-8 illustrates the time series of minimum pit shell elevation data (New Acland not included), extracted from mine survey data and used as input for the Regional Model 2025's transient simulation. To simulate coal mining operations, a conductance value of 5,000 m²/d was assigned to all relevant cells. This value is high enough to allow efficient water outflow without causing numerical instability.

Table 6-4: Status and key attributes of coal mines in the Surat CMA

Mine	Status	Start–end	Target seam	Excavated overburden	Pit depth (m)[1]
Wandoan Coal Project (Glencore)	Proposed	2031–2105	Juandah Coal Measures (Kogan to Wambo)	Alluvium, Springbok Sandstone	24–60
Elimatta New Hope (New Hope Group)	Proposed	2029–2058	Juandah Coal Measures (Kogan to Wambo)	Alluvium, Springbok Sandstone	50–150
Cameby Downs (Yancoal)	Operational	2009–2053	Upper Juandah Coal Measures (Kogan, Macalister and Nangram)	Springbok Sandstone	40–110
Kogan Creek (CS Energy)	Operational	2000–2042	Upper Juandah Coal Measures (Macalister and Nangram)	-	40–60
Wilkie Creek (Peabody)	Care and maintenance	1995–2030	Upper Juandah Coal Measures (Macalister)	-	30–60
New Acland (New Hope Group)	Operational	2001–2043	Taroom Coal Measures (Acland-Sabine, Waipanna and Balgowan)	Main Range Volcanics	30–60
Commodore (Queensland Power Company)	Operational	2001–2037	Taroom Coal Measures (Commodore)	Alluvium	15–50

Note:
1. Estimated pit depth

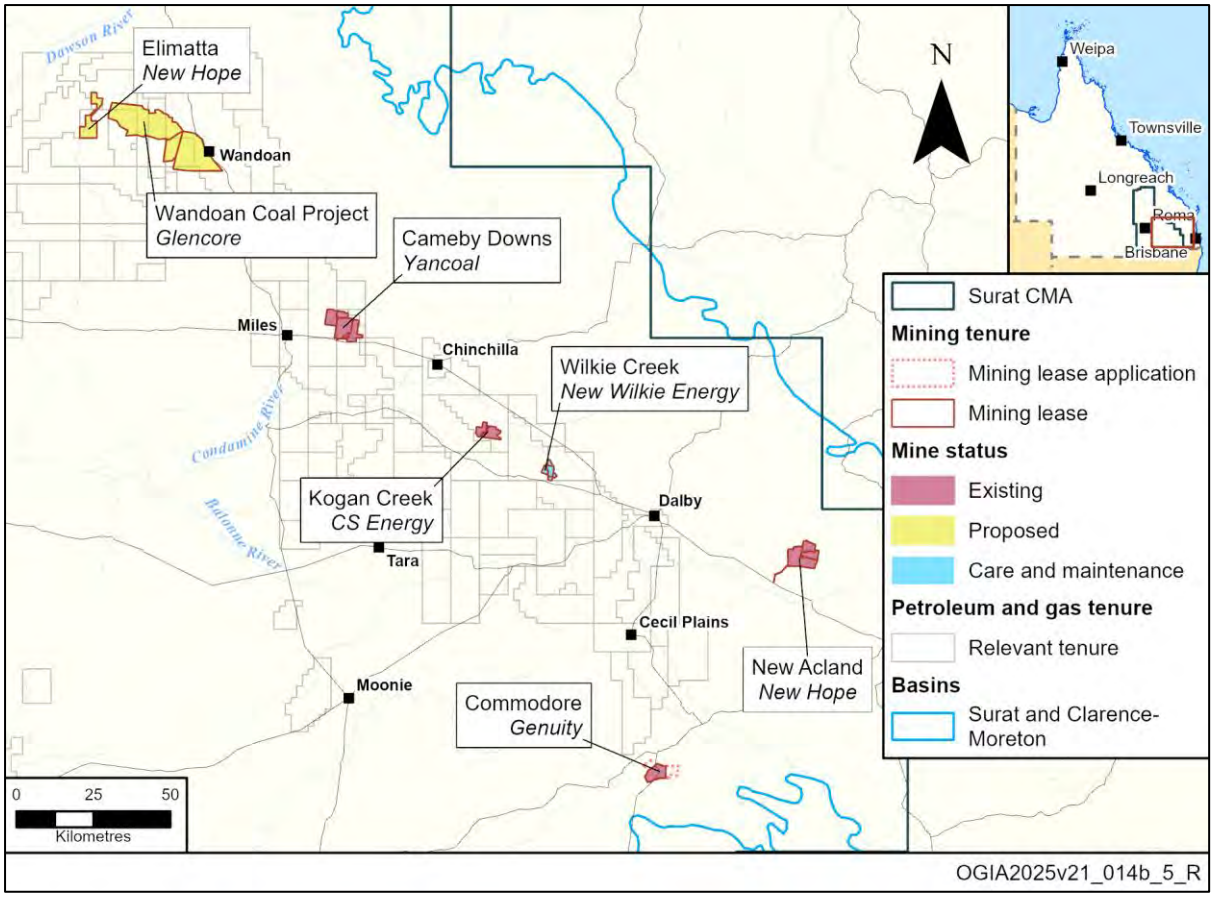

Figure 6-7: Location and status of coal mines in the Surat CMA

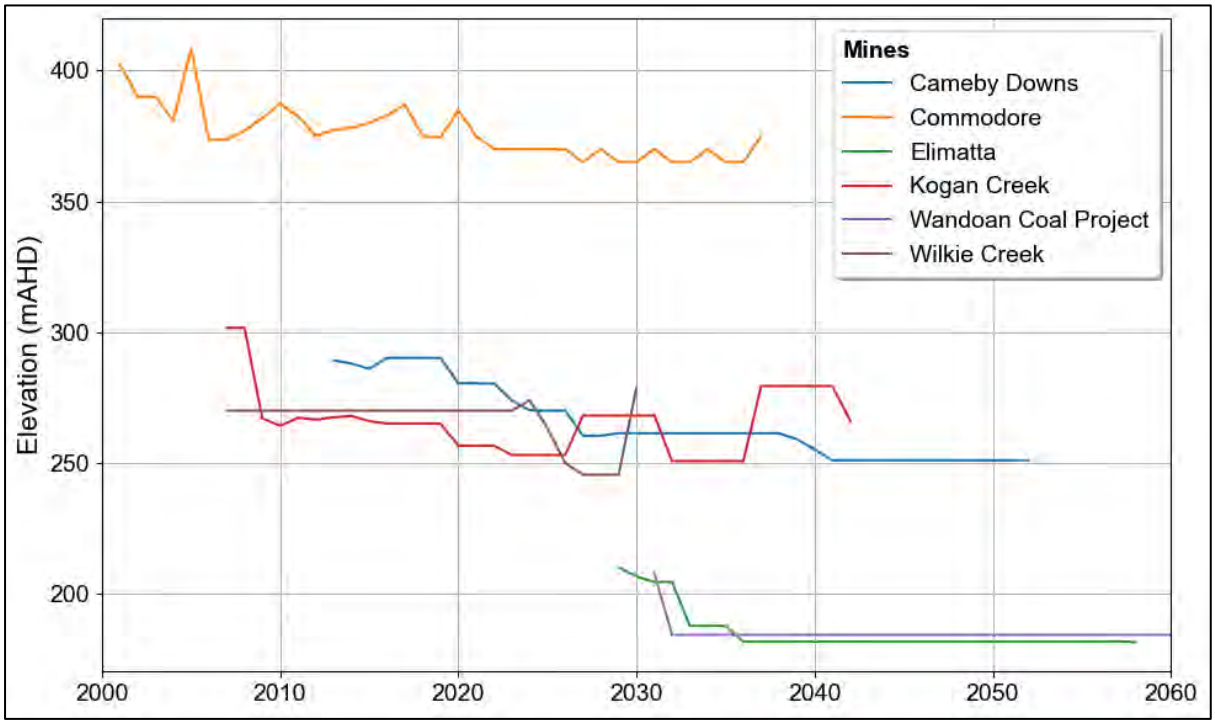

Figure 6-8: Minimum pit shell elevation time series of coal mines included in the Regional Model 2025

6.3.2.4 CSG extraction

6.3.2.4.1 Historic CSG extraction

Information on historic CSG wells during the period January 1995 to December 2023 was obtained from the Queensland Government QDEX database and CSG well information provided to OGIA by individual tenure holders, including well inlet information and monthly actual water extraction volumes for each CSG well. Through comparison of CSG well screen information with stratigraphic picks based on geophysical logs, OGIA has also identified that about 13% of CSG wells (around 1,270 wells) may be partially completed into the lower parts of the Springbok Sandstone.

CSG wells are represented in the groundwater model using the MODFLOW-USG Drain package according to the methodology reported in OGIA (2019b). The model attribution process of drains representing CSG wells is based on well location and inlet information. Where well inlet information is missing, CSG drains are assigned to all layers of the CSG-producing formation – a maximum of six model layers in the Walloon Coal Measures and a maximum of two model layers in each of the Bandanna and Cattle Creek formations. A ‘rule surface’ also constrains this default layer assignment in some places of the model area, to account for areas such as the Condamine Alluvium, where CSG well inlets are not typically placed within 150 m of the ground surface or 30 m of the base of the Condamine Alluvium.

Figure 6-9 provides the locations of historical and future CSG wells that are represented in the model by drain conditions. Drains are assigned to the relevant target formations (Walloon Coal Measures, Bandanna Formation and Cattle Creek Formation) up to the end of the transient calibration period (December 2022). A small number of wells are shown outside of current CSG development areas – these pertain to pilot and exploration wells, such as the Glenburnie site, located southwest of Cecil Plains. Figure 6-9 also shows the location of model grid cells with CSG drains assigned to the lower Springbok Sandstone.

Monthly water extraction volumes recorded for CSG wells define whether CSG drains are active. As development of a well takes place, the assigned elevation to the CSG drain is lowered at a rate that reflects a notional bottom-hole pressure versus time curve, based on data supplied by the tenure holder operating the well. Water production as a result of the descending drain elevation is based on the Peaceman equation (Peaceman 1978). An enhanced local conductance was used in the implementation of the Peaceman equation for water production, to consider the increased connection among coal seams through CSG wells. Full implementation details are reported in Chapter 4 of OGIA (2019b).

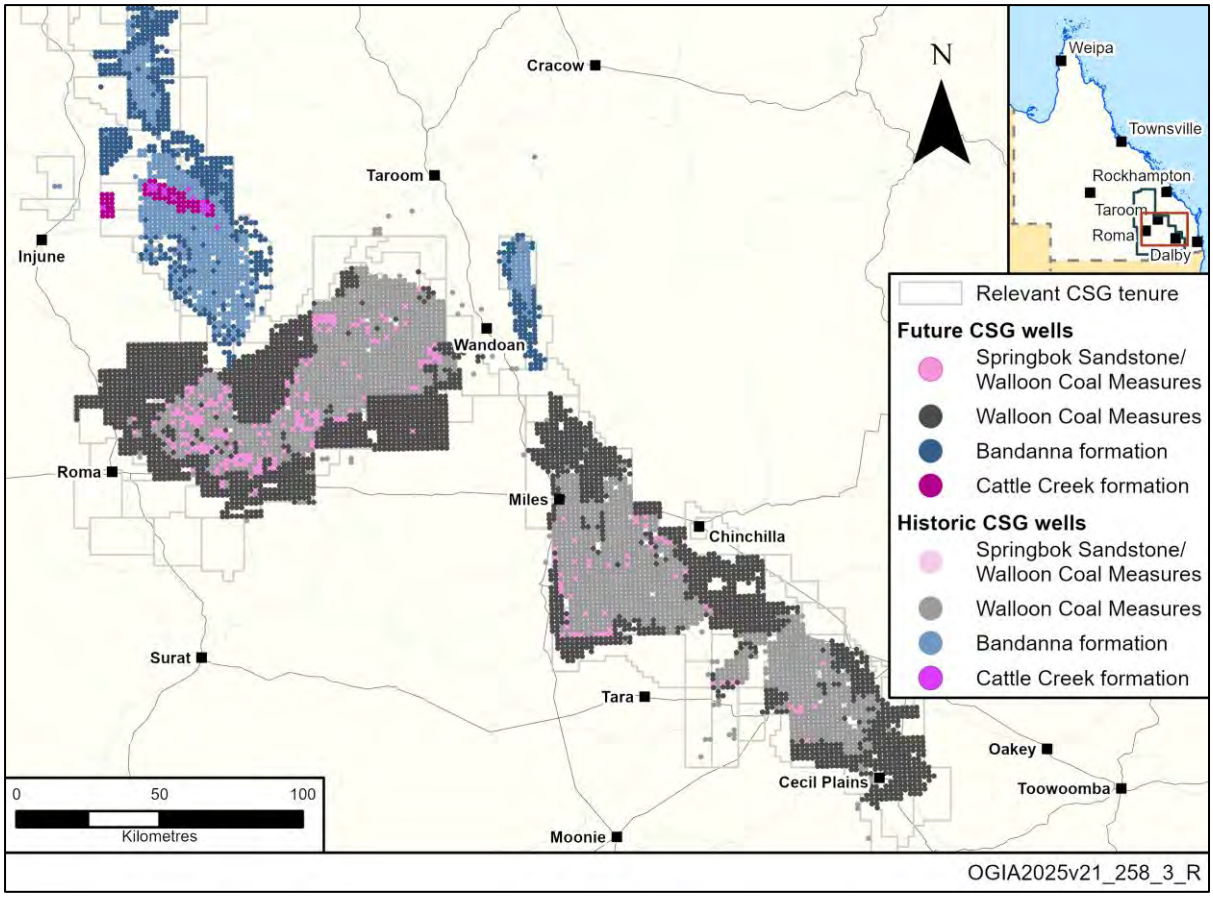

Figure 6-9: Historic and future CSG well locations included in the Regional Model 2025

6.3.2.4.2 Future CSG extraction

Emplacement and activation of future CSG wells in the Regional Model 2025 relies on existing CSG well data and CSG development plans that are provided by tenure holders as part of this UWIR cycle. For the UWIR 2021, tenure holders provided their development plans as shapefiles based on sub-blocks of their respective tenure areas. Tenure holders attributed each sub-block with the target formation, the number of wells planned to produce, and the production start and end dates. Some additional metadata was also provided, such as gas field names and whether the sub-block would contain deviated wells. OGIA used this information as input to a workflow that created theoretical locations within the respective sub-blocks, with spacing of the wells determined by the quantity of planned wells. CSG wells are activated according to the start and end dates for each CSG development area provided by the tenure holders.

The UWIR 2025 introduces a hybrid approach to the development plan submission. Tenure holders provided their development plans in two parts, relating to existing and future wells. For existing wells, each tenure holder provided surface location (coordinates), inlet ‘from’ and ‘to’ locations (coordinates), target formation, top and bottom formation subdivisions, appraisal start and end, production start and end (planned), and other gas field metadata. For future development plans, tenure holders could choose to provide their future development plans as sub-block files (similar to the previous UWIRs) or well files (with information at the well level). Origin and Santos provided their development plans in the sub-block file format. OGIA ran a similar workflow to the UWIR 2021 for these sub-block files. Arrow, QGC and Senex provided their development plans as well files. OGIA uses the information at the well level to place the future wells when such well files are available.

6.3.2.4.3 Deviated wells

The Drain packages for the UWIR 2025 account for the deviation of wells from vertical paths. A deviated well is defined as one where the inlet's starting and ending points have different X and Y coordinates. It is important to note that this definition is applied herein on the UWIR grid (which has a cell size of 1,500 metres) and focuses solely on the inlet segment of CSG wells. These factors may contribute to differences in how deviated CSG wells are classified by various stakeholders.

For modelling purposes, inlet paths are assumed to follow straight lines connecting the starting and ending points of the inlets. All cells intersected by these assumedly straight paths are classified as drain cells, and the descending drain elevations are calculated in the same way as for cells intersected by vertical wells.

6.3.2.5 Dual-porosity and dual-phase flow approximation

As for the UWIR 2021 model, a dual-porosity formulation is used to represent the different properties and responses of coal and interburden (non-coal) material within the CSG reservoir. MODFLOW-USG supports the use of dual-porosity media by defining a mobile domain (coal seams) and immobile domain (interburden) for each dual-porosity layer. The two domains are linked through what is called a "dual-domain flow transfer rate" (DDFTR), which is further specified in the UWIR 2019 modelling report (OGIA 2019b). Mathematically, CSG drains are only connected to the mobile domains of dual porosity cells. The fraction of the mobile domain is based on derived coal proportions from available geophysical logs.

The coal seams desaturate when being depressurised due to CSG extraction, as a result of the desorption of gas from the coal matrix and subsequent dual-phase flow of gas and water to CSG wells. This desaturation process of the coal seams is approximated using a modified van Genuchten equation that has been implemented by OGIA in MODFLOW-USG. This approach has been tested, reviewed and accepted as part of previous UWIR models and is described in detail in OGIA (2019d).

6.3.2.6 CSG-induced subsidence

The Regional Model 2025 simulates CSG-induced subsidence using an integrated approach based on a methodology that differs from that of the UWIR 2021. InSAR data is used to constrain the geomechanical parameters in the coupled hydro-mechanical model. This integrated methodology has been peer-reviewed and published in high-impact journals (Aghighi, Cui, Schöning, Espinoza, et al. 2024; Aghighi, Cui, Schöning & Pandey 2024a; Cui et al. 2025). A brief discussion is provided herein and more information can also be found in the aforementioned publications by OGIA.

6.3.2.6.1 Background

Pore pressure depletion during CSG extraction leads to an increase in effective stresses, causing a reduction in pore volume and cleat aperture in coal, resulting in poromechanical compaction. Additionally, gas desorption from the coal matrix can lead to the contraction of the solid constituent of coal – a process referred to as coal shrinkage. This process is unique to sorptive rocks, such as coal and shale, whereas poromechanical compaction can occur in all rocks, including coal and interburden materials. Figure 6-10 illustrates the two relevant processes contributing to the total compaction (Δb) of coal measures.

Anthropogenic land subsidence related to groundwater extraction and conventional oil or natural gas reservoir developments has been the focus of many studies (Figueroa-Miranda et al. 2018; Geertsma 1973; Motagh et al. 2017; Xu et al. 2008). Conversely, CSG-induced subsidence, accounting for

desorption-induced coal shrinkage, has been studied and modelled in only a limited number of existing studies (Aghighi, Cui, Schöning, Espinoza, et al. 2024; M. S. Masoudian et al. 2019). Wu et al. (2018) included coal shrinkage in a 2D CSG-induced subsidence model with uniform layer-wide properties and showed that the contribution of desorption-induced strain to subsidence is obvious. With a COMSOL model parameterised with typical hydraulic and mechanical properties in Australian CSG development regions, Masoudian et al. (2019) implemented the concept of 'internal and external swelling' that was originally proposed by Liu et al. (2011). The 'external swelling' component of coal shrinkage is defined as the proportion contributing to the bulk compaction of coal seams (defined as 'bulk shrinkage' in this report). The modelling results of Masoudian et al. (2019) suggest that shrinkage is essentially dominating CSG-induced subsidence. These existing studies rely on simple parameterisation and parameter values from expert knowledge; no model calibration was involved. They aim to provide a scientific understanding of the driving mechanisms of CSG-induced subsidence. It is challenging to use such COMSOL models at the regional scale to support real-world decision-making for groundwater management and impact assessment, due to long model running times and software availability to the groundwater community.

On the other hand, a large number of models have been developed, including analytical, semi-analytical and numerical models, to simulate land subsidence in the context of groundwater pumping (Guzy & Malinowska 2020). To support real-world decision-making, numerical models are preferred due to their ability to incorporate spatial heterogeneity and more flexible boundary conditions. For the popular numerical groundwater flow simulator MODFLOW (Harbaugh 2005b; Langevin et al. 2017), a few packages have been developed, such as SUB and CSUB, to simulate the compaction of hydrogeologic units. These commonly used subsidence packages cannot simulate CSG-induced subsidence, however, since they do not consider coal shrinkage. To tackle these challenges, OGIA has developed and implemented an integrated workflow to model CSG-induced subsidence.

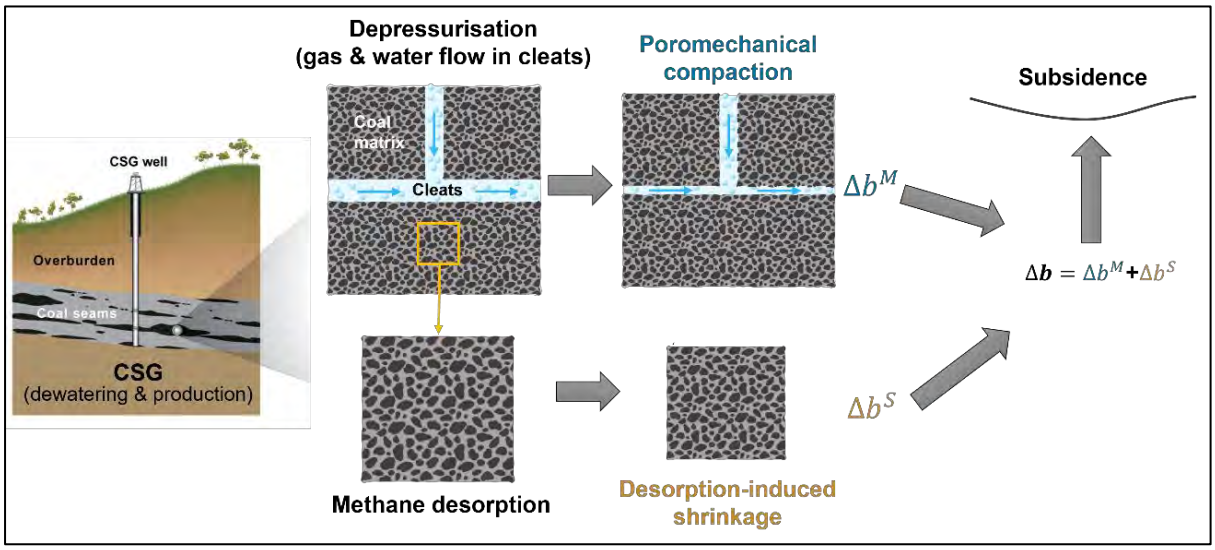

Figure 6-10: Schematic diagram of two relevant processes contributing to the total compaction (Δb) of coal measures, modified from Aghighi et al. (2024)

6.3.2.6.2 Subsidence calculation

OGIA developed a subsidence package for MODFLOW-USG that models both poroelastic compaction and coal shrinkage. The theory that underpins the package is briefly presented below and a more comprehensive and robust discussion can be found in Aghighi et al. (2024).

Poromechanical compaction

Typical CSG reservoirs are characterised by dimensions that are laterally extensive compared to their thickness. As a result, production-induced compaction occurs primarily in the vertical direction. To estimate this compaction, analytical models based on the uniaxial strain condition are commonly employed.

Hooke's law for linear elastic material is expressed as follows:

$$\varepsilon_{xx} = \frac{1}{E}\left[\Delta\sigma'_{xx} - \nu\left(\Delta\sigma'_{zz} + \Delta\sigma'_{yy}\right)\right] \quad \textbf{(6.3)}$$

$$\varepsilon_{yy} = \frac{1}{E}\left[\Delta\sigma'_{yy} - \nu(\Delta\sigma'_{zz} + \Delta\sigma'_{xx})\right] \quad \textbf{(6.4)}$$

$$\varepsilon_{zz} = \frac{1}{E}\left[\Delta\sigma'_{zz} - \nu\left(\Delta\sigma'_{xx} + \Delta\sigma'_{yy}\right)\right] \quad \textbf{(6.5)}$$

where:

E and ν are the drained Young's modulus and Poisson's ratio of the bulk material, respectively,

ε is the strain,

σ is the stress,

$'$ indicates the effective stress,

Δ denotes changes with respect to the reference situation.

Applying the assumption of negligible lateral strains ($\varepsilon_{xx} = \varepsilon_{yy} = 0$) on Hooke's law leads to:

$$\Delta\sigma'_{xx} = \Delta\sigma'_{yy} = \frac{\nu}{1-\nu}\Delta\sigma'_{zz} \quad \textbf{(6.6)}$$

Stresses from overlying rocks and fluids applied to a subsurface hydrogeological unit are shared by the solid skeleton and the pore fluid. The former stress, called effective stress, is responsible for skeletal deformations. If it is assumed the change of total vertical stress can be ignored, the change of vertical effective stress during pumping then becomes:

$$\Delta\sigma'_{zz} = \alpha_b \Delta p_f \quad \textbf{(6.7)}$$

where p_f is the fluid pressure and α_b is the Biot's coefficient. The Biot's coefficient is related to the relative contribution of the skeleton and solid particles to the bulk strain and is defined as:

$$\alpha_b = 1 - \frac{C_s}{C} \quad \textbf{(6.8)}$$

where C_s is the compressibility of solid rock particles and the and C is the drained compressibility of the porous medium. In groundwater-dependent subsidence analysis, α_b is often assumed to be 1; the same assumption is applied here.

Substituting Equations (6.6) and (6.7) into Equation (6.5) gives:

$$\varepsilon_{zz} = \frac{\alpha_b \Delta p_f}{\frac{E(1-\nu)}{(1+\nu)(1-2\nu)}} \quad \textbf{(6.9)}$$

and replacing $\varepsilon_{zz} = \frac{\Delta b}{b}$ gives:

$$\Delta b = \alpha_b c_m b \Delta p_f \tag{6.10}$$

$$c_m = \frac{(1+\nu)(1-2\nu)}{E(1-\nu)} \tag{6.11}$$

where b is the thickness of the porous medium; Δb is the change of the thickness due to poroelastic compaction; and c_m is the compaction coefficient or uniaxial compressibility.

Based on Equation (6.11), the values of c_m can be derived from E and ν if they are available.

Desorption-induced coal shrinkage

In the current study, the ratio of volumetric change caused by matrix shrinkage to the reference volume is defined as the shrinkage strain (denoted by ε^S). The shrinkage strain can be related to the reduction in pore fluid pressure. Gray (1987) suggested a simple linear relationship between the shrinkage strain and pore fluid pressure:

$$\Delta\varepsilon^S = k_{ep}\Delta p_f \tag{6.12}$$

where $k_{ep}$is the coefficient of proportionality.

Levine's study (1996) suggested that a linear relationship overestimates the shrinkage strain. An improved model based on the Langmuir-type relationship was proposed:

$$\varepsilon^S = \varepsilon_L \frac{p_f}{p_{L\varepsilon} + p_f} \tag{6.13}$$

where ε_L is the maximum of the sorption-induced strain (hereafter Langmuir strain) and $p_{L\varepsilon}$ is the Langmuir pressure that is the pressure corresponding to half of ε_L.

The Langmuir-type relationship is commonly employed to characterise sorption strain (Harpalani & Schraufnagel 1990; Palmer & Mansoori 1998a; Robertson & Christiansen 2006; Wu et al. 2010). Langmuir strain parameters are actually curve-fitting values derived from laboratory tests measuring coal shrinkage under various pore fluid pressures. These parameters are typically obtained from adsorption and swelling experiments, with their application to desorption and shrinkage processes relying on the assumption that sorption processes are reversible (physical adsorption).

The Langmuir strain (ε_L) can be related to Langmuir volume (V_L) by a linear relationship (Harpalani & Chen 1992):

$$\varepsilon_L = \beta_h V_L \tag{6.14}$$

where β_h is the ratio coefficient.

In the absence of experimental data for shrinkage strain, Equation (6.14) is often used to estimate the Langmuir strain from V_L (Robertson 2005). Such data was used in the current study to derive the prior range of these parameters. Limited ε_L and V_L data from the literature led to β_h = 1.06 kg/m^3.

The sorption-induced volumetric strain (Shi & Durucan 2004; Palmer & Mansoori 1998a) is given by:

$$\Delta\varepsilon^S = -(\varepsilon^S - \varepsilon_i^S) = -\varepsilon_L\left(\frac{p_f}{p_{L\varepsilon} + p_f} - \frac{p_{fi}}{p_{L\varepsilon} + p_{fi}}\right) \tag{6.15}$$

where $p_{fi}$is the initial reservoir pressure at the reference state.

It is noted that Equation (6.15) is based on the assumption that both the current and initial pressures are less than the critical desorption pressure. Shrinkage strain increases as pressure decreases (noting the sign convention of compressive stress and strain being positive). In other words, since $p_{fi} > p_f$ (as production implies), thus $\varepsilon_i^S > \varepsilon^S$.

The Langmuir strain (ε_L) in Equation (6.15) can be measured under various boundary conditions, resulting in either a volumetric or uniaxial value, depending on the experimental setup (for example, pressure cells for volumetric measurements or triaxial cells for uniaxial measurements). Since uniaxial strain is the standard parameter for subsidence modelling, it is essential to ensure consistency when using the Langmuir strain in such models. Available Langmuir strains are commonly provided as volumetric values and must be converted to their uniaxial equivalents for use in subsidence modelling. The uniaxial Langmuir strain can be calculated from the corresponding volumetric strain as follows:

$$\varepsilon_{UL} = \varepsilon_L \frac{K}{H_{us}} \tag{6.16}$$

where *K* is the bulk modulus of coal and H_{us} is uniaxial compaction modulus, also referred to as oedometer modulus ($H_{us} = (d\sigma_{zz})/(d\varepsilon_{zz})$).

The derivation of Equation (6.16) can be found in Aghighi et al. (2024). The desorption-induced coal shrinkage under uniaxial strain condition can be defined as:

$$\Delta b = b\varepsilon_{UL}\left(\frac{p_f}{p_{L\varepsilon} + p_f} - \frac{p_{fi}}{p_{L\varepsilon} + p_{fi}}\right) \tag{6.17}$$

6.3.2.6.3 Coupled groundwater and subsidence modelling

Based on Equations (6.10) and (6.17), the total compaction under uniaxial strain condition, including poroelastic compaction and bulk shrinkage, can be derived as follows:

$$\Delta b = c_m b\alpha_b \Delta p_f + b\varepsilon_{UL}\left(\frac{p_f}{p_{L\varepsilon} + p_f} - \frac{p_{fi}}{p_{L\varepsilon} + p_{fi}}\right) \tag{6.18}$$

It is noted that Equation (6.18) is negative during CSG depressurisation, which means a reduction in thickness. Pressure changes in Equation (6.18) can be obtained from a groundwater model. Compressibility provides another linkage between the groundwater model and the subsidence model. Specific storage is the volume of water that is released from per unit volume of saturated aquifer. The specific storage is defined as:

$$S_s = \gamma_w(\alpha_b c_m + \Phi c_w) \tag{6.19}$$

where γ_w is specific weight of water ($\gamma_w = \rho g$); ρ is water density; g is the gravitational acceleration; Φ is the effective porosity; and c_w is water compressibility.

The compaction coefficient can then be written as:

$$c_m = \frac{1}{\alpha_b}\left(\frac{S_s}{\gamma_w} - c_w\Phi\right) \tag{6.20}$$

where the impact of coal shrinkage on storage properties of coal seams is neglected.

Combining Equations (6.18) and (6.20) and changing pressure to head ($p = \gamma_w H$) lead to:

$$\Delta b = S_s b \Delta H - \Phi c_w b \Delta H + b \varepsilon_{UL} \left(\frac{H_f}{H_{L\varepsilon} + H_f} - \frac{H_{fi}}{H_{L\varepsilon} + H_{fi}} \right) \quad \textbf{(6.21)}$$

where H_f and $H_{f\mathrm{i}}$ are the current and initial pressure heads; and $H_{L\varepsilon}$ is the Langmuir head corresponding to the Langmuir pressure ($p_{L\varepsilon}$).

The terms on the right-hand side of Equation (6.21) represent the thickness change due to poromechanical compaction, fluid expansion and coal shrinkage, respectively. It is noted that the concept of 'specific storage' is normally defined to measure the storage capacity of the saturated part of an aquifer that is a function of aquifer compressibility and the compressibility of the water itself. During CSG depressurisation, when the pressure in a cell is below the critical desorption pressure, water production is primarily controlled by the drainable porosity (specific yield) of the porous media. Thus, for desaturated cells during the modelling, the specific storage parameter is only used by the subsidence model, although the two models are still linked by reservoir pressure.

Surface subsidence can be approximated as the cumulative settlement of all underlying geological units when formation shielding or bridging effects are ignored (Aghighi, Cui, Schöning & Pandey 2024b). For a groundwater system with m hydrogeological units, this can be expressed mathematically as:

$$\Delta b_t = \sum_{i=1}^{m} \Delta b_i \quad \textbf{(6.22)}$$

where Δb_t is the total subsidence; and Δb_i is the contribution from layer i (for coal measures, Δb_i is the sum of the poroelastic compaction and shrinkage-induced compaction; for non-coal units, Δb_i equals to the poroelastic compaction).

6.3.2.6.4 Bridging

Competent geological layers can impede the impact of subsurface coal extraction or compaction of coal seams from fully or partially reaching the ground surface. This phenomenon, known as 'formation bridging' (or simply bridging), can reduce subsidence induced by both underground coal mining and CSG extraction. Figure 6-11 schematically shows simple bridging scenarios: absence of bridging (a) and presence of bridging (b), where a producing CSG well intersects a coal seam and its overlying sandstone formation (hanging wall). The extent and magnitude of formation bridging depend on several factors, including the area of coal extraction, the depth of the coal seam, the magnitude of compaction, the mechanical properties of the overburden, the presence of discontinuities and the sorption properties of the coal.

OGIA has developed an analytical model, based on the plate theory, to assess the impact of bridging on CSG-induced subsidence (Aghighi, Cui, Schöning & Pandey 2024b). Results of this study show that formation bridging can only occur, if at all, during the early phase of a CSG well's life cycle, when the drainage radius is relatively small. Taking a conservative approach and based on both the hydro-geomechanical study conducted as part of UWIR 2021 (Schlumberger 2021) and the analysis outlined in Aghighi et al. (2024b), OGIA assumes negligible bridging in modelling subsidence for the UWIR 2025.

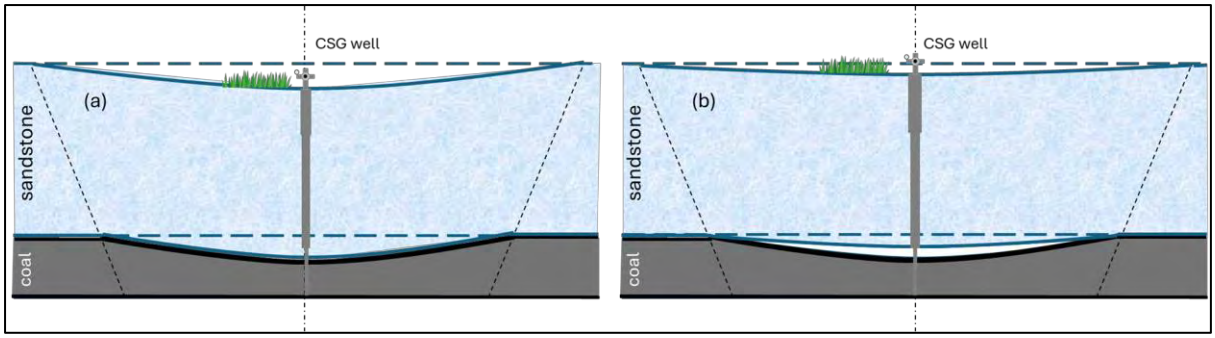

Figure 6-11: Schematic of settlement of a sandstone formation (a) without and (b) with formation bridging

6.4 Stochastic model calibration and uncertainty analysis

6.4.1 Methodology

A clear distinction exists between the highly parameterised inversion used to produce a 'base calibrated model' and uncertainty analyses that sample from the posterior parameter distribution. The former suppresses unnecessary heterogeneity while retaining features consistent with geological principles; the latter seeks to represent all plausible heterogeneity that remains compatible with historical system response. The degree to which parameter uncertainty is reduced depends on the calibration dataset's information content.

For the UWIR model, a combined approach was adopted, using PEST_HP developed by Doherty (2020) and PESTPP-IES developed by White (2018). A minimum error variance solution provides a useful precursor to uncertainty analysis because of the following:

- It anchors the inversion to a solution that aligns closely with expert geological expectations, supporting better model structure exploration.
- A full Jacobian-based calibration typically yields a lower model-to-measurement misfit than rank-deficient methods, particularly for data relevant to impact assessment.
- Posterior sampling with PESTPP-IES can be more efficient when initial fields are conditioned by the minimum error variance solution, requiring fewer iterations to achieve a good fit.

Accordingly, calibration-constrained parameter realisations were generated by:

- using PEST_HP to derive the minimum error variance parameter set, representing the heterogeneity required to match observed behaviour
- randomly sampling from a Gaussian distribution centred on the calibrated field, with standard deviations informed by expert hydrogeological judgement
- applying the Iterative Ensemble Smoother (PESTPP-IES) for Monte Carlo–based uncertainty analysis.

6.4.1.1 Minimum error variance

As noted previously, the first phase of stochastic model calibration and uncertainty analysis was undertaken using the PEST_HP software suite (Doherty 2020). Model calibration represents an 'inverse problem', whereby parameters are adjusted until model outputs achieve an acceptable fit with observed system states. Because the calibration dataset does not uniquely determine parameter values, this inverse problem is mathematically 'ill-posed'. Nevertheless, a single parameter set can be

identified by selecting the one that provides an adequate fit to the calibration dataset while deviating as little as possible from pre-calibration parameter values. Since these prior values partly reflect expert knowledge, the resulting parameter field can be considered to represent ‘minimised error variance’. Among the infinite number of parameter sets that could reproduce the calibration dataset, this field occupies a central position in parameter space, thereby distributing and minimising the risk of error.

Calibration with PEST_HP was implemented through highly parameterised inversion, with uniqueness enforced by Tikhonov regularisation (Tikhonov 1963a, 1963b). This approach constrains parameter adjustments to occur in ways that are geologically plausible, by penalising departures from preferred conditions. In practice, these conditions were expressed through ‘prior information’ equations that required parameters to remain close to their initial values. Parameter covariance matrices further controlled these departures, ensuring that pilot-point based spatial parameters deviated collectively rather than individually.

For the Regional Model 2025, PEST_HP calibration required adjustment of 22,393 parameters against a dataset of 118,830 observations (described in section 6.4.4 and summarised in Appendices B1 and B2). This process also employed 12,577 regularisation equations.

6.4.1.2 Iterative Ensemble Smoother (IES)

The IES method was implemented using PESTPP-IES, part of the PEST++ suite. The algorithm is described in Chen & Oliver (2013, 2017) and White (2018). PESTPP-IES begins with an ensemble of random parameter fields, each representing a sample from the prior (pre-calibration) parameter probability distribution. Through successive iterations, these realisations are updated until they represent samples from the posterior (post-calibration) distribution, which captures residual parameter uncertainty arising from:

- the limited information content of the calibration dataset
- measurement noise (including ‘structural noise’ caused by model imperfections in simulating real-world behaviour).

A key strength of the IES approach is its efficiency: regardless of the number of adjustable parameters, the number of model runs per iteration equals the size of the ensemble. This enables the inclusion of far more parameters than could otherwise be estimated, providing greater flexibility to represent system detail and thereby supporting a more comprehensive characterisation of post-calibration predictive uncertainty. Furthermore, the randomised computation of the Jacobian (the matrix of partial derivatives of model outputs with respect to adjustable parameters) helps avoid entrapment in local objective-function minima, thereby enhancing the reliability of the resulting posterior parameter fields and predictive probability distributions.

6.4.1.3 Prior parameter ensemble

The smaller the number of random parameter fields in an ensemble, the greater the risk of anomalous parameter correlations. For example, in the UWIR Regional Model 2025, recharge applied to a given stress period cannot influence water levels in earlier periods, and water levels observed at distant locations are generally insensitive to local parameter changes. While PESTPP-IES includes a ‘localisation’ option that allows users to pre-specify Jacobian elements (often as zero) when relationships are already known, this was not adopted by OGIA as it would have introduced significant numerical inefficiency, given the dimensionality of the problem. Consequently, some spurious

correlations were not explicitly excluded from the empirical Jacobian matrix. Nonetheless, Chen and Oliver (2013) emphasise that the impact of such correlations diminishes as ensemble size increases and they recommend using an ensemble at least as large as the number of uniquely identifiable pieces of information in the calibration dataset – that is, the effective dimensionality of the solution space. On this basis, PESTPP-IES was implemented with 3,000 parameter-field realisations to provide adequate sampling of parameter space.

Random parameter fields were generated using the PEST utility RANDPAR2_MKL (Doherty 2018). A total of 3,000 realisations were produced using a random number generator, with Gaussian probability distributions assumed for all parameters (or their log10-transformed equivalents). Means were centred on the calibrated 'base' parameter values, and parameter bounds were strictly enforced (Appendix C). For non-pilot-point parameters, no prior correlations were imposed; their uncertainties were defined solely by their standard deviations. These were calculated as one quarter of the adopted calibration parameter range (equivalent to approximately 95% confidence limits), with an upper limit of 0.5 applied in log space. Prior uncertainties for zonal and layer-wide parameters are presented in Appendix G1.

For pilot-point parameters, full covariance matrices were applied based on spatially variable variograms. These variograms reflect both the expected range of property values (for example, hydraulic conductivity across different aquifer materials) and the degree of spatial continuity. An exponential variogram was used, expressed as Equation (6.23):

$$\mathrm{C(h)} = \mathrm{C(0)}\left(1 - \mathrm{e}^{-\frac{\mathrm{h}}{\mathrm{a}}}\right) \quad \textbf{(6.23)}$$

where:

h depicts the separation between any two pilot points,

C(0) expresses parameter covariance at zero pilot-point separation (the variogram 'sill'), this being the innate variance of the parameter,

a is a length parameter or integral scale, which defines a variogram range of approximately 3a (Deutsch & Journel 1992).

The variogram '*a*' value was assigned on a pilot-point-specific basis to account for the upscaling inherent in pilot-point parameterisation. Specifically:

- the mean separation between a pilot-point and its eight nearest neighbours was calculated
- the assigned '*a*' value was set to 25% greater than this mean separation.

This approach ensures that dense pilot-point networks capture short-range heterogeneity, whereas sparser distributions represent only long-range variability. Variogram sills for pilot-point hydraulic properties and subsidence-specific parameters (Langmuir strain and Langmuir pressure) ranged from 0.01 to 0.25 (in log space), corresponding to standard deviations of 0.1 to 0.5 (in log space).

6.4.2 Calibration stages

MODFLOW-USG can handle a combination of steady and transient flow fields across different stress periods. In the historic calibration simulation, three calibration stages are run concurrently, with initial heads automatically transferred from one flow regime to the next.

The first simulation stage represents pre-1947 steady-state conditions prior to any groundwater extraction from the Surat CMA. Its main purpose was to incorporate a set of head measurements unaffected by uncertain pumping regimes into the calibration dataset. While all groundwater head measurements within the Regional Model 2025 domain postdate the onset of water extraction, some early measurements are considered relatively unaffected by pumping.

The second simulation stage involved a pre-1995 steady-state representation of hydraulic conditions prior to the commencement of CSG extraction from the Surat and Bowen basins in 1995. This stage served two purposes:

- to add to the calibration dataset a set of observations assumed to reflect pre-CSG extraction steady-state conditions
- to provide initial heads for the subsequent transient simulation stage.

The third calibration stage is a transient historical simulation covering a 28-year period from 1 January 1995 to 31 December 2022 (336 monthly stress periods). This stage incorporates the progressive expansion of CSG extraction over time, along with (to a lesser extent) the effects of spatiotemporal variations in non-CSG extraction and the dynamics of diffuse rainfall recharge. Together, these factors enable history-matching of groundwater responses under post-CSG conditions.

6.4.3 Parameterisation

The parameterisation strategy adopted for calibration and uncertainty analysis remained largely consistent with that used in the UWIR 2021 model, with adjustments made to accommodate spatial disposition of coal shrinkage parameters – namely, the Langmuir strain and Langmuir pressure parameters, and the unknown (estimable) noise term associated with the initial measurement for each InSAR time-series location (henceforth referred to as ‘InSAR offsets’).

The amount of coal shrinkage is commonly estimated using a Langmuir-type non-linear relationship between coal shrinkage strain and pressure. This empirical relationship involves two curve-fitting parameters: the maximum sorption-induced strain under infinite pore fluid pressure (i.e., Langmuir strain) and the Langmuir pressure for sorption-induced strain which is the pressure corresponding to half of the Langmuir strain (Palmer & Mansoori 1998b; Pan & Connell 2012). These two parameters are obtained from laboratory measurements on coal samples. In the absence of laboratory measurements, these parameters are obtained from their relationship with Langmuir isotherm parameters relating to gas content (Harpalani & Chen 1992). Due to the scarcity of data on these parameters, the latter approach is used to estimate the Langmuir coal shrinkage parameters for the current UWIR. This method requires Langmuir volume and pressure data which are extracted from methane adsorption reports for cored CSG wells. For a more detailed discussion, refer to Section 6.3.2.6.

The Langmuir volume and pressure data were inferred from the analysis of several available methane adsorption reports for cored CSG wells, including some located in the Condamine area, as well as the reported ranges of these parameters in the literature. OGIA is reviewing the current prior ranges of these parameters by incorporating methane adsorption reports from more development areas across the Surat CMA. Furthermore, OGIA is exploring ways to obtain additional data from laboratory methane sorption experiments to directly measure the shrinkage parameters of different coal seams across the CMA. Where necessary, Monte Carlo analyses are being utilised to obtain prior data for the Langmuir coal shrinkage parameters. Separate suites of pilot point parameters for the Langmuir strain and Langmuir pressure respectively were adopted for the three geological sub-units of the

Walloon Coal Measures. Within the Upper and Lower Juandah CM (and the numerical layers therein), these properties were assumed to be vertically homogeneous. The pilot point specifications are provided in Table 6-5 and Table 6-6 below. Note that Langmuir pressure head is used herein in the interest of consistency with pressure representation in groundwater modelling.

Table 6-5: Parameter specifications for Langmuir strain (dimensionless)

Stratigraphic unit	Model layer(s)	Number of pilot points	Initial	Minimum	Maximum
Upper Juandah CM	12, 13	285	7.39E-03	5.60E-05	1.75E-02
Lower Juandah CM	14, 15, 16	312	7.39E-03	5.60E-05	1.75E-02
Taroom CM	17	324	6.86E-03	8.09E-06	1.86E-02

Table 6-6: Parameter specifications for Langmuir pressure head (m)

Stratigraphic unit	Model layer(s)	Number of pilot points	Initial	Minimum	Maximum
Upper Juandah CM	12, 13	285	567.0	151.0	1281.0
Lower Juandah CM	14, 15, 16	312	567.0	151.0	1281.0
Taroom CM	17	324	519.0	91.0	861.0

Pilot point locations for the Langmuir strain and Langmuir pressure parameters are shown in Appendix G9 and G10. There are also 3,186 estimable InSAR offset parameters; the adopted estimable range was -30 mm (i.e. subsidence) to +30 mm (i.e. uplift) with an initial value of 0 mm. The parameter bounds for hydraulic conductivity and storage are provided in Appendix C1 and Appendix C2, respectively. Further details on model parameterisation of other parameters can be found in the OGIA (2021b).

6.4.4 Observations

For UWIR 2025, the pre-1947 and pre-1995 steady-state observations used in UWIR 2021 were retained. For convenience, these are summarised in Section 6.4.4.1 and 6.4.4.2.

6.4.4.1 1947 steady-state targets

Table **6-7** below summarises the stratigraphic distribution of the 1947 steady-state calibration dataset. As highlighted in previous UWIRs, observed head data from deeper parts of the basin at this early stage of development are very limited. This calibration step comprises 651 observations, with locations shown in Appendix D1. Contour maps of simulated water levels from the 1947 steady-state simulation are provided in Appendix E1. Scatter plots of measured versus modelled heads for the 1947 targets are presented in Appendix E2, and residual distributions (measured minus modelled water levels) are shown in Appendix E3.

Table 6-7: Steady-state pre-1947 water level calibration targets by formation

Formation	Layers	Targets
Cenozoic Formations	1	147
Upper Cretaceous Formations	2	27
Wallumbilla Formation	3	38
Bungil Formation	4	58
Mooga Sandstone	5	73
Orallo Formation	6	66
Gubberamunda Sandstone	7	80
Westbourne Formation	8	0
Springbok Sandstone Upper	9	8
Springbok Sandstone Lower	10	6
Walloon Non-Productive-Zone	11	1
Upper Juandah Coal Measures	12, 13	7
Lower Juandah Coal Measures	14, 15, 16	21
Taroom Coal Measures	17	12
Durabilla Formation	18	0
Hutton Sandstone Upper	19	67
Hutton Sandstone Lower	20	10
Upper Evergreen Formation	21	0
Boxvale Sandstone	22	4
Lower Evergreen Formation	23	0
Precipice Sandstone	24	14
Moolayember Formation	25	0
Clematis Group	26	2
Rewan Group	27	0
Bandanna Formation Non-Productive-Zone	28	0
Bandanna Formation Upper	29	0
Bandanna Formation Lower	30	0
Upper Permian	31	9
Cattle Creek Non-Productive-Zone	32	0
Cattle Creek Formation Upper	33	0

Formation	Layers	Targets
Cattle Creek Formation Lower	34	0
Lower Permian	35	1
Total		651

Groundwater flow is conceptualised as occurring parallel to the general-head boundary (GHB) along the western edge of the model domain, with GHB cell locations shown in Appendix F. Boundary heads are adjusted during calibration and are parameterised using pilot points spaced at 9 km intervals, where a zero lateral head difference is imposed in the east-west direction. These zero-gradient observations, introduced in the same layers as the GHB boundary conditions, total 341. The locations of the paired GHB observations are provided in Appendix D2.

6.4.4.2 1995 steady-state targets

6.4.4.2.1 Heads – Condamine Alluvium and Main Range Volcanics

Steady-state 1995 water levels were sourced from two datasets: for the Condamine Alluvium, from the 'KCB Condamine Model' (KCB 2011), and for the Main Range Volcanics, via spatial interpolation of observed groundwater levels. These values were applied directly as drain elevations to all relevant MODFLOW-USG cells in the model domain.

To ensure simulated heads within these cells rose to the assigned drainage surface, the same water levels were also included as calibration observations. Because drains prevent heads from exceeding their elevation, this constraint effectively limited simulated levels to at the observed drainage surface as much as possible. In total, 278 head observations were generated for the Condamine Alluvium footprint of the Regional Model 2025 and 386 for the Main Range Volcanics. Their locations are shown in Appendix D3.

Scatter plots of modelled versus observed heads (Appendix E4) illustrate the imposed restriction, with simulated values prevented from exceeding the measured water levels (i.e. drain elevations).

6.4.4.2.2 Heads – other stratigraphic units

Processing of groundwater head data yielded 5,888 measurements for calibration of the 1995 steady-state simulation. Their distribution across model layers and stratigraphic units is summarised in Table 6-8.

A ΔH value was computed for every head observation to identify locations where the steady-state assumption is most likely violated. Refer to Section 5.4.3 of OGIA (2019b) for details. Observations with $\Delta H >$ 5 m were flagged as significant and assigned to a "penalty" group.

For all observations the residual is defined as $r = h_o - h_m$ (observed minus simulated). For members of the penalty group, we use an asymmetric residual that tolerates under-prediction up to ΔH but penalises over-prediction:

- If $h_m \in [h_o - \Delta H, h_o]$, set $r = 0$
- If $h_m < h_o - \Delta H$, set $r = (h_o - \Delta H) - h_m$
- If $h_m > h_o$, use the conventional residual $r = h_o - h_m$

This reflects the expectation that, under gradually increasing groundwater extraction, steady-state heads computed by the model should be at or below the transient heads that are observed; modest under-predictions are therefore forgiven, while over-predictions are penalised.

So, for example, if h_o = 300 mAHD and ΔH = 10 m, any h_m between 290 and 300 mAHD yields zero misfit. If h_m =288 mAHD, r = (300 - 10) - 288 = 2m. If h_m = 302 mAHD, r = 300 - 302 = -2m.

Locations of traditional and penalty observations are provided in Appendices D4 and D5, respectively. Maps of simulated groundwater contours for the 1995 steady-state period are shown in Appendix E5. Scatter plots of observed versus modelled heads and residual maps are presented in Appendices E6–E7 (traditional group) and E8–E9 (penalty group).

Table 6-8: Steady-state 1995 water level calibration targets by formation

Formation	Layers	Targets
Cenozoic Formations	1	1,483
Upper Cretaceous Formations	2	116
Wallumbilla Formation	3	94
Bungil Formation	4	180
Mooga Sandstone	5	398
Orallo Formation	6	340
Gubberamunda Sandstone	7	448
Westbourne Formation	8	0
Springbok Sandstone Upper	9	102
Springbok Sandstone Lower	10	47
Walloon Non-Productive-Zone	11	9
Upper Juandah Coal Measures	12, 13	121
Lower Juandah Coal Measures	14, 15, 16	312
Taroom Coal Measures	17	187
Durabilla Formation	18	0
Hutton Sandstone Upper	19	1,045
Hutton Sandstone Lower	20	249
Upper Evergreen Formation	21	0
Boxvale Sandstone	22	36
Lower Evergreen Formation	23	0
Precipice Sandstone	24	227
Moolayember Formation	25	0

Formation	Layers	Targets
Clematis Group	26	122
Rewan Group	27	0
Bandanna Formation Non-Productive-Zone	28	1
Bandanna Formation Upper	29	42
Bandanna Formation Lower	30	10
Upper Permian	31	186
Cattle Creek Non-Productive-Zone	32	0
Cattle Creek Formation Upper	33	5
Cattle Creek Formation Lower	34	0
Lower Permian	35	128
Basement	36	0
Total		5,888

6.4.4.2.3 Other Targets

The following calibration targets were also included in the current model as per UWIR 2019 (OGIA 2019b):

- A total of 260 vertical head difference observations, the locations of which are shown in Appendix D6 (and Appendix E10 for residuals map). These comprised the following:
    - 96 differences between head in the Condamine Alluvium (layer 1) and that in an underlying Surat Basin layer (layers 12 to 17)
    - 164 differences between head in the Main Range Volcanics (layer 1) and a head in an underlying Surat Basin layer (layers 12 to 20).
- Simulated inflow to the Condamine Alluvium from adjacent and underlying strata could be up to 10,000 ML/yr before a penalty was applied, acknowledging uncertainty in the conceptual estimate1995-2022 transient targets

6.4.4.2.4 Consumptive groundwater extraction

Groundwater extraction for non-CSG purposes is simulated using the MODFLOW-USG well (WEL) package. Each water supply well is assigned either its metered extraction rate or an estimated value as discussed in Section 6.3.2.2. For conventional petroleum and gas wells, rates are based on metered data. All simulated wells are subject to automatic reductions (“derating”) if simulated heads fall below a user-defined elevation, taken as either the top of the well screen or the top of the model cell containing the well if screen information is absent.

To avoid unrealistic derating (e.g., from underestimation of local hydraulic conductivity), the transient calibration dataset includes estimated time series of groundwater extraction from each of the major aquifers represented in the model. For these aquifers, the target is achieved if total simulated extraction exceeds 50% of estimated actual extraction for the Walloon Coal Measures, and 80% for

all other formations. Thresholds below 100% are applied given the greater uncertainty in groundwater extraction estimates compared with surface water, particularly where flow metering is limited to a small number of wells and does not extend far back in time.

Table 6-9 presents target extractions at the end of the transient historic simulation (December 2022), while Figure 6-12 shows the total extraction rate across all formations for the same period.

Table 6-9: Estimated and targeted groundwater extraction rates for Dec-2022

Stratigraphic unit (model layer/s)	Extraction (ML/yr)	
	Estimated actual	Targeted
Gubberamunda Sandstone (layer 7)	8,225	6,580
Springbok Sandstone (layers 9 and 10)	688	550
Walloon Coal Measures (layers 11 to 17)	4,358	2,179
Hutton Sandstone (layers 19 and 20)	17,850	14,280
Boxvale Sandstone (layer 22)	208	166
Clematis Sandstone (layer 26)	1,115	892

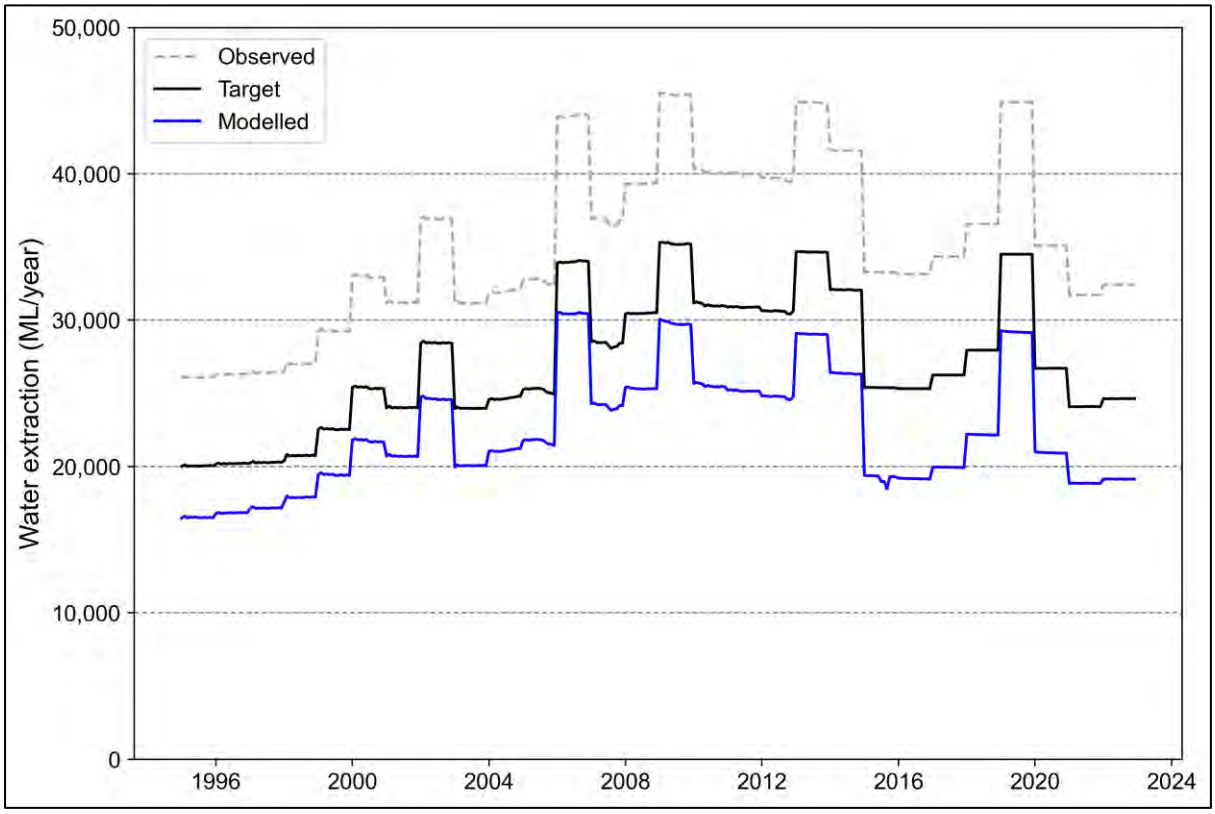

Figure 6-12: Total transient historic non-CSG extraction (1995 to 2022)

6.4.4.2.5 Measured CSG water extraction rates

Monthly groundwater extraction records are available for all active CSG wells within the Surat CMA. These data were used to history-match the Regional Model 2025 against time-series of total CSG groundwater extraction from the following formations:

- Walloon Coal Measures
- Bandanna Coal Measures
- Cattle Creek Formation

In addition, history matching was carried out against total CSG extraction volumes for 30 CSG development areas (8 of which ceased operations prior to the end of the calibration period). These areas, along with their observed production volumes for December 2022, are summarised in Table 6-10 as an example. Time-series plots comparing modelled and observed CSG extraction rates by formation and by development area are presented in Appendix E11.

Table 6-10: CSG development areas and CSG groundwater extraction rates for Dec-2022

	Extraction (ML/yr)	
Development area	**Measured**	**Modelled**
Alfredson	317	115
Arcadia	172	197
Atlas	510	598
CDA	5,413	6,058
Combabula	3,591	4,321
Condabri	2,418	2,357
Fairview Bandanna	5,486	5,029
Fairview Cattle Creek	80	116
KNJV	437	348
Murrungama	82	44
NDA	4,366	5,828
Peat Bandanna	3	1
Ramyard	0	4
Riley	37	22
Roma	3,366	4,320
Scotia	103	874
SDA	2,598	3,099
South	3,721	3,621
Spring Gully Bandanna	3,646	872

Development area	Extraction (ML/yr)	
	Measured	Modelled
Talinga Orana	10,693	8,205
Western Surat Gas Project	722	626
Outside	102	500

6.4.4.2.6 Transient groundwater level observations and observed temporal trends

Groundwater level observations in key units form a substantial part of the 2025 transient calibration dataset. The selection of groundwater level observations relies on a scripted workflow and expert knowledge. After a thorough process to verify aquifer attribution and the representativeness of water level measurements, the following criteria were applied:

- time series with records between 1995 and 2022
- a minimum of 4 head measurement records
- at least one year of data
- attributed to one of the following formations: Springbok Sandstone (layers 9 and 10), Walloon Coal Measures (layers 12-17), Hutton Sandstone (layers 19 and 20), Boxvale Sandstone (layer 22), Precipice Sandstone (layer 24) and Bandanna Coal Measures (layers 29 and 30).

After the above filtering, expert knowledge was further applied to select monitoring locations and records for inclusion in the transient calibration dataset. The following principles were followed during this process.

- Groundwater bores are mainly screened to a single aquifer
- Only one calibration point was selected per model cell except when the multiple points do not temporarily overlap
- Groundwater levels are representative of the regional groundwater conditions
- There is no obvious conflict with nearby bores that cannot be explained

Table 6-11 summarizes the number of monitoring locations for each of the aforementioned formations that have been used for the history matching of the transient groundwater model, which amounted to a total of 13,936 processed measurements for 585 monitoring locations. This is an increase by 98 monitoring locations compared to the dataset used for the calibration of the UWIR 2021 model. Also note that the Regional Model 2025 is calibrated against groundwater level data up to December 2022, whereas the UWIR 2021 model has been calibrated against data until December 2019.

Similar to the UWIR 2021 model, groundwater level observation groups for the Walloon Coal Measures and Precipice Sandstone have been further subdivided. For the Upper Juandah Coal Measures, Lower Juandah Coal Measures and Taroom Coal Measures, monitoring points were assigned to separate observation groups depending on their proximity to CSG activities. This subdivision has been made to improve the calibration against more subtle temporal head trends further away from CSG areas compared to the large observed drawdown within active CSG extraction areas. For the Precipice Sandstone a similar subdivision has been made to distinguish between

monitoring points that are showing increasing groundwater levels due to their proximity to aquifer reinjection sites.

Consistent with the calibration approach adopted for the UWIR 2021 model, temporal head differences have been calculated for each observation point using the first head observation at each monitoring point as reference head. This generated a further 13,351 temporal head change observations relating to the 585 monitoring locations with transient head data used for model calibration. These are introduced to emphasize the importance of replicating temporal trends, such as observed drawdown in the Walloon Coal Measures, Springbok Sandstone and Hutton Sandstone. See Appendix D7 for locations.

Groundwater level contours representing conditions at the end of the transient calibration period (December 2022) are provided as Appendix E12 for every model layer. Scatter plots of observed versus modelled groundwater levels are provided as Appendix E13.

Table 6-11: Groundwater level monitoring sites by formation used for transient model calibration

Formation	Layers	Regional Model 2021	Regional Model 2025
Upper Springbok Sandstone	9	29	35
Lower Springbok Sandstone	10	27	33
Upper Juandah Coal Measures	12, 13	79	102
Lower Juandah Coal Measures	14, 15, 16	84	101
Taroom Coal Measures	17	77	102
Upper Hutton Sandstone	19	91	94
Lower Hutton Sandstone	20	14	22
Boxvale Sandstone	22	1	1
Precipice Sandstone	24	68	72
Upper Bandanna Formation	29	6	9
Lower Bandanna Formation	30	8	14
Total		487	585

6.4.4.2.7 Transient vertical head difference observations

Based on the observed head data, a dataset of interlayer vertical head differences has also been generated and added to the transient calibration dataset. As discussed in Doherty and Hunt (2010), this can be an important type of information to estimate vertical hydraulic conductivities and the connectivity between different hydrogeological units. Observed vertical head differences to constrain the vertical hydraulic conductivity of these layers are based on pairs of monitoring points that are situated above and below the aforementioned aquitard layers and within 1 km of each other. In most cases, the selected observation points are within 100 m of each other. Table 6-12 below shows the

vertical head pairs and targeted parameters for the Regional Model 2025. See Appendix D8 for locations of vertical head difference calibration targets used in the transient calibration.

An example of observed vertical head differences is provided for nested monitoring site 160759A_160951A in Figure 6-13. It shows observed and modelled vertical head difference based on head monitoring information for the Taroom Coal Measures and Hutton Sandstone. The data for this site shows a vertical head difference of more than 200 metres, which is important information to constrain the vertical hydraulic conductivities between these two formations in the Regional Model 2025.

Table 6-12: Transient vertical head difference targets by formation

Stratigraphic unit pair	Targeted parameter	Model layer		Number of observation locations
		Upper	Lower	
Condamine Alluvium-GAB	Kv Condamine transition zone (layer 2)	1	9, 10, 12, 13, 14, 15, 16, 17	25
Gubberamunda Sandstone – Upper Springbok Sandstone	Kv Westbourne Formation (layer 8)	7	9	19
Lower Springbok Sandstone – Upper Walloon Coal Measures	Kv Walloon non-productive zone (layer 11)	10	12, 13	27
Internal Walloon Coal Measures	Kv Walloon Coal Measures (layers 12 to 17)	12,13	14, 15, 16, 17	67
Lower Walloon Coal Measures – Upper Hutton Sandstone	Kv Durabilla Formation (layer 18)	17	19	29
Durabilla – Upper Hutton Sandstone	Kv Durabilla Formation & Upper Hutton Sandstone	18	19	6
Upper – Lower Hutton Sandstone	Kv Hutton Sandstone (layers 19 and 20)	19	20	4
Boxvale Sandstone – Precipice Sandstone	Kv Lower Evergreen Formation (layer 23)	22	24	1
Precipice Sandstone – Bandanna Formation	Kv Precipice & Bandanna Formation	24	29	1
Total				179

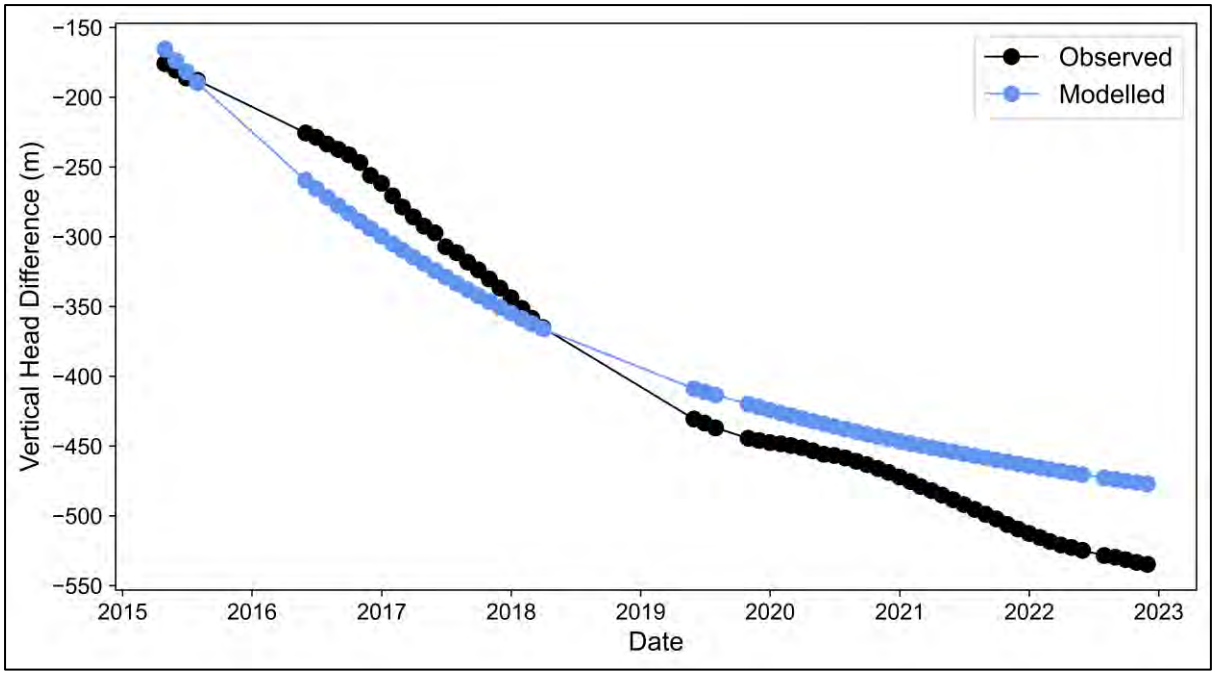

Figure 6-13: Transient vertical head difference between Taroom Coal Measures and Upper Hutton Sandstone (160759A_160951A)

6.4.4.2.8 InSAR

InSAR data from 2015 to 2022 of two descending Sentinel-1 tracks were used to constrain geomechanical parameters. Given the very large number of potential InSAR time series, a systematic method of data reduction was necessary to identify a manageable set of calibration targets. The dataset was screened and subdivided using a combination of time-series analysis and filtering criteria. Only InSAR points with temporal coherences of higher than 0.6 and distances to nearby CSG wells of less than 10 km were included in the calibration dataset.

To support data reduction, fortnightly InSAR observations were decomposed using Seasonal-Trend decomposition (STL) to separate long-term trends from seasonal variability. A linear regression was then applied to the extracted trend component to estimate the slope (in mm/day), providing a direct measure of long-term subsidence or uplift. Sites were then classified as auxiliary (i.e. detailed time series omitted) if either their motion was minor. “Minor motion” was defined as meeting at least one of: trend slope ≥ −0.0035 mm/day (equivalent to approximately 10mm fall over eight years); the most negative displacement was greater than −10 mm (i.e. didn’t reach 10 mm of subsidence); or the average displacement since June 2017 was positive (uplift). These minor-motion sites were summarised by their mean value only.

In high-density areas, spatial down-sampling was applied to preserve coverage while reducing site count. The study area was partitioned into a 2.5 km × 2.5 km grid; within each cell, the site nearest to the within-cell centroid was retained as the representative location, ensuring spatial representativeness. For the retained sites, their quarterly time series were used for model calibration. Sites removed by this step were also classified as auxiliary; for these, time series were summarised by the mean and by a trend slope estimated via ordinary least squares, assuming evenly spaced monthly observations.

Overall, this process produced 2,265 non-zero-weighted InSAR mean statistics and 809 trend-slope statistics at auxiliary sites. The remaining time series data (resampled to quarterly frequency) were

employed at 921 InSAR locations spanning June 2017 to December 2022, yielding a concise yet spatially and temporally comprehensive calibration dataset.

A comprehensive set of plots comparing modelled and observed InSAR time series for all sites is presented in Appendix E19. Visual inspection of the time series indicated that the model successfully captured the dominant subsidence signal associated with reservoir pressure decline. These comparisons provide a detailed visual assessment of the calibration quality and the spatial variability of model performance across the regional model area.

Modelled and observed summary statistics for the auxiliary group are presented in Appendix E20 to evaluate the model's regional performance. This assessment was based on statistical pairing of observed and simulated mean displacement and trend slope values. The resulting 1:1 scatter plots demonstrate a strong linear relationship and low bias, indicating that the model reproduces both the magnitude and direction of long-term ground movement trends with acceptable accuracy. These auxiliary comparisons provide additional confidence in the model's capacity to simulate regional-scale subsidence behaviour.

6.4.4.2.9 Other targets

The following additional targets were applied in the Regional Model 2025:

- Vertical head differences and water saturation within coal-bearing layers in areas of active CSG extraction (see Appendices E14 and E15).
- Measured reinjection rates for Precipice Sandstone reinjection areas, along with head targets to ensure simulated heads do not exceed surface elevation, which would otherwise result in zero reinjection rates and reduce model sensitivity to observed data (see Appendices E13).
- Heads, vertical head differences, and water saturation derived from existing dual-phase CSG reservoir models developed by CSG companies (see Appendices E16-E18).

6.4.5 Calibration performance

While the previous sections have presented the model calibration results with multiple scatterplots, time series and residual maps for different groups of calibration targets, this section is to provide a high-level summary to the calibration performance of the regional model. Model-to-measurement misfit was evaluated using inferential statistics, including the scaled root mean square (SRMS), scaled mean sum of residuals (SMSR), and Pearson's correlation coefficient (R), as described by Middlemis et al. (2001) in the groundwater modelling context.

Table 6-13 provides a statistical summary of the performance of the PEST_HP-calibrated transient groundwater levels across the key stratigraphic units used for impact assessment. SRMS and SMSR values are generally between 5% and 10% in the major formations and correlation coefficients are close to unity except for the Springbok Sandstone. With overall SRMS and SMSR values of 4.8% and 2.5%, respectively, the calibration was considered appropriate for conditioning the prior parameter distribution.

Table 6-13: Calibration performance statistics for transient groundwater levels in key hydrogeological units

Stratigraphic unit / model layer	SRMS (%)	SMSR (%)	Pearson's R
Springbok Sandstone (layers 9 and 10)	11.8	7.7	0.73
Walloon Coal Measures (layers 12 to 17)	6.4	3.6	0.91
Upper Juandah Coal Measures (layers 12 to 13)	*8.2*	*5.4*	*0.84*
Lower Juandah Coal Measures (layers 14 to 16)	*7.1*	*4.5*	*0.91*
Taroom Coal Measures (layer 17)	*7.6*	*3.6*	*0.92*
Hutton Sandstone (layers 19 and 20)	3.4	2.2	0.98
Precipice Sandstone (layer 24)	5.9	3.4	0.96
Bandanna (layers 29 and 30)	9.1	7.1	0.95
All units	**4.8**	**2.5**	**0.93**

As discussed in the previous section, the subsidence relevant parameters were calibrated using InSAR time series, referenced to a baseline date of acquisition. The calibration focused on reproducing the spatial and temporal patterns of measured ground motion across the regional model domain, with emphasis on areas that experience CSG depressurisation. Overall, the model provided a good representation of the observed subsidence magnitudes and trends. For the majority of InSAR monitoring points, the temporal evolution of simulated ground movement closely followed that of the observations, both in direction and in rate of change. A scatter plot for the entire transient InSAR calibration targets is presented in Appendix E21. SRMS and SMSR values for transient InSAR calibration targets are 3.8% and 0.2%, respectively.

For PESTPP-IES, most realisations achieved an acceptable fit by the third iteration, as reflected in a marked reduction in both the mean and standard deviation of the objective function. Subsequent iterations were indicative of an ensemble "collapse," where parameter sets converge and the range of uncertainty may be underestimated. Accordingly, the parameter ensemble from the third iteration was selected as the posterior parameter probability distribution.

6.4.6 Calibrated parameters

Samples from the posterior parameter probability distribution were obtained by ranking all the 3000 calibrated model realisations according to their total objective function values. From this ranking, the lowest 1000 realisations were retained, and 500 of these were then randomly selected for predictive uncertainty analysis. This approach slightly reduces the spread of the posterior parameter estimates but ensures that the selected fields emphasise cases where the model-to-measurement misfit is minimised. Importantly, the overall range of total objective function values within this subset remains comparable to that of the full ensemble, indicating that the representativeness of the parameter space is largely preserved.

The resulting parameter fields provide a robust basis for exploring the statistical characteristics of any model parameter. As an illustration, Appendix G1 presents histograms of posterior probability

distributions for both zonal parameters and layer-wide parameter types, highlighting how the uncertainty structure differs across parameter groupings.

The spatial variability of a pilot point parameter's statistical properties can be illustrated by mapping each statistic to the location of its corresponding model parameter. Appendices G2 through G10 present the spatial distribution of the calibrated "base" values of the pilot point parameter. Appendices G11 through G19 then show the spatial distribution of the standard deviation of the base-10 logarithm of the parameter, representing the posterior uncertainty diagnostic. Note that Langmuir strain (EL) and Langmuir pressure (PL) properties (Appendix G9 to G10; Appendix G18 to G19) are only applicable within areas affected by CSG depressurisation for the subsidence calculations. Accordingly, for presentation purposes, these parameter fields have been clipped to the pilot-point footprint using a 5 km interior buffer.

6.4.7 Steady-state water balance

The water balance for the 1947 and 1995 steady-state simulations is provided in Table 6-14 and

Table 6-15 respectively. These correspond to the "base" calibrated parameter set only for ease of interpretation. Also note that net flux into the layer is positive.

Consistent with earlier versions of the regional model, both the pre-development (1947) and pre-CSG development (1995) water balances indicate only minor outflows along the southern model boundary to the remainder of the GAB - 4,674 ML/yr and 2,389 ML/yr, respectively. These outflows represent less than 1% of applied recharge, with the remainder contributed locally to shallow groundwater systems, where it is lost through evaporation or contributes to surface water baseflow. Under steady-state conditions, the non-CSG extraction demand of approximately 29,000 ML/yr is met primarily by reducing discharge to these shallow systems.

Table 6-14: Water balance in each model layer for the 1947 steady-state simulation ("base" calibrated parameter set)

Stratigraphic unit(s)	Model layer	Recharge (ML/yr)	Non-CSG extraction (ML/yr)	Surficial drainage (ML/yr)	Net GHB flux (ML/yr)	Net interlayer flux (ML/yr)
Alluvia, Basalt and Cenozoic Sediments	1	372,945	0	-392,623	0	19,678
Upper Cretaceous	2	3,540	0	-2,410	0	-1,130
Wallumbilla Formation	3	12,081	0	-7,226	0	-4,854
Bungil Formation	4	11,590	0	-6,541	404	-5,453
Mooga Sandstone	5	25,871	0	-10,017	-2,010	-13,844
Orallo Formation	6	9,425	0	-10,024	0	599
Gubberamunda Sandstone	7	13,562	0	-8,409	-1,195	-3,958
Westbourne Formation	8	16,161	0	-16,064	0	-97
Upper Springbok Sandstone	9	28,185	0	-27,918	-12	-255
Lower Springbok Sandstone	10	3,044	0	-3,063	-25	44
Walloon Coal Measures non-productive zone	11	0	0	0	0	0
Upper Juandah-1 Coal Measures	12	2,284	0	-2,346	-1	63
Upper Juandah-2 Coal Measures	13	371	0	-374	-8	11
Lower Juandah-1 Coal Measures	14	1,518	0	-1,455	-7	-57
Lower Juandah-2 Coal Measures	15	881	0	-867	-6	-8
Lower Juandah-3 Coal Measures	16	832	0	-819	-8	-5

Stratigraphic unit(s)	Model layer	Recharge (ML/yr)	Non-CSG extraction (ML/yr)	Surficial drainage (ML/yr)	Net GHB flux (ML/yr)	Net interlayer flux (ML/yr)
Taroom Coal Measures	17	1,098	0	-1,021	-9	-67
Durabilla Formation	18	2,177	0	-1,580	0	-597
Upper Hutton Sandstone	19	31,095	0	-32,802	-142	1,848
Lower Hutton Sandstone	20	850	0	-847	-165	163
Upper Evergreen	21	19,311	0	-19,154	0	-157
Boxvale Sandstone	22	386	0	-368	-2	-16
Lower Evergreen	23	16,083	0	-14,910	0	-1,174
Precipice Sandstone	24	25,283	0	-33,635	-1,487	9,839
Moolayember Formation	25	6,204	0	-7,470	0	1,266
Clematis Sandstone	26	50,619	0	-48,288	0	-2,330
Rewan Group	27	4,987	0	-5,346	0	359
Bandanna Formation non-productive zone	28	0	0	0	0	0
Upper Bandanna Formation	29	3,844	0	-3,851	0	7
Lower Bandanna Formation	30	0	0	0	0	0
Undifferentiated Bowen Basin strata	31	3,566	0	-3,586	0	19
Cattle Creek Formation non-productive zone	32	0	0	0	0	0
Upper Cattle Creek Formation	33	0	0	0	0	0

Stratigraphic unit(s)	Model layer	Recharge (ML/yr)	Non-CSG extraction (ML/yr)	Surficial drainage (ML/yr)	Net GHB flux (ML/yr)	Net interlayer flux (ML/yr)
Lower Cattle Creek Formation	34	0	0	0	0	0
Undifferentiated Bowen Basin strata	35	1,170	0	-1,275	0	104
Totals		**668,962**	**0**	**-664,288**	**-4,674**	**0**

Table 6-15: Water balance in each model layer for the 1995 steady-state simulation ("base" calibrated parameter set)

Stratigraphic unit(s)	Model layer	Recharge (ML/yr)	Non-CSG extraction (ML/yr)	Surficial drainage (ML/yr)	Net GHB flux (ML/yr)	Net interlayer flux (ML/yr)
Alluvia, Basalt and Cenozoic Sediments	1	373,126	0	-383,585	0	10,459
Upper Cretaceous	2	3,540	-963	-1,866	0	-711
Wallumbilla Formation	3	12,081	-392	-5,866	0	-5,823
Bungil Formation	4	11,590	-747	-5,552	859	-6,151
Mooga Sandstone	5	25,871	-2,711	-8,784	-751	-13,624
Orallo Formation	6	9,425	-3,174	-8,876	0	2,626
Gubberamunda Sandstone	7	13,562	-6,252	-7,809	-862	1,361
Westbourne Formation	8	16,161	0	-16,011	0	-150
Upper Springbok Sandstone	9	28,185	-265	-27,716	1	-206
Lower Springbok Sandstone	10	3,044	-112	-3,052	-19	138
Walloon Coal Measures non-productive zone	11	0	-40	0	0	40

Stratigraphic unit(s)	Model layer	Recharge (ML/yr)	Non-CSG extraction (ML/yr)	Surficial drainage (ML/yr)	Net GHB flux (ML/yr)	Net interlayer flux (ML/yr)
Upper Juandah-1 Coal Measures	12	2,284	-111	-2,231	-1	59
Upper Juandah-2 Coal Measures	13	371	-164	-348	-7	148
Lower Juandah-1 Coal Measures	14	1,518	-149	-1,356	-5	-8
Lower Juandah-2 Coal Measures	15	881	-244	-784	-4	151
Lower Juandah-3 Coal Measures	16	832	-329	-746	-5	248
Taroom Coal Measures	17	1,098	-262	-876	-5	46
Durabilla Formation	18	2,177	0	-1,527	0	-650
Upper Hutton Sandstone	19	31,095	-5,164	-28,258	-74	2,401
Lower Hutton Sandstone	20	850	-1,139	-826	-115	1,230
Upper Evergreen	21	19,311	0	-19,116	0	-194
Boxvale Sandstone	22	386	-194	-350	-1	159
Lower Evergreen	23	16,083	0	-14,873	0	-1,210
Precipice Sandstone	24	25,283	-4,898	-28,996	-1,400	10,012
Moolayember Formation	25	6,204	0	-7,404	0	1,200
Clematis Sandstone	26	50,619	-1,655	-46,861	0	-2,102
Rewan Group	27	4,987	0	-5,329	0	342
Bandanna Formation non-productive zone	28	0	-11	0	0	11
Upper Bandanna Formation	29	3,844	-67	-3,812	0	35

Stratigraphic unit(s)	Model layer	Recharge (ML/yr)	Non-CSG extraction (ML/yr)	Surficial drainage (ML/yr)	Net GHB flux (ML/yr)	Net interlayer flux (ML/yr)
Lower Bandanna Formation	30	0	-11	0	0	11
Undifferentiated Bowen Basin strata	31	3,566	0	-3,567	0	1
Cattle Creek Formation non-productive zone	32	0	-2	0	0	2
Upper Cattle Creek Formation	33	0	-13	0	0	13
Lower Cattle Creek Formation	34	0	-33	0	0	33
Undifferentiated Bowen Basin strata	35	1,170	0	-1,273	0	103
Totals		669,144	-29,103	-637,652	-2,389	0

6.4.8 Transient water balance for the Walloon Coal Measures

Transient water balance results for the period January 1995 through to the end of the historic simulation period in December 2022 for the Walloon Coal Measures are shown in Figure 6-14. These are provided for the “base” calibrated parameter set only. The plot indicates that the CSG industry’s additional extraction demand is largely being supplied from (coal and interburden) storage within the Walloon Coal Measures, with only small contributions from increased inflows from adjacent strata or reduced lateral or surface outflows to the surface.

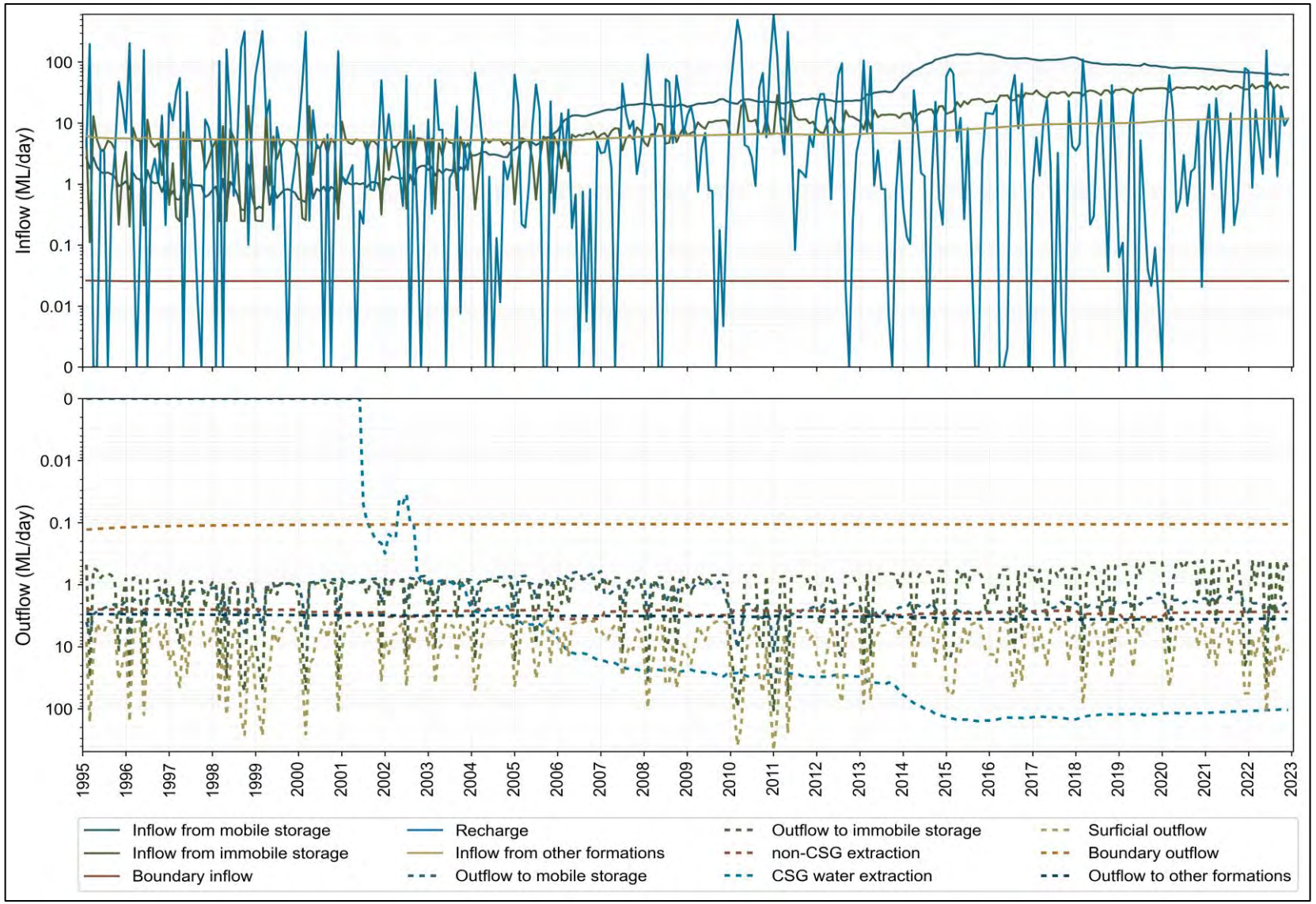

Figure 6-14: Water balance of the Walloon Coal Measures for the transient calibration period ("base" calibrated parameter set)

6.5 Model predictions

Posterior probability distributions for selected predictions were generated by running the predictive model with 500 calibration-constrained parameter sets. To interpret the large number of outputs, a statistical approach was applied: the 5th (P5), 50th (P50), and 95th (P95) percentiles of each output were calculated for every grid cell (or interpolated to points of interest) from the 500 realisations. Outputs falling outside the P5 to P95 range were classified as outliers.

6.5.1 Drawdown Impacts

As outlined in Section 2, a key objective of this model is to evaluate regional drawdown impacts from CSG and coal mining developments. Drawdown is defined as the difference in simulated groundwater level between a no-development scenario (with only consumptive water use) and a development scenario (including petroleum and gas and coal mining). Trigger thresholds apply for each aquifer, with bores considered impacted when drawdown exceeds 2 m in unconsolidated aquifers or 5 m in consolidated aquifers.

Following the methodology in Section 6.4.1, 500 model simulations were undertaken to assess uncertainty in drawdown predictions. Appendix G20 presents maps of the P5, P50, and P95 maximum all-time (LAA) drawdown impacts in critical aquifer and coal layers, while Appendix G21 provides time series of predicted impacts at selected sites. Table 6-16 summarises the area within each formation predicted to exceed the relevant drawdown threshold at any point in the future.

Table 6-16: Area of maximum all-time (LAA) drawdown impact by formation

Stratigraphic units	Model layers	Trigger threshold (m)	Area (km^2)		
			P5	P50	P95
Cenozoic aged units	1	2	92.25	171	285.75
Main Range Volcanics	1	5	11.25	18	27
Upper Cretaceous aged units	2	5	38.25	150.75	382.5
Wallumbilla Formation	3	5	0	0	0
Bungil Formation	4	5	0	0	0
Mooga Sandstone	5	5	0	0	0
Orallo Formation	6	5	0	0	0
Gubberamunda Sandstone	7	5	0	0	36
Westbourne Formation	8	5	2652.75	3703.5	5701.5
Upper Springbok Sandstone	9	5	10298.25	12127.5	13551.75
Lower Springbok Sandstone	10	5	13461.75	15063.75	16726.5
Walloon Coal Measures non-productive zone	11	5	13704.75	15342.75	17104.5
Upper Juandah	12 and 13	5	18823.5	20335.5	22263.75

Stratigraphic units	Model layers	Trigger threshold (m)	Area (km^2)		
			P5	P50	P95
Lower Juandah	14 to 16	5	21755.25	24061.5	26489.25
Taroom Coal Measures	17	5	20787.75	23242.5	26203.5
Durabilla Formation	18	5	11812.5	14474.25	17219.25
Hutton Formation	19, 20	5	2963.25	4752	6277.5
Upper Evergreen Formation	21	5	0	18	83.25
Boxvale Sandstone	22	5	0	0	6.75
Lower Evergreen Formation	23	5	2.25	2.25	20.25
Precipice Sandstone	24	5	2196	2715.75	3438
Moolayember Formation	25	5	63	119.25	312.75
Clematis Sandstone	26	5	130.5	292.5	585
Rewan Group	27	5	1869.75	2621.25	3836.25
Bandanna non-productive zone	28	5	11657.25	13911.75	17201.25
Upper Bandanna Formation	29	5	13662	15696	18576
Lower Bandanna Formation	30	5	13783.5	15912	19066.5
Lower Bowen 1	31	5	96.75	416.25	1046.25
Cattle Creek Formation non-productive zone	32	5	985.5	1032.75	1122.75
Upper Cattle Creek Formation	33	5	1012.5	1059.75	1147.5
Lower Cattle Creek Formation	34	5	969.75	1019.25	1113.75
Lower Bowen 2	35	5	796.5	882	981

6.5.2 Net flux impacts to the Condamine Alluvium

A key predictive output for the impact assessment is the CSG-induced flux between the Condamine Alluvium and the underlying Great Artesian Basin. In the Regional Model 2025, this is calculated as the difference in net zonal fluxes between the development and no-development scenarios, referred to as the Condamine differential net flux. Consistent with the spatiotemporal depressurisation beneath the Condamine Alluvium, the differential net flux peaks in late 2047, ranging stochastically between 1,390 and 1,775 ML/yr (P5 to P95), with a median (P50) of 1,591 ML/yr. Thereafter, the differential flux declines as groundwater levels recover following the end of CSG development. Over the 100-year period from 2011, the average differential net flux is projected to range between 835 and 1,002 ML/yr (P5 to P95), with a P50 of 920 ML/yr (refer to Figure 6-15). Note that negative values are used in the figure to demonstrate that more water is flowing out of the Condamine Alluvium.

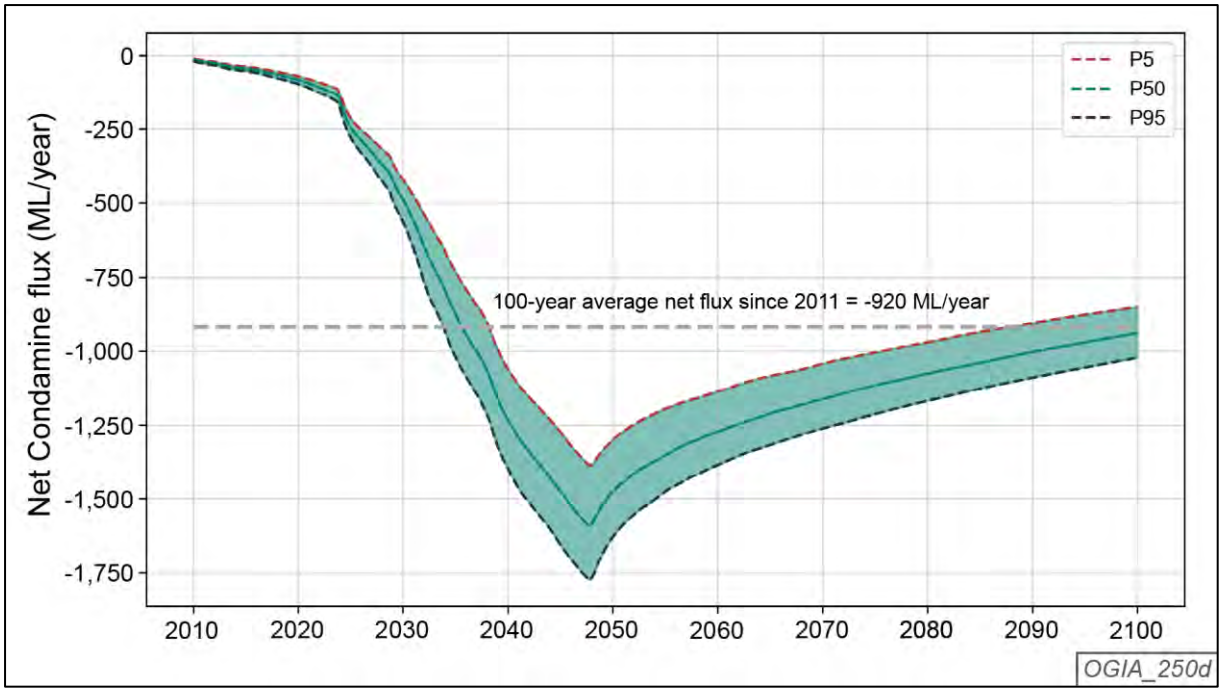

Figure 6-15: CSG-induced differential net flux for the Condamine Alluvium

6.5.3 CSG water extraction

Predicted total CSG water extraction from the Walloon Coal Measures, Bandanna Formation, and Cattle Creek Formation is shown in Figure 6-16, Figure 6-17 and Figure 6-18, with P5, P50, and P95 outputs derived from the posterior 500 model realisations.

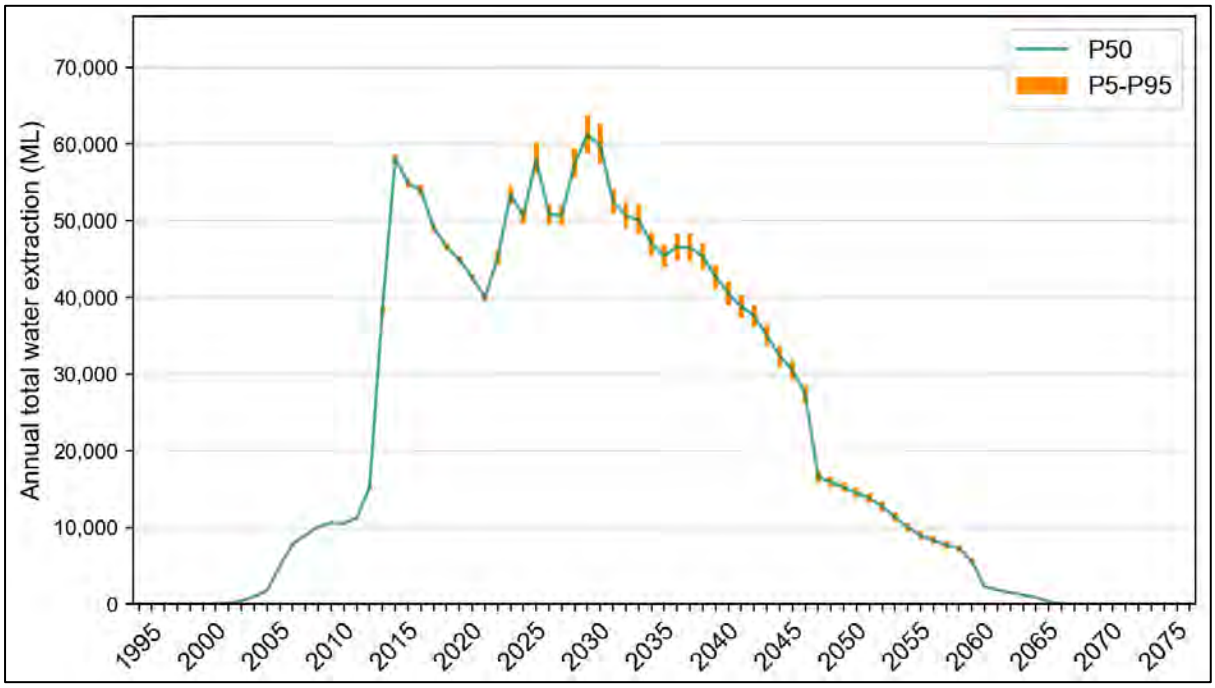

Figure 6-16: Modelled CSG water extraction with uncertainty from Walloon Coal Measures

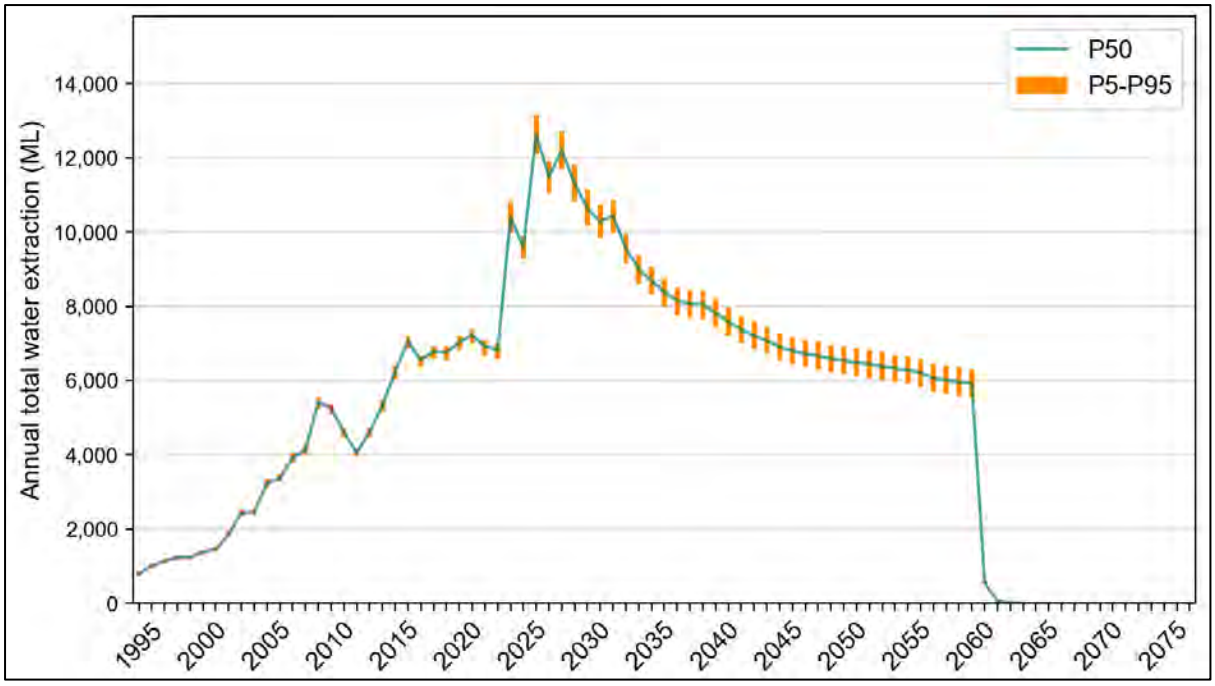

Figure 6-17: Modelled CSG water extraction with uncertainty from Bandanna Formation

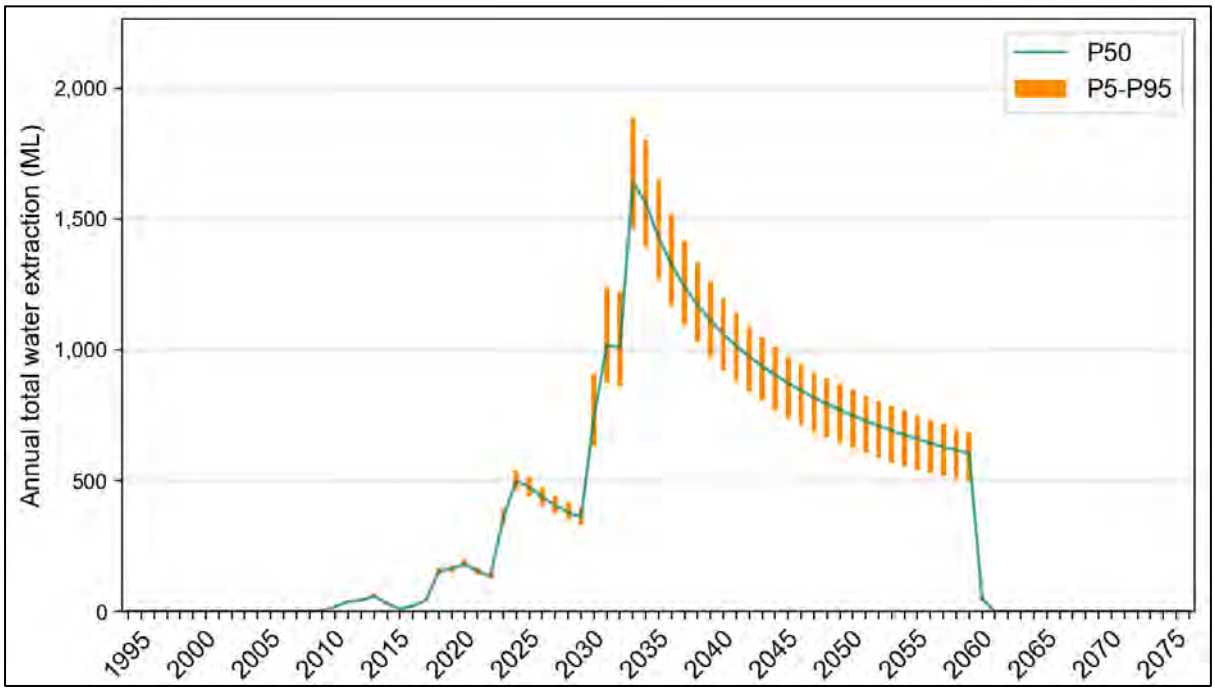

Figure 6-18: Modelled CSG water extraction with uncertainty from Cattle Creek Formation

For the Walloon Coal Measures, the predicted extraction range is relatively narrow, reflecting the substantial amount of history-matching data available for this unit. In contrast, the Bandanna and Cattle Creek formations exhibit wider predictive ranges, consistent with the more limited data available for these deeper CSG reservoirs. It is important to note that these stochastic prediction intervals are based on a single development profile based on the data from different tenure holders and therefore do not capture uncertainty associated with alternative development plans.

6.5.4 Pit Inflows

While the model was not calibrated to historical sump water volumes from coal mining, pit inflow predictions from groundwater were generated for reference (Figure 6-19). The total water extraction from coal mines through the development period is predicted to be less than 1000 ML, consistent with analytical estimates reported by OGIA (2021b). This represents only a small fraction of the cumulative water extraction from CSG and coal developments. By comparison, CSG operations in the Walloon Coal Measures extracted around 53,500 ML (P50) in 2024.

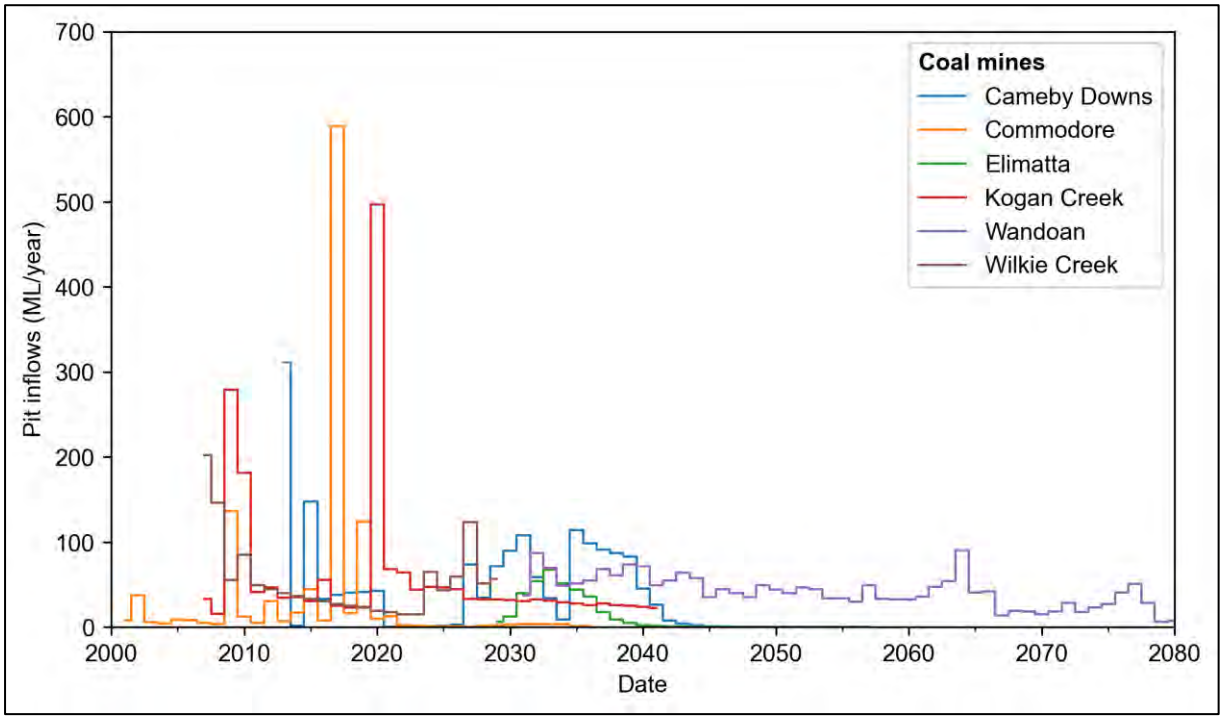

Figure 6-19: Predicted pit inflows (P50) for various mines in the Surat CMA

6.5.5 Subsidence

This section presents and analyses the subsidence results and the derived ground slope change. Following notes need to be kept in mind throughout this section:

- The term "subsidence" specifically refers to CSG-induced subsidence unless stated otherwise.
- Subsidence is represented as negative in modelling. This assumption is consistent with the respective sign convention in geomechanics, hydrogeology, and remote sensing. However, for ease of reading and comprehension, an absolute value of subsidence is sometimes used for discussing results herein. Accordingly, the 5th percentile (P5) of subsidence where it is expressed as a negative value is equivalent to the 95th percentile (P95) of subsidence where it is considered as positive.
- It is important to note that OGIA's current subsidence model focuses on the Walloon Coal Measures, which include the Upper and Lower Juandah Coal Measures and the Taroom Coal Measures. These coal measures represent the main source of subsidence. They have greater areal extent and thickness as well as shallower depth compared to the Bandanna and Cattle Creek Formations, the other two target formations for CSG operations in the Surat CMA. The other two formations will be included in the future model when more data are available.

6.5.5.1 Predictive subsidence

The analysis of subsidence modelling results primarily includes short- and long-term spatial distribution, statistical evaluation and uncertainty analysis. As discussed in Chapter 2, IAA and LAA of groundwater level impact can be derived by trigger thresholds and assessment periods defined in the Water Act. However, such definition does not exist for subsidence assessment in the Water Act. For information purpose, IAA and LAA maps are derived in this section using a threshold of 10 mm. The IAA map is the maximum subsidence within three years of the UWIR release (by 2028 for this UWIR). The LAA map is the maximum subsidence at any time in the future. They provide insights into the spatial distribution of maximum subsidence over short and long terms. It is important to emphasise that the IAA and LAA results are formed from subsidence at different times. As a result, slope changes cannot be calculated based on IAA and LAA rasters. The subsidence by the end of year 2060 is used for slope change calculation.

Maximum subsidence maps

Figure 6-20 (a) and (b) present the IAA and LAA maps, respectively based on the P50 of 500 stochastic realisations of subsidence. The IAA and LAA maps show that subsidence is likely to reach a maximum of approximately 250 mm and 300 mm (in absolute terms), respectively, although it is likely to remain 100 mm or less for most parts of the area affected by subsidence. These maxima occur in two specific areas: near the Horrane Fault and east of Condamine town.

A comparison of the IAA and LAA maps also reveals that the extent of the affected areas expands over time as future CSG fields undergo development. Notably, the affected area extends further into the footprint of the Condamine Alluvium. However, it remains confined within the WCM footprint as implied by the subsidence model.

Figure 6-21 presents the P5, P50 and P95 subsidence map by the end of year 2060, with the P50 map highlighted as the primary focus. The P5 and P95 maps provide insights into the range of possible subsidence outcomes, while the P50 map represents the median or most likely scenario. Together, these maps offer a better understanding of subsidence variability in the areas affected by CSG developments.

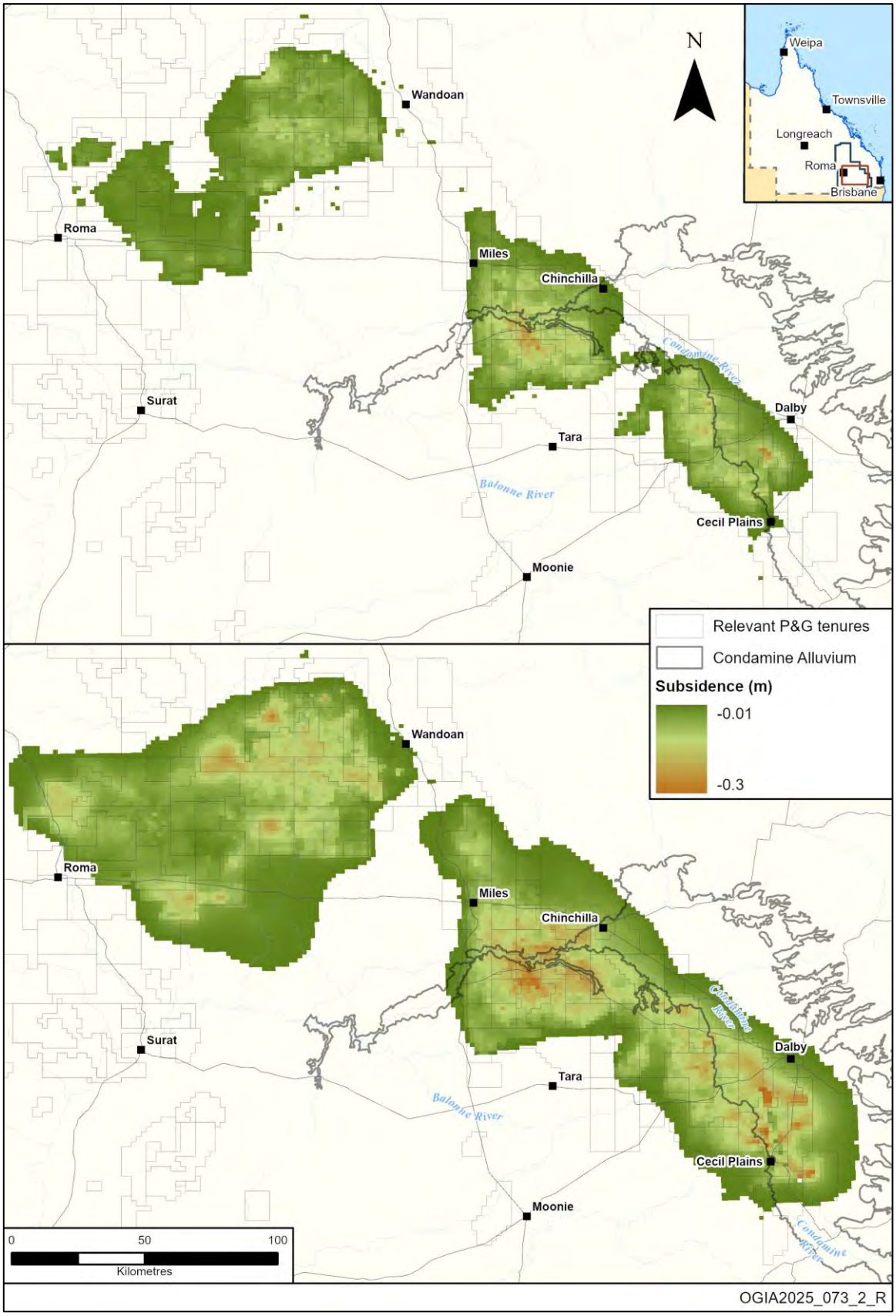

Figure 6-20: P50 of the short-term (top: IAA) and long-term (bottom: LAA) maximum subsidence

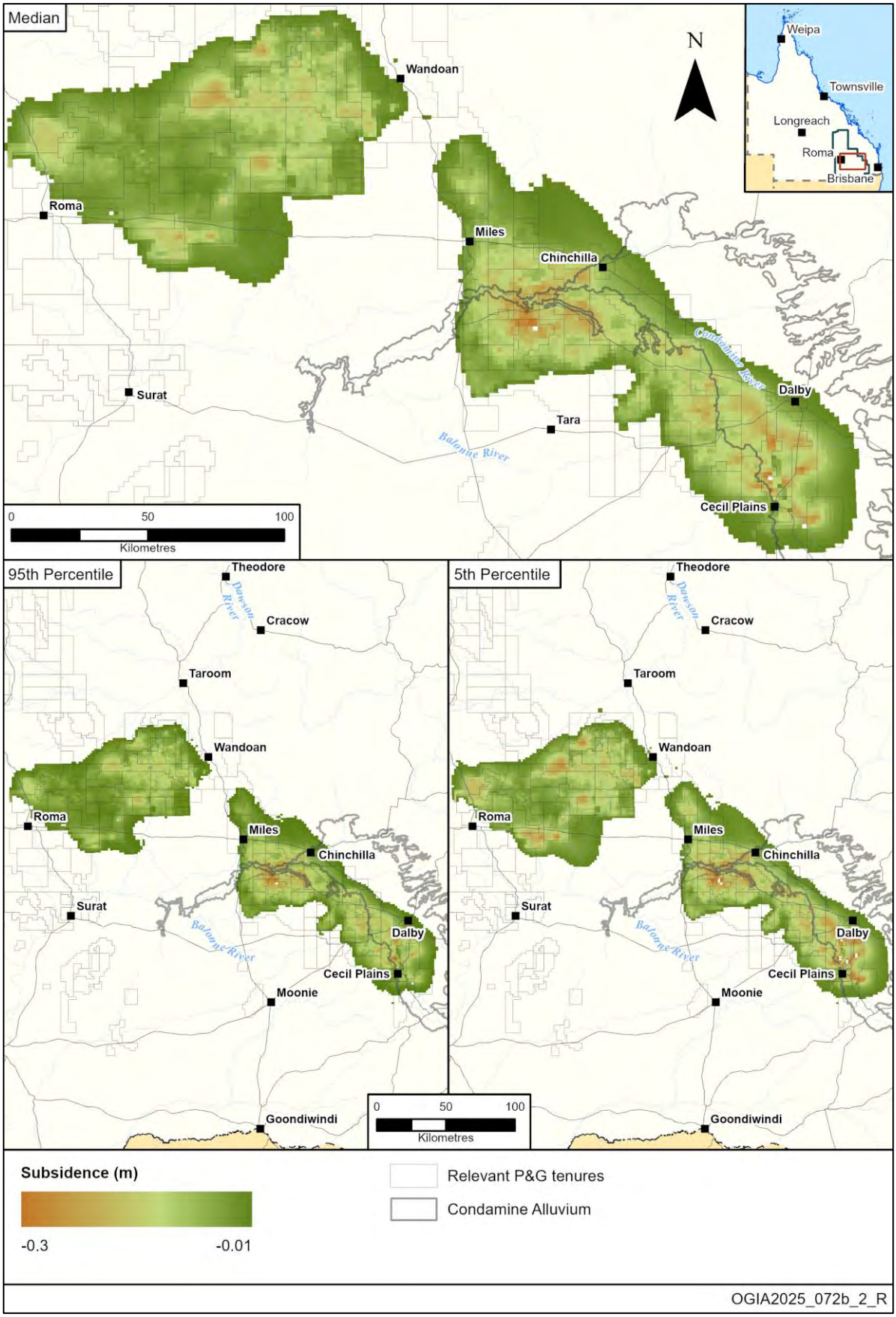

Figure 6-21: Maps corresponding to P50 (a), P5 (b) and P95 (c) of the subsidence for year 2060, with the P50 map highlighted as the primary focus

6.5.5.1.1 Subsidence time series at selected locations

Subsidence time series at different locations can provide an insight into the spatiotemporal variation of subsidence across the WCM. Figure 6-22 (a) displays selected locations on the LAA map. These locations are divided into three groups based on their maximum predictive subsidence (in absolute term) being less than 25 mm, between 25 mm and 150 mm (inclusive) and greater than 150 mm (Figure 6-22 (b), (c) and (d), respectively).

Figure 6-22 shows that most selected locations experience a rapid increase in subsidence during the early stages of CSG extraction. The historical progression of this subsidence was calibrated using field observations, primarily derived from InSAR data. Predictive results indicate that the relatively high rate of subsidence continues until sometime between 2040 and 2060 at these locations when the depressurisation stops. Thereafter, subsidence either continues to grow at a significantly reduced rate or begins to reverse, with the ground moving upward following the initial downward movement. This transition can be attributed to changes in groundwater levels as predicted by the model.

Locations within CSG tenures in the Condamine Alluvium extent, especially those situated close to the Horrane Fault, reach subsidence greater than 100 mm in the time from 2040 to 2060.

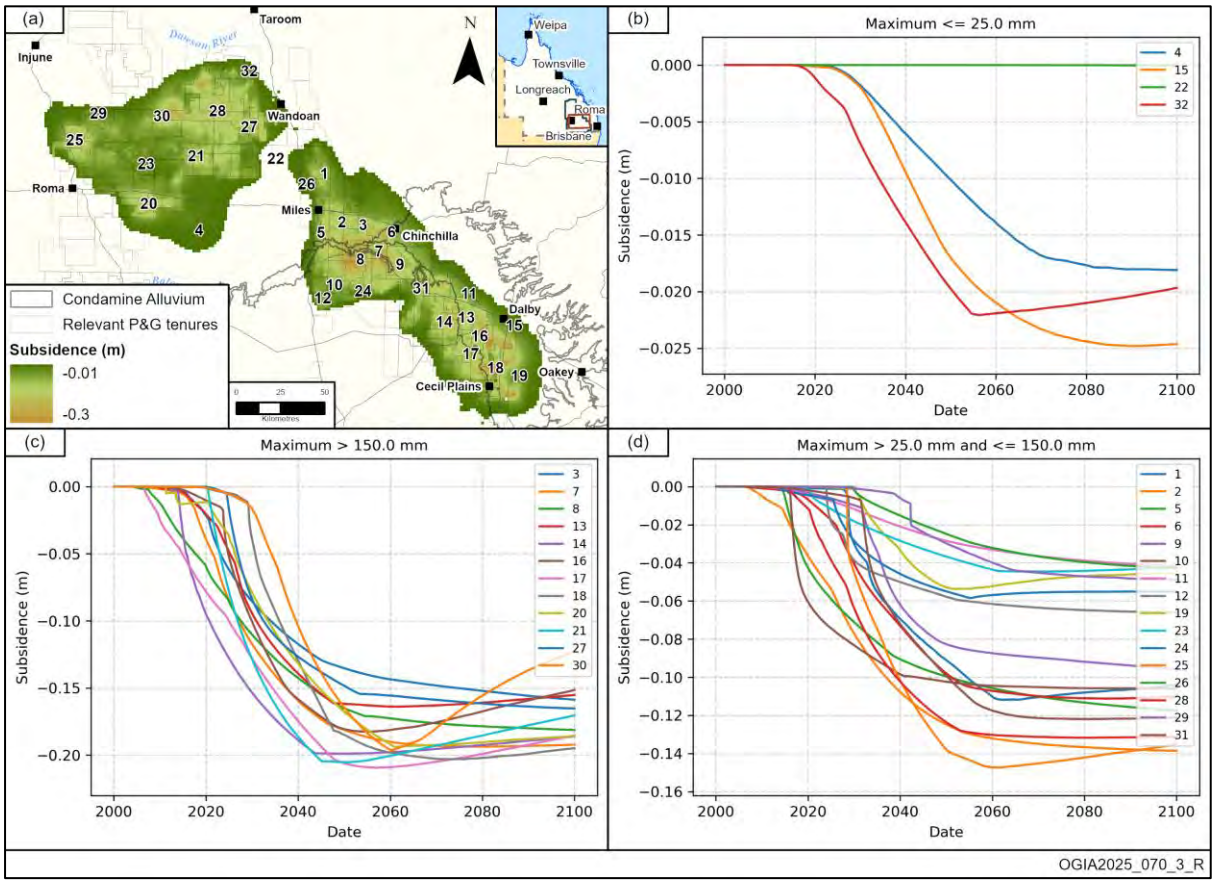

Figure 6-22: (a) Selected locations displayed on the LAA map. (b), (c) and (d) P50 percentile subsidence time series (2000-2100) at selected locations across the WCM where the maximum predicted subsidence (in absolute term) is less than 25 mm, between 25 mm and 150 mm (inclusive) and greater than 150 mm, respectively.

6.5.5.1.2 Evolution of subsidence areas

The number of surficial grid cells experiencing subsidence serves as a proxy for estimating the area of ground surface affected by subsidence. Figure 6-23 presents P50 time series of surficial cell count with subsidence exceeding various thresholds in the range of 50 mm to 300 mm. Plots in these figures provide insights into the spatial and temporal progression of subsidence area. Figure 6-23 demonstrates that greater subsidence, both in terms of magnitude and area, occurs as CSG developments progress and expand. This reflects the relationship between subsidence and CSG-induced drawdown. The trends in these figures suggest that the area of subsidence for lower thresholds reaches their peak over a much longer period, whereas higher thresholds peak relatively quickly.

For instance, Figure 6-23 (a) indicates that cells experiencing subsidence exceeding 50 mm first appear in 2006 and reach their peak in 2093 at approximately 4700 cells. In contrast, cells exceeding 200 mm of subsidence reach their peak count of around 190 cells much earlier, in 2059. This difference highlights the expected behaviour that lower thresholds of subsidence are more widespread, occur earlier, and persist for longer durations compared to higher thresholds.

Table 6-17 summarises the predicted time series of cell counts exceeding various subsidence thresholds. It includes the maximum number of cells recorded for each threshold, the start and end years of the occurrence period, and the specific year in which the maximum cell count occurred. By providing these details, the table highlights trends and critical points in subsidence activity over time, offering insights into the extent and timing of subsidence.

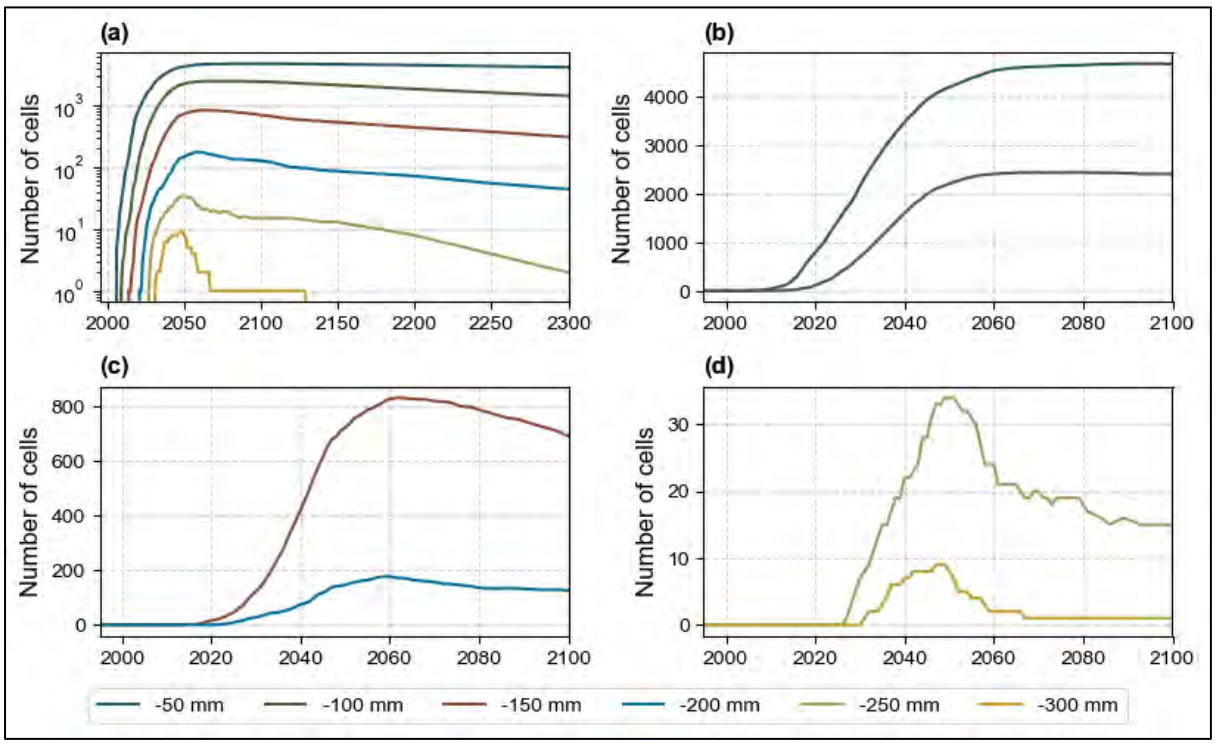

Figure 6-23: Number of cells with subsidence exceeding various threshold versus year (extracted from P50 subsidence results). It shows that the rate of decline in the number of cells, and hence the area of subsidence, is steeper for greater subsidence thresholds. Larger subsidence thresholds, such as 250mm or 300mm, exhibit a more rapid reduction in affected cell counts compared to smaller thresholds like 50 mm.

Table 6-17: Summary of modelled time series data for cell counts exceeding subsidence thresholds

Subsidence threshold (mm)	Start year	End year	Year of max count	Max count	% of surficial cells
-10m	2003	>2100	2199	7798	8.038
-50	2006	>2100	2093	4691	4.836
-100	2009	>2100	2078-2079	2445	2.520
-150	2014	>2100	2062	831	0.857
-200	2021	>2100	2059-2060	177	0.182
-250	2027	>2100	2049-2051	34	0.035
-300	2031	>2100	2047-2049	9	0.009
-350	2040	2049	2044-2049	2	0.002

6.5.5.2 Changes in ground slopes due to CSG-induced subsidence

Highly developed farming systems within parts of the Surat CMA, such as the Condamine Alluvium, rely on low-slope landforms. As such, it is important to assess the potential impact of subsidence on farming operations through changes in land slope. This assessment involves calculating the slope of the ground surface after modifying the surface elevations to reflect the effects of subsidence. OGIA has developed an integrated workflow to assess farm-scale impact of CSG-induced subsidence (Schoning et al. 2025). Sub-regional/local scale subsidence modelling is recommended in such workflow. The purpose of the slope maps presented herein should be used as a screen tool to identify area of interest due to its coarse grid resolution.

OGIA employs Landlab Software (Barnhart et al. 2020; Hobley et al. 2017) to estimate slope and aspect of ground surface based on the popular Horn method (Horn 1981). The workflow uses predicted subsidence of a specific time to adjust the region's DEM. Slope change is then determined by comparing the slope of the modified DEM with that of the reference DEM. The 2006 9-second DEM of Queensland is used as the reference for this analysis.

The year 2060 was selected as the representative time for analysing long-term subsidence, based on current CSG development plans in south-east Queensland. The workflow incorporates stochastic subsidence predictions to generate 500 realisations of slope change across the WCM. Figure 6-24 presents the absolute value of median (P50) slope changes in 2060 relative to the 2006 reference DEM. The map highlights predicted changes in slope within the Condamine Alluvium, with relatively higher slope changes observed near the Horrane Fault. This can be attributed to the compartmentalisation effect and the juxtaposition of layers, which restrict horizontal flow along the fault. The resulting differential drawdown patterns on either side of the fault cause variations in subsidence magnitude and rate, leading to changes in ground slopes.

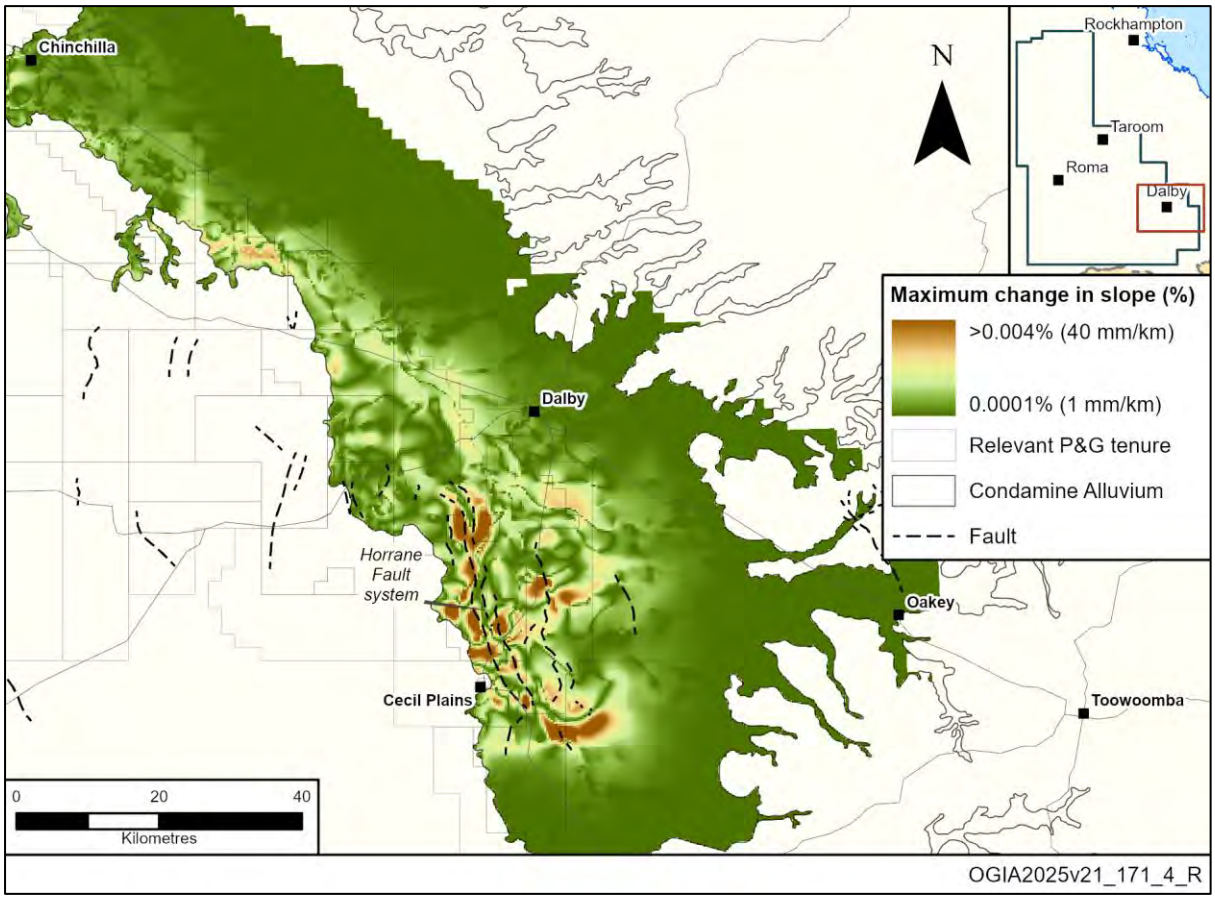

Figure 6-24: Predicted change in ground slope due to CSG-induced subsidence (year 2060 vs year 2006)

7 New Acland groundwater model

7.1 Overview

OGIA has reviewed several hydrogeological investigations undertaken on behalf of New Acland Coal Pty Ltd (NAC) for the New Acland Mine (NAM). More recently, this includes the Underground Water Model Review Report by SLR (2024) prepared in accordance with Condition 24 of the Associated Water License (AWL) granted in October 2022 for commencement of the Stage 3 expansion (operations commenced in May 2023).

Based on an assessment of the hydrogeological information to date - including geophysical logs, groundwater monitoring data, potential impact pathways along faults, and pit inflow volumes, and a sensitivity analysis of critical parameters including recharge multipliers and storage parameters, OGIA has concluded that:

- the hydrogeological conceptualisation of potential groundwater pressure propagation from the NAM is broadly consistent with the available data; and
- the numerical groundwater model presented in SLR (2024) is fit for purpose to assess groundwater pressure impacts in the area.

Accordingly, this model was adopted to predict potential impacts from the NAM for UWIR 2025. The approach will continue to be reviewed and refined as new data become available.

The following section provides a brief overview of the architecture and methodology of the New Acland groundwater model. For a detailed description of the conceptual framework, model setup, parameterisation, calibration, and uncertainty analysis, the reader is referred to SLR (2024).

7.2 Model architecture

SLR (2024) developed a MODFLOW-USG Transport model with a non-uniform hexagonal grid comprising 392,013 nodes (spanning approximately 2,500 square kilometres) across 16 layers containing the Alluvium down to the Marburg Sandstone (see Table 7-1 below). Voronoi cell sizes range from an edge length of 25 m around pumping and monitoring bores to 800 m within the Alluvium. Cells representing open-cut mining areas and drainage channels have edge lengths of around 100 m. Coal and interburden layers in the Walloon Coal Measures of the NAM model are predominantly attributed to the Lower Juandah and Taroom Coal Measures. Non-neighbourhood connections are incorporated for the geological faults to represent the juxtaposition of hydrological units along their throw.

Table 7-1: NAM Model Layers (SLR Consulting Australia 2024)

Model Layer	Layer Name/Geologic Unit	Lithology	Indicative Thickness (m)
1	Alluvium	Gravels, sands, silts and clays	Average of 8.6m, minimum of 0.5m
2	Main Range Volcanics/Basalt	Alkaline basalt	Up to 250m
3	Miscellaneous Walloon Coal Measures	Interbedded fine-grained sandstone, siltstone and coal	Variable
4	Wonkers Coal Sequence	Interbedded fine-grained sandstone, siltstone and coal	Average of 35m
5	Interburden	Mudstone, siltstone, and fine-grained sandstone	Average of 24m
6	Waipanna Coal Sequence	Interbedded fine-grained sandstone, siltstone and coal	Average of 33m
7	Interburden	Mudstone, siltstone, and fine-grained sandstone	Average of 36m
8	Acland Coal Sequence (Above Underground Mines)	Interbedded fine-grained sandstone, siltstone and coal	6m
9	Acland Coal Sequence Historic Underground Mines	-	2m
10	Acland Coal Sequence	Interbedded fine-grained sandstone, siltstone and coal	Average of 50m
11	Interburden	Mudstone, siltstone, and fine-grained sandstone	Average of 24m

Model Layer	Layer Name/Geologic Unit	Lithology	Indicative Thickness (m)
12	Balgowan Coal Sequence (Above Underground Mine)	Interbedded fine-grained sandstone, siltstone and coal	7m
13	Balgowan Coal Sequence Historic Underground Mine	-	2.6m
14	Balgowan Coal Sequence	Interbedded fine-grained sandstone, siltstone and coal	Average of 35m
15	Durabilla Formation	Mudstone, siltstone, and fine-grained sandstone	Average of 25m
16	Marburg Sandstone	Sandstone interbedded with siltstone, shale, and minor mudstone	Average of 250m

The transfer of outputs from the NAM model to the Regional Model 2025 is achieved through the linkage of corresponding layers, as outlined in Table 7-2.

Table 7-2: Relationship between NAM model layers and the UWIR 2025 regional model layers

Layers of the NAM model	Layers of the Regional Model 2025
1	1
2	1
3 - 7	14 - 16
8 - 14	17
15	18
16	19 - 20

7.3 Process representation

7.3.1 Recharge and surficial processes

Diffuse rainfall infiltration was incorporated into the model using the Recharge (RCH) package. For the historic period, rainfall recharge was applied as a percentage of SILO Grid Point data, with seasonal variation introduced using AWRA-L (Bureau of Meteorology) model outputs, with zone-specific recharge multipliers applied during calibration. For all backfilled areas, the initial recharge of the spoil is set to 2.5% of actual rainfall, which is allowed to vary during calibration. Long-term average rainfall was adopted for steady-state and predictive periods.

Vegetation-driven groundwater losses were simulated using the Evapotranspiration (EVT) package. Two zones were defined: areas undisturbed by mining activities and areas affected by mine development, including adjacent wetlands. At ground surface, evapotranspiration was assigned a

long-term average rate of 700 mm/yr (Bureau of Meteorology), decreasing linearly to zero at maximum root depths. Root depths were permitted to vary between 0.5 m and 10 m during model calibration.

Four major creeks (Oakey, Myall, Gowrie and Westbrook) are represented in the model using the River (RIV) package, which enables bi-directional exchange with the groundwater system, governed by the relative responses of the streams and aquifer during seasonal wet periods. Creek-bed incision depths range from 1 to 10 m below the surrounding topography. Creek-bed conductance values were derived from the a priori creek geometry intersection with each model cell, together with estimates of the vertical hydraulic conductivity (Kz) of the riverbed material for each reach. Consequently, streambed conductance exhibited spatial variability along the channel reaches.

7.3.2 Consumptive water use

Groundwater extraction from nearly 2,500 bores is simulated in the model using the Well (WEL) package. The AUTOFLOWREDUCE option is enabled, which automatically reduces pumping rates as groundwater levels approach the base elevation of a pumped cell. Extraction rates are based on consumptive water use estimates from the 2018 NAM model (except for updated data pertaining to NAC extraction bores within the Main Range Volcanics.

7.3.3 Coal mining

Excavated coal material is represented via the drain (DRN) package, with the drain cell elevations set to the base of the target coal seam for each pit, nominally the base of the Acland Coal Sequence (Taroom Coal Measures). Additionally, the Time-varying Materials (TVM) package was employed to simulate increases to the hydraulic conductivity and specific storage of voids (atmospheric conditions) and backfill (disturbed overburden material).

7.3.4 Faults

Two major fault lines are represented in the model: the F5 Fault, located to the north of the Stage 3 project area, and the MDL_01 Fault, located to the southwest. Both faults trend northwest-southeast and exhibit throws of up to 50 m (SLR Consulting Australia 2018). Fault-affected cells, where juxtaposition of layers occurs, are addressed in the model through non-neighbouring connections. Faults are also represented as distinct hydraulic property zones, allowing the calibrated model to simulate observed fault-specific barrier and conduit behaviours.

7.4 Calibration and uncertainty analysis

PESTPP-IES developed by White et al. (2018) as used to match the following observation types:

1. the initial water level observed for each bore in the monitoring network
2. temporal differences in observed water levels relative to the initial measured water level of (1).
3. drawdowns from a 3-day constant rate pumping test (with monitored recovery) of the Acland Coal Sequence on the downthrown side of the *MDL_01* Fault
4. a one-sided penalty term for pit inflows that exceed a given peak threshold.

The following parameter types were estimated:

- formation-scale hydraulic properties (Kx, Kx/Kz, Ss)

- pilot point based hydraulic property (Kx, Kx/Kz, Ss) multipliers for the Waipanna, Acland and Balgowan coal sequence layers, as well as the Marburg Sandstone and Main Range Volcanics layers
- pilot point based specific yield (Sy) multipliers in the Main Range Volcanics layer
- pilot point based hydraulic property (Kx, Kx/Kz, Ss) multipliers for each fault
- zonal (undisturbed versus disturbed) evapotranspiration extinction depth
- zonal multipliers for recharge rate
- layer-based multipliers for well extraction
- elevation of general head boundaries for each layer
- riverbed vertical conductivity for different reaches
- hydraulic properties (Kx, Kx/Kz, Sy, Ss) of spoil material

The parameter estimation process yielded 268 calibrated models used to develop uncertainty analysis for predictions based on their performance against historical data.

7.5 Scenarios

Impact drawdown was based on the difference in hydraulic head between two scenarios included in SLR (2024):

1. *Null Mining* – representing all non-mining stresses under the assumption that mining activities had never commenced
2. *AWL Condition 4 Mine Plan* - incorporates all historical and proposed (Stage 3) mining operations at New Acland, modified to account for Condition 4 of the AWL

Given that UWIR 2025 is only assessing impacts of associated water use, a minor modification was made to the *AWL Condition 4 Mine Plan* scenario whereby mine water supply bores were removed. The only associated water considered in the model is that from the drains representing mining pits.

The predictive scenarios are simulated over the period from 01/01/1900 to 31/07/2038, encompassing 174 stress periods. The simulation begins with a 100-year warm-up phase (January 1900 to August 2001), during which stress period lengths range from 7 to 40 years. This is followed by three distinct development phases:

1. Transient calibration period – quarterly stress periods from August 2001 to July 2023, excluding the fault pumping test (2) below.
2. Fault pumping test – short-term stress periods of 6 hours from 14/11/2016 to 30/11/2016.
3. Future mining scenario – annual stress periods from August 2023 to July 2038

A separate pseudo steady-state simulation with a maximum of 1,000 years was undertaken for each parameter realisation prior to the predictive simulation run. The stress period is completed when the ratio of the net rate of change of storage terms to the net total water budget rate (storage plus boundary flow rates) terms reduces to 0.1%. Output heads are then passed to the starting heads for the predictive simulation run using a modified basic (BAS) package. This step ensured the steady-

state component of the prediction converges appropriately. Furthermore, the output times were modified to align with the UWIR 2025 regional model as closely as possible, to minimise temporal interpolation errors.

8 Integration of impacts for UWIR 2025

As discussed in Chapter 5 of this document, a suite of models was utilised for impact assessment in UWIR 2025. The Regional Model 2025 was used for the prediction of cumulative impacts from CSG, conventional gas and coal mines in the Northern and Central areas as well as the Commodore mine in the South (see Chapter 6). Impact predictions at the New Acland mine were produced separately via the Acland Model (see Chapter 7). Overall cumulative impacts were thereby obtained through superposition of the cumulative impact predictions from the Regional Model 2025 and the Acland model impacts. Although the concept is derived from linear systems, it can also be used for mildly nonlinear systems with acceptable errors (O'Reilly 1987). For nonlinear systems, the composite impact from the superposition is therefore an approximation of the actual accumulative impact. Furthermore, given the distant proximity the New Acland mine, overlapping impacts with CSG operations are expected to be minor (less than the 5 m threshold) and so the above approach is considered suitable for obtaining cumulative impact estimates.

Given the two models both rely on a large number of posterior realisations for predictive uncertainty analysis. There is no direct corresponding relationship between individual realisations from the two models. The superposition was conducted on their statistic outputs. More specifically, statistical time-series of impact (P5, P50, P95) from the Regional Model 2025 were combined with the statistical time-series of impact (P5, P50, P95) from the Acland Model. The superposition of impacts involved three main steps:

1. Resampling of time series outputs of the Acland Model to align with the Regional Model 2025 outputs. Specifically, a linear interpolation was used for the output time alignment.
2. Upscaling the Acland Model impacts to the corresponding UWIR grids using an area-weighted approach. When layer merging is required before the superposition, the maximum impacts from relevant layers were used as the merged impact following the conservative principle. For example, Taroom Coal Measures was represented by layers 8 to 14 in the Acland Model (Table 7-2). The impact from these layers needs to be merged before it is superposed with the impact of layer 17 in the Regional Model 2025.
3. Superposing the impacts by summing the impacts for the two models.

Figure 8-1 represents a pair of impact time-series from the Regional Model 2025 and Acland Model for a location in the Taroom Coal measures. This plot shows the result of the superposition with the cumulative impact equal to their sum. For cumulative impacts at water bores, bilinear interpolation of cell-based impacts from the merged results (obtained in step 3) was applied to estimate impacts at each bore location. The IAA impact reported in the UWIR 2025 was calculated by superimposing the respective maximum impacts in the two models between January 2026 to December 2028, while the LAA impact using the respective maximum impacts across all time in each model. The superposition only applies to the Condamine Alluvium, Marin Range Volcanics, Walloon Coal Measures and Hutton Sandstone. Maps showing the Merged P5, P50, and P95 for the maximum all time impact can be found in Appendix G20.

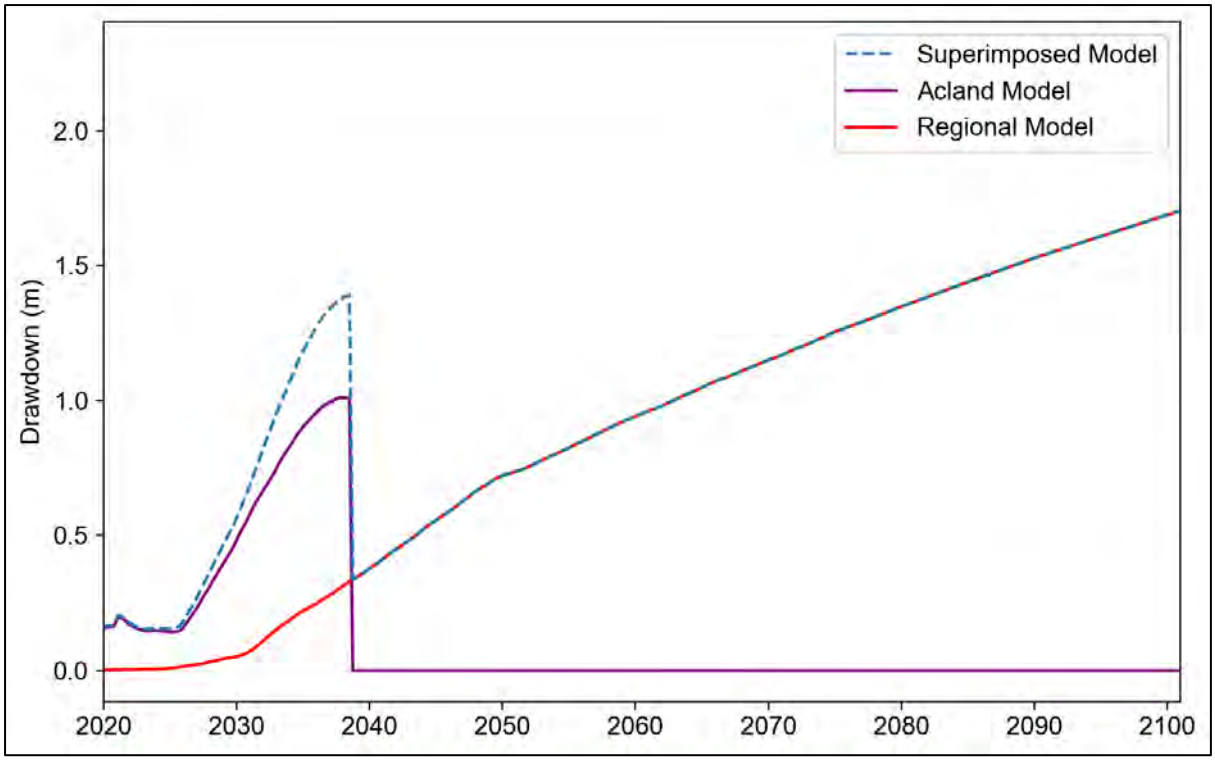

Figure 8-1: An example to show the superposition of the regional and local impact time-series

Figure 8-2 shows three IAA impact heatmaps for the Taroom Coal Measures. The top map presents the cumulative model impacts, while the lower left and right present the Regional Model 2025 and the Acland Model impacts, respectively. The three maps also indicate the position of the example timeseries used in Figure 8-1. It is apparent from Figure 8-2 that impacts from the New Acland mine and nearby CSG development do not coalesce within the three years. Figure 8-3 shows the corresponding LAA maps for the Taroom Coal Measures, where cumulative impacts become relevant.

LAA impacts may occur at fringe areas between the two models, however no receptors have been identified that are not predicted to be impacted by either model independently. This further supports the simplified approach taken for the merging of impacts between the two models.

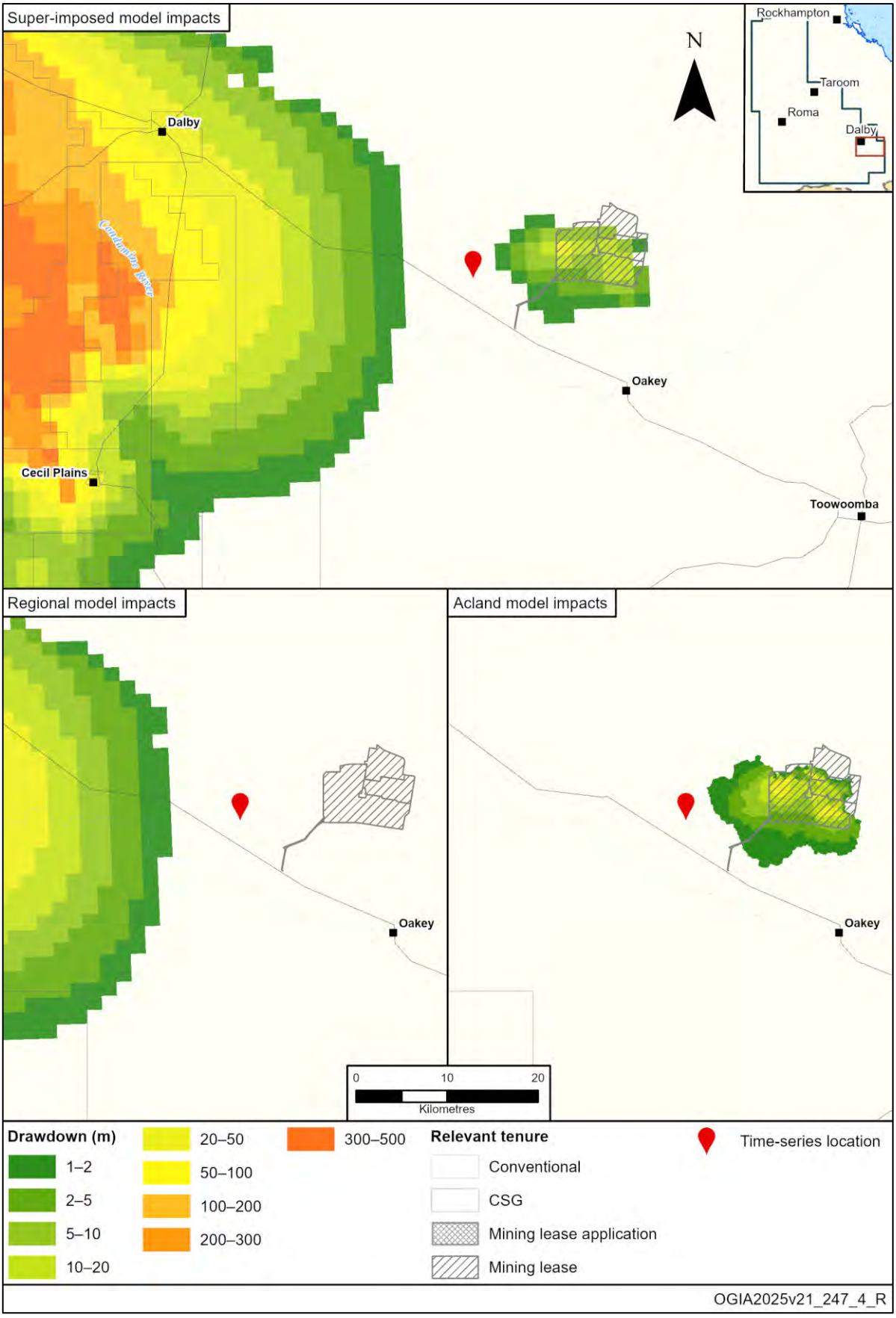

Figure 8-2: P50 of IAA impact in the Taroom Coal Measures based on superposition

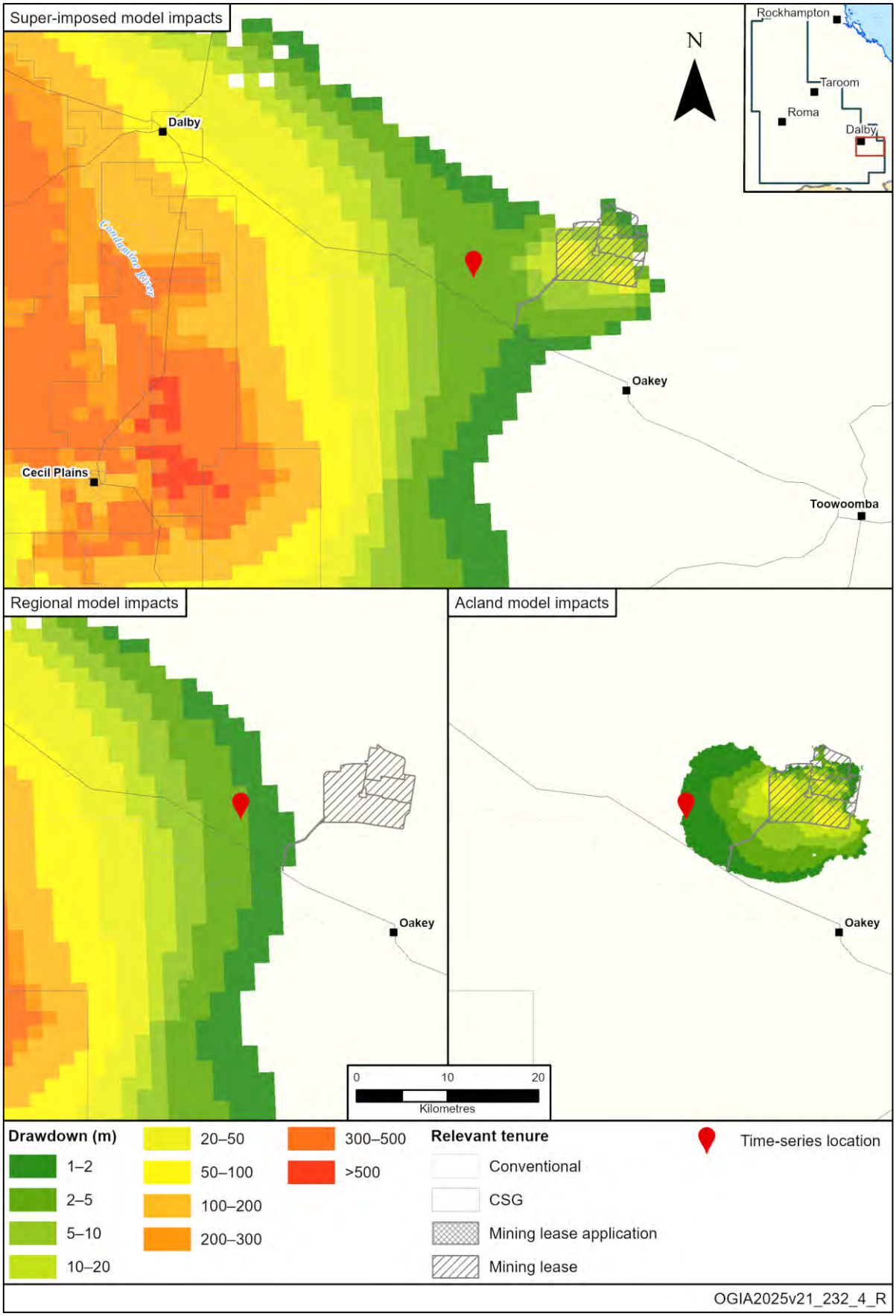

Figure 8-3: P50 of LAA impact in the Taroom Coal Measures based on superposition

9 Conclusions

This report is designed to provide detailed information concerning the groundwater modelling work that underpin the cumulative impact predictions in the UWIR 2025. It details the data, approach and techniques used to address complex modelling challenges, such as dual-phase flow, parameter upscaling, and regional scale CSG-induced subsidence.

Specifically, the primary purpose of the modelling effort is to predict spatiotemporal changes in regional groundwater pressures within the Surat CMA due to resource development, encompassing CSG, coal mining, and conventional oil and gas activities. The modelling is required to achieve several statutory and technical objectives, including:

- **Defining Impact Areas:** Identifying the IAA and LAA, which delineate regions where groundwater levels are predicted to decline by more than the statutory trigger thresholds (two meters for unconsolidated aquifers or five meters for consolidated aquifers) within the next three years (IAA) or at any time in the future (LAA).
- **Identifying Assets at Risk:** Identifying specific IAA and LAA bores and potentially affected springs (where source aquifer pressure is predicted to decline by more than 0.2 m at any time).
- **Quantifying Flow:** Predicting impacts to the rate and volume of groundwater movement between coal formations and key aquifers in the Surat CMA.
- **Estimating Groundwater Extraction:** Estimating the quantity of groundwater expected to be extracted by CSG and coal mining tenure holders.
- **Regional Scale Subsidence Assessment:** Estimating the extent of CSG-induced subsidence and slope change within the Surat CMA at a regional scale.

9.1 Drawdown and impact magnitudes

In the CSG and coal target formations (Walloon Coal Measures and Bandanna Formation), predicted maximum all-time impacts are generally less than 500 m across most areas. Within the shallow units, the Upper Juandah and Lower Juandah Coal Measures, typical impact ranges from 100 m to 300 m. In the lowermost unit (Taroom Coal Measures), depressurisation near CSG wells commonly ranges between 200 m and 500 m, although declines exceeding 500 m may occur locally. For the major underlying aquifers, only minor impacts around 10 metres are predicted in the Hutton Sandstone and Precipice Sandstone. Impacts in the overlying Springbok Sandstone remain below 100 m for most areas.

9.2 Spatial footprint changes

The predicted impact footprint in the Bandanna Formation shows significant contraction in UWIR 2025, although the area of more than 500 m drawdown impact is increased, mainly due to changes in planned development. In the Precipice Sandstone, the one-metre impact footprint is significantly wider east of the Precipice-Bandanna contact zone compared to UWIR 2021, attributed mainly to improved calibration on local water production and minor changes to the production profile.

9.3 Predicted water extraction and flux

The average annual volume of associated water extraction predicted for the life of the industry in UWIR 2025 is about 46,000 ML/year, which is marginally less than the 54,000 ML/year predicted in the UWIR 2021. Critically, the predicted impact pattern in the overlying Condamine Alluvium remains broadly similar to the previous UWIR, with impacts on groundwater levels remaining less than a metre. The average net loss of water (flux) from the Condamine Alluvium to the underlying bedrocks is predicted to be about 920 ML/year over the next 100 years, which is marginally less than the 1,270 ML/year predicted in the UWIR 2021.

9.4 Regional-scale CSG-induced subsidence and slope change

The CSG-induced ground motion is likely to remain less than 150 mm for most parts of the area affected by subsidence, though localized areas may experience subsidence greater than 250 mm. The maximum change in regional ground slope is generally predicted to be less than 0.001% (10 mm over 1 km), potentially reaching up to 0.004% (40 mm over 1 km) in areas near the Horrane Fault within the Condamine Alluvium footprint.

References

Aghighi, MA, Cui, T, Schöning, G, Espinoza, N & Pandey, S 2024, 'Subsidence associated with dewatering and gas extraction from coal seams: Contribution of desorption-induced coal shrinkage', *Journal of Hydrology*, vol. 637, p. 131355.

Aghighi, MA, Cui, T, Schöning, G & Pandey, S 2024a, 'A novel methodology for assessing the potential for formation bridging in coal seam gas fields: A case study from southern Queensland', *Gas Science and Engineering*, vol. 126, p. 205321.

Aghighi, MA, Cui, T, Schöning, G & Pandey, S 2024b, 'A novel methodology for assessing the potential for formation bridging in coal seam gas fields: A case study from southern Queensland', *Gas Science and Engineering*, vol. 126, no. December 2023.

Barnhart, KR, Hutton, EWH, Tucker, GE, Gasparini, NM, Istanbulluoglu, E, Hobley, DEJ, Lyons, NJ, Mouchene, M, Nudurupati, SS, Adams, JM & Bandaragoda, C 2020, 'Short communication: Landlab v2.0: a software package for Earth surface dynamics', *Earth Surface Dynamics*, vol. 8, no. 2, pp. 379–397.

Bui Xuan Hy, A, Burcet, M, McDermott, I & Schöning, G 2025, *Geological model of the Condamine Alluvium area*, Office of Groundwater Impact Assessment (OGIA), Department of Local Government, Water and Volunteers, Queensland Government, Australia, accessed from <https://www.ogia.water.qld.gov.au/publications-reports>.

Chen, Y & Oliver, DS 2013, 'Levenberg-Marquardt forms of the iterative ensemble smoother for efficient history matching and uncertainty quantification', *Computational Geosciences*, vol. 17, no. 4, pp. 689–703.

Chen, Y & Oliver, DS 2017, 'Localization and regularization for iterative ensemble smoothers', *Computational Geosciences*, vol. 21, no. 1, pp. 13–30.

Cranfield, LC 2017, *Mapping of Surat Basin coal seam gas reservoir units*, Department of Natural Resources and Mines, Queensland.

Crosbie, R, Raiber, M, Wilkins, A, Dawes, W, Louth-Robins, T & Gao, L 2022, 'Quantifying diffuse recharge to groundwater systems of the Great Artesian Basin, the NSW coalfields and surrounds',.

Cui, T, Schoning, G, Gallagher, M, Aghighi, MA & Pandey, S 2025, 'A Coupled Hydro-Mechanical Modeling Framework to Concurrently Simulate Coal Seam Gas Induced Subsidence and Groundwater Impacts', *Water Resources Research*, vol. 61, no. 8, p. e2024WR039280.

Deutsch, CV & Journel, AG 1992, 'GSLIB: Geostatistical Software Library and User's Guide', , p. 340.

Doherty, J 2018, 'PEST: Model-Independent Parameter Estimation User Manual Part II: PEST Utility Support Software (7th Edition)', accessed from <Downloadable from www.pesthomepage.org>.

Doherty, J 2020, 'PEST_HP, PEST for Highly Parallelized Computing Environments',.

Doherty, J 2021, ‘A Simple Lumped Parameter Model for Unsaturated Zone Processes’,.

Doherty, J & Hunt, R 2010, *Approaches to Highly Parameterized Inversion: A Guide to Using PEST for Groundwater-Model Calibration*,.

Erasmus, D, Flook, S, Foster, L, Gallagher, M, Bui Xuan Hy, A, Lowry, S, Beck, D & Pandey, S 2024, *Methodology for the assignment of aquifers to bores in the Surat and southern Bowen basins*, Office of Groundwater Impact Assessment (OGIA), Department of Regional Development, Manufacturing and Water, Queensland Government. Australia, accessed from <https://www.ogia.water.qld.gov.au/publications-reports>.

Figueroa-Miranda, S, Tuxpan-Vargas, J, Ramos-Leal, JA, Hernández-Madrigal, VM & Villaseñor-Reyes, CI 2018, ‘Land subsidence by groundwater over-exploitation from aquifers in tectonic valleys of Central Mexico: A review’, *Engineering Geology*, vol. 246, pp. 91–106.

Geertsma, J 1973, ‘Land Subsidence Above Compacting Oil and Gas Reservoirs’, *Journal of Petroleum Technology*, vol. 25, no. 6, pp. 734–744.

GHD 2012a, *Report for Queensland Water Commission (QWC), Stage 2 Surat Cumulative Management Area Groundwater Model Report*, Office of Groundwater Impact Assessment, Brisbane.

GHD 2012b, *Report for Queensland Water Commission (QWC), Stage 2 Surat Cumulative Management Area Groundwater Model Report*, Office of Groundwater Impact Assessment, Brisbane.

Gray, I 1987, ‘Reservoir Engineering in Coal Seams: Part 2-Observations of Gas Movement in Coal Seams’, *SPE Reservoir Engineering*, vol. 2, no. 01, pp. 35–40.

Guzy, A & Malinowska, AA 2020, ‘State of the art and recent advancements in the modelling of land subsidence induced by groundwater withdrawal’, *Water (Switzerland)*, vol. 12, no. 7.

Harbaugh, AW 2005a, ‘MODFLOW-2005 : the U.S. Geological Survey modular ground-water model--the ground-water flow process’, *Techniques and Methods*, accessed July 19, 2024, from <https://pubs.usgs.gov/publication/tm6A16>.

Harbaugh, AW 2005b, *MODFLOW-2005, The U.S. Geological Survey modular ground-water model—the Ground-Water Flow Process*, U.S. Geological Survey, Reston, VA.

Harpalani, S & Chen, G 1992, ‘Effect of gas production on porosity and permeability of coal’, in *Proceedings of the Symposium of Coalbed Methane R and D in Australia*, pp. 67–73.

Harpalani, S & Schraufnagel, RA 1990, ‘Shrinkage of coal matrix with release of gas and its impact on permeability of coal’, *Fuel*, vol. 69, no. 5, pp. 551–556.

Herckenrath, D, Doherty, J & Panday, S 2015, ‘Incorporating the effect of gas in modelling the impact of CBM extraction on regional groundwater systems’, *Journal of Hydrology*, vol. 523, pp. 587–601.

Hobley, DEJ, Adams, JM, Nudurupati, SS, Hutton, EWH, Gasparini, NM, Istanbulluoglu, E & Tucker, GE 2017, 'Creative computing with Landlab: an open-source toolkit for building, coupling, and exploring two-dimensional numerical models of Earth-surface dynamics', *Earth Surface Dynamics*, vol. 5, no. 1, pp. 21–46.

Horn, BKP 1981, 'Hill Shading and Reflectance Map', *IEEE*, vol. 69, pp. 14–47.

KCB 2011, *Central Condamine Alluvium, Stage IV - Numerical Modelling, Final Report*, Department of Environment and Resource Management, Brisbane.

Langevin, CD, Hughes, JD, Banta, ER, Niswonger, RG, Panday, S & Provost, AM 2017, *Documentation for the MODFLOW 6 Groundwater Flow Model*, accessed August 9, 2024, from <https://pubs.usgs.gov/publication/tm6A55>.

Levine, JR 1996, 'Model study of the influence of matrix shrinkage on absolute permeability of coal bed reservoirs', *Geological Society, London, Special Publications*, vol. 109, no. 1, p. 197.

Liu, J, Chen, Z, Elsworth, D, Qu, H & Chen, D 2011, 'Interactions of multiple processes during CBM extraction: A critical review', *International Journal of Coal Geology*, vol. 87, no. 3–4, pp. 175–189.

Masoudian, M, Leonardi, C, Chen, Z & Underschultz, J 2019, 'Towards the development of a baseline for surface movement in the Surat Cumulative Management Area', *The APPEA Journal*, vol. 59, no. 1, p. 95.

Masoudian, MS, Leonardi, C, Chen, Z & Underschultz, J 2019, 'The Effect of Sorption-Induced Shrinkage on the Ground Surface Movement Above Gas-Producing Coalbeds', *53rd U.S. Rock Mechanics/Geomechanics Symposium*, no. June, p. ARMA-2019-0123.

Middlemis, H., Merrick, N., Ross, J., and Rozlapa, K 2001, *groundwater Flow Modelling Guideline*, Murray-Darling Basin Commision, Perth, Australia.

Motagh, M, Shamshiri, R, Haghshenas Haghighi, M, Wetzel, HU, Akbari, B, Nahavandchi, H, Roessner, S & Arabi, S 2017, 'Quantifying groundwater exploitation induced subsidence in the Rafsanjan plain, southeastern Iran, using InSAR time-series and in situ measurements', *Engineering Geology*, vol. 218, pp. 134–151.

OGIA 2016a, 'Underground Water Impact Report for the Surat Cumulative Management Area', , p. 270, accessed from <https://www.dnrm.qld.gov.au/__data/assets/pdf_file/0003/409359/uwir-submission-summary.pdf>.

OGIA 2016b, *Groundwater modelling report for the Surat Cumulative Management Area*, Brisbane, Queensland.

OGIA 2016c, *Hydrogeological Conceptualisation Report for the Surat Cumulative Management Area*, OGIA, Department of Natural Resources and Mines, Brisbane.

OGIA 2019a, *Underground Water Impact Report for the Surat Cumulative Management Area*, Brisbane, Queensland.

OGIA 2019b, *Groundwater Modelling Report - Surat Cumulative Management Area*, Brisbane, Queensland.

OGIA 2019c, *Updated Geology and Geological Model for the Surat Cumulative Management Area*, Brisbane, Queensland.

OGIA 2019d, *Groundwater Modelling Report - Surat Cumulative Management Area*, Department of Natural Resources, Mines and Energy, Queensland Government, Brisbane, Queensland, accessed from <https://www.ogia.water.qld.gov.au/publications-reports>.

OGIA 2021a, *Underground Water Impact Report 2021 for the Surat Cumulative Management Area*, Brisbane, Australia.

OGIA 2021b, *Modelling of cumulative groundwater impacts in the Surat CMA: approach and methods (OGIA21CD15)*, Department of Regional Development, Manufacturing and Water, Queensland Government, Brisbane, Queensland, accessed from <https://www.ogia.water.qld.gov.au/publications-reports>.

OGIA 2021c, *Geological modelling - source data, information and method (OGIA21CD03)*, Brisbane, Queensland.

OGIA 2025, *Underground Water Impact Report 2025 for the Surat Cumulative Management Area*, Office of Groundwater Impact Assessment, accessed from <https://www.ogia.water.qld.gov.au/publications-reports>.

O'Reilly, J 1987, 'Nonlinear control systems: An introduction. A. Isidori, Lecture Notes in Control and In formation Sciences, vol. 12, Springer-Verlag, Berlin, 1981. No. of pages: 297. Price: DM 45', *International Journal of Adaptive Control and Signal Processing*, vol. 1, no. 1, pp. 93–93.

Palmer, I & Mansoori, J 1998a, 'How Permeability Depends on Stress and Pore Pressure in Coalbeds: A New Model', *Spe Reservoir Evaluation & Engineering*, vol. 1, no. 06, pp. 539–544.

Palmer, I & Mansoori, J 1998b, 'How Permeability Depends on Stress and Pore Pressure in Coalbeds: A New Model', *SPE Reservoir Engineering (Society of Petroleum Engineers)*, vol. 1, no. 6, pp. 539–543.

Pan, Z & Connell, LD 2012, 'Modelling permeability for coal reservoirs: A review of analytical models and testing data', *International Journal of Coal Geology*, vol. 92, pp. 1–44.

Panday 2021, 'USG-Transport Version 1.8.0: Block-Centered Transport Process for USG. GSI Environmental',.

Peaceman, DW 1978, 'Interpretation of Well-Block Pressures in Numerical Reservoir Simulation.', *Soc Pet Eng AIME J*, vol. 18, no. 3, pp. 183–194.

Queensland Water Commission 2012, *Underground water impact report for the Surat Cumulative Management Area*, Queensland Water Commission, Brisbane.

Robertson, EP 2005, 'Measurement and Modeling of Sorption-Induced Strain and Permeability Changes in Coal', *Idaho National Lab.(INL), Idaho Falls, ID (United States)*, no. INL/EXT-06-11832.

Robertson, EP & Christiansen, RL 2006, *A Permeability Model for Coal and Other Fractured, Sorptive-Elastic Media*, Society of Petroleum Engineers, Canton, Ohio, USA.

Schlumberger 2021, '3D Mechanical Earth Model - Geomechanical Study to determine compaction and subsidence from Walloon Coal Measures dewatering in Condamine Alluvium area.', , no. June.

Schoning, G, Pandey, S, Cui, T, Burcet, M, Erasmus, D, Gallagher, M, Aghighi, MA, Quici, V, Zhang, Y & Flook, S 2025, *Methodology for the assessment of farm-scale changes caused by coal seam gas-induced subsidence: a pilot study on the western Condamine Alluvium*, Office of Groundwater Impact Assessment (OGIA), Department of Local Government, Water and Volunteers, Queensland Government, Australia.

Shi, JQ & Durucan, S 2004, 'Drawdown Induced Changes in Permeability of Coalbeds: A New Interpretation of the Reservoir Response to Primary Recovery', *Transport in Porous Media*, vol. 56, no. 1, pp. 1–16.

SLR Consulting Australia 2018, *New Acland Stage 3 Project 2017-2018 Groundwater Model Update Numerical Model Report*, Brisbane, Australia.

SLR Consulting Australia 2024, *NAC 2023 Numerical Groundwater Model Update*, Brisbane, Australia.

Smallacombe, J, Singh, D, Erasmus, D, Flook, S & Pandey, S 2024, *Water bores and groundwater use in the Surat and southern Bowen basins*, Office of Groundwater Impact Assessment (OGIA), Department of Regional Development, Manufacturing and Water, Queensland Government, Brisbane, Queensland, accessed from <https://www.ogia.water.qld.gov.au/publications-reports>.

Tikhonov, AN 1963a, 'Solution of incorrectly formulated problems and the regularization method', *Soviet Mathematics Doklady*, vol. 4.

Tikhonov, AN 1963b, 'Regularization of Incorrectly Posed Problems', *Soviet Mathematics Doklady*, vol. 4, no. 6.

White, JT 2018, 'A model-independent iterative ensemble smoother for efficient history-matching and uncertainty quantification in very high dimensions', *Environmental Modelling & Software*, vol. 109.

Wu, G, Jia, S, Wu, B & Yang, D 2018, 'A discussion on analytical and numerical modelling of the land subsidence induced by coal seam gas extraction', *Environmental Earth Sciences*, vol. 77, no. 9, pp. 1–13.

Wu, Y, Liu, J, Elsworth, D, Chen, Z, Connell, L & Pan, Z 2010, 'Dual poroelastic response of a coal seam to CO2 injection', *International Journal of Greenhouse Gas Control*, vol. 4, no. 4, pp. 668–678.

Xu, Y-S, Shen, S-L, Cai, Z-Y & Zhou, G-Y 2008, 'The state of land subsidence and prediction approaches due to groundwater withdrawal in China', *Natural Hazards*, vol. 45, no. 1, pp. 123–135.

This page is intentionally blank.

Office of Groundwater Impact Assessment
Department of Local Government,
Water and Volunteers
GPO Box 2247, Brisbane, Queensland 4001
13 QGOV (13 74 68)
ogia@dlgwv.qld.gov.au
www.ogia.water.qld.gov.au

Queensland Government